Spring 2002

Assessing ice storm damage to hardwood forest canopies using the Advanced Solid-State Array Spectroradiometer (ASAS) and Landsat TM imagery

James Stuart Burnett
University of New Hampshire, Durham

INFORMATION TO USERS

This manuscript has been reproduced from the microfilm master. UMI films the text directly from the original or copy submitted. Thus, some thesis and dissertation copies are in typewriter face, while others may be from any type of computer printer.

The quality of this reproduction is dependent upon the quality of the copy submitted. Broken or indistinct print, colored or poor quality illustrations and photographs, print bleedthrough, substandard margins, and improper alignment can adversely affect reproduction.

In the unlikely event that the author did not send UMI a complete manuscript and there are missing pages, these will be noted. Also, if unauthorized copyright material had to be removed, a note will indicate the deletion.

Oversize materials (e.g., maps, drawings, charts) are reproduced by sectioning the original, beginning at the upper left-hand corner and continuing from left to right in equal sections with small overlaps.

Photographs included in the original manuscript have been reproduced xerographically in this copy. Higher quality 6" x 9" black and white photographic prints are available for any photographs or illustrations appearing in this copy for an additional charge. Contact UMI directly to order.

ProQuest Information and Learning
300 North Zeeb Road, Ann Arbor, MI 48106-1346 USA
800-521-0600

UMI®

ASSESSING ICE STORM DAMAGE TO HARDWOOD FOREST CANOPIES USING THE ADVANCED SOLID-STATE ARRAY SPECTRORADIOMETER (ASAS) AND LANDSAT TM IMAGERY

BY

JAMES S. BURNETT

BA Bowdoin College, 1972
MALS Dartmouth College, 1978
MS University of New Hampshire, 1998

DISSERTATION

Submitted to the University of New Hampshire
in Partial Fulfillment of
the Requirements for the Degree of
Doctor of Philosophy
in
Natural Resources

May, 2002

This dissertation has been examined and approved.

Dr. Barrett N. Rock, Dissertation Director
Professor of Natural Resources
Complex Systems Research Center
University of New Hampshire, Durham, NH

Dr. Richard W. Birnie
Professor of Earth Sciences
Dartmouth College, Hanover, NH

Dr. Christopher Eagar
Adjunct Professor of Natural Resources
University of New Hampshire, Durham, NH
Research Ecologist, USDA Forest Service,
Durham, NH

William Frament
Remote Sensing Specialist
USDA Forest Service, Durham, NH

Dr. James R. Irons
ASAS Instrument Scientist
NASA - Goddard Space Flight Center
Greenbelt, MD

Dr. Mary E. Martin
Research Assistant Professor of Natural Resources
Complex Systems Research Center
University of New Hampshire, Durham, NH

April 22, 2002
Date

DEDICATION

To my parents, Josh and Tay Burnett.

ACKNOWLEDGEMENTS

I especially want to thank my wife, Kris, for supporting me in this endeavor from conception to completion. In many ways our family life was turned upside down. She helped us land on our feet as my number one constructive critic and supporter.

There are many people connected with the University of New Hampshire I would like to thank. My masters degree advisor, Dick Weyrick, and the professors who introduced me to remote sensing, Russ Congalton, Barry Rock, and Mary Martin. There are also my fellow graduate students at UNH to thank – Steve Hale, Petya Entcheva – and the support crew in the "Rock" lab – Ryan Huntley and Anya Whittington. It was important to have a group of colleagues with whom to share ideas and solve problems. The computer systems technicians in Morse Hall (RCC) were also very helpful in addressing the many computer-related problems that invariably occur. Thank you, Faith Sheridan and Alison Magill, for helping with logistical matters related to the UNH Natural Resources Department program and procedures.

The NASA Space Grant Fellowship program provided generous funding support for my ice damage assessment project. These funds came to me through grants from both UNH and Dartmouth College. David Bartlett is the director of the Space Grant program at UNH, which funded my first year of research, and Prof. Dick Birnie is Chair of the Earth Sciences Department and director of Space Grant funds at Dartmouth, which supported the last two years of research. These funds were critical to the successful completion of my project.

The cordial and enthusiastic assistance that I received at Dartmouth came from Dick Birnie. Dick provided Space Grant funding, the use of the Earth Science

Department's remote sensing and GIS lab, and immeasurable amounts of energy, interest, and advice, all of which helped bring my project to a successful conclusion. Thank you, Dick.

Many United States Forest Service (USFS) personnel lent their experience and expertise during the fieldwork phase of the project and in some of the initial global positioning systems (GPS) and geographic information systems (GIS) work. Wayne Millen, of the Androscoggin District of the USFS, granted permission for the field crew to collect samples and make measurements in study areas throughout the White Mountain National Forest (WMNF). Wayne also shared data and methods that his crews had collected and used in their ground assessment of the ice damage from the storm. Bill Frament shared the Forest Service's sketch map ice damage assessment data and Bill Campbell helped me to locate potential target areas for overflights and to collect GPS data. Chris Eagar shared other ground data that the Forest Service had collected following the ice storm of January 1998. Tom Luther helped create a GPS points file from collected data. All these efforts were essential to establishing the conditions on the ground that were to be compared to the conditions as interpreted from the remotely sensed imagery of the ice storm damage.

Forest Service personnel and scientists connected with Hubbard Brook Experimental Forest, Thornton, NH, and Bartlett Experimental Forest, Bartlett, NH, were cooperative and helpful while data was being collected in their forests. Wayne Martin helped us get started at Hubbard Brook and Chris Costello and Mike Medieros provided photos of the ice damage and helped me select study sites in the forest.

My project never would have gotten off the ground – literally – had it not been for NASA. Jim Irons, Carol Russell, Phil Dabney, Mike Bur, and Bill Kovalick, all of Goddard Space Flight Center (GSFC), were especially helpful in the use of the ASAS sensor to acquire imagery of ice-damaged sites in the WMNF. Jim and Carol are responsible for much of the early research done in the development and use of ASAS, Phil and Mike provided on-flight technical expertise and data preprocessing in the lab, and Bill developed the program to adapt the atmospheric correction model (6S) to ASAS data. My visit to GSFC to speak with scientists working on projects similar to mine – Charlie Wathall, Abuelgasim, Stefan Sandimeier, and K. Ranson – was also very informative.

TABLE OF CONTENTS

LIST OF TABLES

LIST OF FIGURES

ABSTRACT

ASSESSING ICE STORM DAMAGE TO HARDWOOD FOREST CANOPIES USING THE ADVANCED SOLID-STATE ARRAY SPECTRORADIOMETER (ASAS) AND LANDSAT TM IMAGERY

By

James S. Burnett

University of New Hampshire, May 2002

A major ice storm in January 1998 damaged 17 million acres of forestland in the Northeastern United States and Quebec Province. In July 1998 the airborne multiangle hyperspectral sensor, Advanced Solid-State Array Spectroradiometer (ASAS), acquired imagery for nine ice damaged target areas in the White Mountain National Forest (WMNF). Ice damage was also measured *in situ* at 288 sample plots. Radiance values for nadir ASAS images were normalized and the blue shift of the red edge was represented as the radiance value at 714 nm (714nr). The 714nr for 210 sites in 3 damage classes differentiated severely damaged sites from moderately and lightly damaged sites. The classification map of 714nr in 3 damage classes produced an overall accuracy of 54%. The effectiveness of off-nadir ASAS imagery (+/-45°, +/-26° view angle) to differentiate levels of ice damage was evaluated. It was determined that the red edge features of normalized ASAS data were not significantly affected by view angle, and that when compared to off-nadir views, the nadir view was most effective for detecting damage. Three vegetation indices, Vegetation Index (VI), NDVI, and TM 5/4, were applied to a single post-event (August 1998) TM image and classification mapping

and accuracy assessment methods were applied. The overall accuracies of the 3 indices to map 3 levels of damage were 68% for VI, 72% for NDVI, and 76% for TM 5/4. Finally, the effectiveness of the ASAS 714nr approach was compared to 3 Landsat TM change detection analyses using pre- and post-event differences in VI, NDVI, and TM 5/4 to detect ice damage. The overall accuracies of the 3 indices to map 3 levels of damage using change detection were 78% for VI, 82% for NDVI, and 78% for TM 5/4.

CHAPTER I

INTRODUCTION

In January of 1998, unusual weather patterns contributed to a major "100-year-event" ice storm throughout northern New England and New York and Quebec, Canada. Estimates of losses to natural resources in the United States alone exceed $1 billion. The United States Forest Service (USFS) reported 17 million acres of damaged forestlands in this area. It is important to detect, assess, and map forest disturbance, such as ice storm damage, on a regional scale quickly and accurately (Linnane, 1998).

Ideal conditions for ice accumulation on tree branches and stems occur when water droplets form in a warm (above-freezing) layer of air aloft and descend through a thin layer of cold (below-freezing) layer of air near the Earth's surface (Ludlum, 1976). For three days early in January 1998, New Hampshire weather conditions favorable for ice accumulation on exposed surfaces prevailed. Tree branches and stems - particularly hardwood species such as sugar maple, red maple, paper birch, white ash, and red oak - situated between 600-750 meters in elevation on hilly and mountainous areas were affected. As ice accumulated on limb and stem surfaces, as much as 10 cm in some areas of the state, these appendages bent over or failed causing wide-scale damage to the forest. The damage left a patchwork of gaps in the canopy, which greatly reduced the amount of green vegetation that had existed when the canopy was undamaged and closed. The evidence of damage – exposed broken stems and branches and woody debris on the ground – was visible across the landscape and particularly from the air. The nature of the

damage offers a unique opportunity to test remote sensing detection of ice damage to the forest canopy.

Following a forest disturbance event the USFS relies initially on sketch mapping as its primary damage assessment instrument. Sketch mapping is a subjective process in which two or more sketch map artists fly over the disturbed area, assess differing levels of damage, and combine their interpretations into a single coverage. Later, more comprehensive and detailed assessments are usually made using aerial photographs (1:8,000 scale). While this is a less subjective process than sketch mapping, a study by Biging et al. (1991) comparing photointerpretation to ground measurements for characterizing forest structures revealed the accuracy for species identification to be between 75% and 85%, while the accuracy of crown closure was less than 40%. Gaps in the forest canopy caused by ice storm damage are directly related to crown closure measurements. In addition, the cost of aerial photography on a regional scale is prohibitive. The method of connecting remotely sensed data to the materials and conditions that actually exist on the ground needs to be improved and made more cost effective using remotely sensed digital imagery. This is particularly true at the regional level where compounded error and economies of scale become an important factor in large-scale forest disturbance assessments.

Initiatives, such as the International Geosphere-Biosphere Program and the United States Global Change Research Program, call for the use of remote sensing technology in efforts to understand the forces behind global change (CEES, 1991). Though much progress has been made in this regard, remote sensing, as an environmental monitoring tool, remains under-utilized. The relationship between ground conditions and what is

measured in airborne and spaceborne spectral reflectance data needs to be better defined so that remotely sensed datasets are used more effectively. The relatively high spatial resolution Multispectral Scanner (MSS) and Landsat Thematic Mapper (TM) satellite series provides an archive of space-borne digital imagery dating back to 1972. System Probatoire d'Observation de la Terre-1 (SPOT 1), launched in 1986, initiated a similarly useful archive of commercial imagery that has been underutilized as an environmental monitoring resource. The successful launch of the satellite-based Terra platform (EOS-AM, April 1999) by the National Aeronautics and Space Administration's Earth Observing program and the NASA EO-1 (November 2000) has made multiangle (Multi-angle Imaging Spectroradiometer, MISR) and hyperspectral (Hyperion) viewing a reality.

The Advanced Solid-State Array Spectrometer (ASAS) airborne sensor offers three special features: It is capable of hyperspatial (2.5-meter pixels at nadir), hyperspectral (62 narrow bands), and multiangle viewing. In this study, the effectiveness of ASAS hyperspectral resolution and multiangle viewing to detect and measure forest canopy damage, such as that caused by ice storms is evaluated and compared to broadband (Landsat TM) methods. The hyperspectral capabilities of ASAS provide the potential to detect and quantify fine-feature spectral reflectance data related to variations in canopy morphology (percent canopy damage to individual trees) and leaf condition (size, chlorophyll content) related to ice storm damage. The multiangle views of forest canopies provide new off-nadir data with the potential to detect and discriminate between differing levels of storm damage. From off-nadir the sensor can view the sides of tree crowns and perhaps detect non-green vegetation and other symptoms of ice damage.

The ASAS investigation was carried out in three steps. First, the hyperspectral capability of ASAS is used to distinguish between the spectral fine-features of the red edge for measuring differing levels of damaged forest canopies. Horler et al. (1980, 1983) showed that the slope and position of the red edge region (approximately 650-750 nm) of the electromagnetic spectrum is directly correlated with leaf chlorophyll content and by extension, levels of green biomass. A shift in the wavelength position of the red edge curve of vegetation spectra in the direction of the blue region of the spectrum is referred to as the blue shift and is seen as an indication of reduced chlorophyll content and/or green biomass (Moss and Rock, 1991), a symptom of ice storm damage to the forest canopy (Rock et al., 1988; Vogelmann et al., 1993). For this study the blue shift is represented by measuring the reflectance value for normalized red edge (653 to 775 nm) values at ASAS 714 nm. This value is referred to as 714nr (714 normalized reflectance). The average value for *in situ* measurements of percent ice damage for study sites and the average 714nr for corresponding sites sensed remotely are used to map three levels of ice damage.

Second, the multiangle viewing capability of ASAS to detect canopy damage is evaluated. ASAS datasets derived from various off-nadir view angles are used to measure spectral reflectance differences in sites with differing levels of ice storm damage to forest canopies. Prior to evaluating the ability of off-nadir views to differentiate levels of canopy damage, data for view angles from +45° to –45° off-nadir were evaluated to determine if off-nadir viewing affects the slope and wavelength position of the red edge curve of an undamaged canopy control site. When ASAS datasets are normalized for five view angles (+/-45, +/-26, and nadir) the red edge spectral signatures are qualitatively

invariant: the shape, slope, and wavelength position of the red edge is not significantly changed. The ability of normalized data from off-nadir views (+45° to –45° off-nadir) to distinguish levels of ice damage to forest canopies is then compared to that of nadir data.

Finally, the ability of 714nr values to detect ice storm damage is compared to the ability of traditional broadband (Landsat TM) canopy damage detection methods. First, the Vegetation Index (VI), NDVI, and Thematic Mapper 5/4 ratio (TM 5/4) are applied to study sites in a post-event (August 1998) TM image and these results are used to map 3 levels of damage. The accuracies of these classification maps are compared to the 714nr classification map results. Second, ASAS results are compared to results of damage assessments with the VI, NDVI, and TM 5/4 when change detection is applied to pre- and post-event Landsat TM scenes to determine levels of damage to forest canopies for corresponding study sites in the WMNF. This phase of the investigation not only evaluates the effectiveness of hyperspectral vs. broadband sensors to detect ice damage, but also evaluates the cost-effectiveness and practicality of using change detection, involving pre- and post-event imagery, vs. single post-event remote sensing methods and using satellite (Landsat) vs. airborne (ASAS) platforms.

The opportunity now exists, following the ice storm, to utilize simple and practical forest canopy damage assessment tools. The damage caused by the recent ice storm in northern New Hampshire provides an opportunity for the evaluation of the hyperspectral, multi-angle viewing capabilities of ASAS and traditional broadband remote sensing instruments to detect, measure, and map forest disturbances, such as ice storm damage. Methods described in these analyses have the potential to improve the accuracy and efficiency of regional ice storm damage assessments.

A practical and effective regional assessment tool could be useful to both public and private landowners. It could provide ice damage assessments that are consistent and fair across the affected landscape. It could facilitate post-event allocation of reparations and cost-share benefits for economic losses at both the state and federal level. Timber salvage operations could be targeted and prioritized by both public and private landowners. Forests with increased risk of wildland fires due to fuel loading could be identified, prioritized, and monitored. Assessments could be archived and studies monitoring the recovery of damage sites could be initiated. In general, an effective ice damage assessment tool would provide baseline documentation useful immediately following the disturbance event and into the future.

The following hypotheses are tested.

Chapter II - ASAS HYPERSPECTRAL RED EDGE MEASUREMENTS

2-1. Values of 714nr for nadir hyperspectral ASAS imagery of variously ice damaged hardwood sites (7.5 x 7.5 m sites, N = 210) can differentiate 3 levels of damage.

2-2. Values of 714nr for nadir hyperspectral ASAS imagery of variously ice damaged hardwood sites (7.5 x 7.5 m sites, N = 210) can be classified with greater than 80% overall accuracy.

Chapter III - ASAS NADIR VS. OFF-NADIR VIEWING

3-1. Red edge features of normalized ASAS datasets are not affected by sensor view angle.

3-2. Values of 714nr for off-nadir hyperspectral ASAS imagery of variously ice damaged hardwood sites (90 x 90 m sites, N = 50+/-) are more effective than nadir imagery at differentiating 3 levels of ice damage to hardwood forest canopies.

Chapter IV – 714nr VS. BROADBAND MEASUREMENTS

4-1. Measurements of TM 5/4, NDVI, and VI for a post-event Landsat TM scene (August 1998) of variously ice damaged hardwood sites (90 x 90-m sites, N = 66) are more effective than 714nr (7.5 x 7.5 m sites, N = 210) at differentiating and mapping 3 levels of ice damage to hardwood forest canopies.

4-2. Measurements of TM 5/4, NDVI, and VI applied to pre- and post-event Landsat TM scenes (August 1996 and 1998) of variously ice damaged hardwood sites (90 x 90 m sites, N = 66) using change detection are more effective than nadir 714nr (7.5 x 7.5 m sites, N = 210) at differentiating and mapping 3 levels of ice damage to hardwood forest canopies.

LITERATURE REVIEW

Forest Decline and Canopy Damage Research

Although spectral features of healthy vs. stressed vegetation and undamaged vs. damaged canopies have not been used specifically to assess ice storm damage, spectral features of vegetation and forest canopies have been explored using spectral signatures derived from spaceborne remote sensing instruments, such as Landsat Multispectral Scanners (MSS) and Landsat Thematic Mapper (TM). Airborne hyperspectral sensors and field spectrometers have been used to measure vegetation health and condition, as well. Red edge features have been the focus of many explorations seeking to differentiate levels of plant stress to various vegetation types (Rock, et al. 1988; Moss and Rock, 1991; Vogelmann, et al. 1993; Zarco-Tejeda, 2000). For example, it was discovered that healthy leaves progress from a stage of active photosynthesis through various stages of senescence as tannins replace chlorophyll (Knipling, 1969). In the early 1980s, further investigations revealed vegetation red edge changes recorded with an airborne spectrometer over an area of sulphide mineralization (Collins et al., 1983; Chang and Collins, 1983; Milton et al., 1983). Early research culminated with the findings of Horler et al. (1980, 1983), which showed that the slope and position of the red edge reflectance region of the electromagnetic spectrum is directly correlated with leaf chlorophyll content. Subsequent vegetation studies documented and applied Horler's findings (Rock et al., 1988; Vogelmann et al., 1993; Zarco-Tejada et al., 2000; Entcheva, 2000).

Because sensors, such as Landsat MSS and TM, do not acquire red edge spectral data, the broadband NDVI has been used to monitor crop conditions since the early 1970s. The index is determined by dividing the difference between reflectance values in

the red and near infrared (NIR) bands by their sum. For example, when using Landsat Thematic Mapper data (TM), NDVI = TM4 – TM3 / TM4 + TM3. In an NDVI image, the brighter the pixel, the greater the photosynthesizing vegetation present (Jensen, 1996). By normalizing the difference between the red and the NIR, NDVI describes the red edge region. The NDVI is traditionally used with multispectral imagery to determine relative values for leaf area index (LAI) and green (vegetative) biomass. The NDVI is used to monitor crops and measure LAI and biomass amounts on continental and global scales, usually by applying imagery from Advanced Very High Resolution Radiometer (AVHRR) imagery with coarse spatial resolution (1 km x 1 km).

Several methods of quantifying red edge features were developed in order to measure change in vegetation health and condition. Various vegetation indices have been applied to multispectral satellite imagery in order to detect changes in vegetation condition symptomatic of forest damage. An assessment of the Visible/Infrared Intelligent Spectrometer (VIRIS) and simulated Thematic Mapper (TMS) data acquired in field and laboratory studies led to development of an imaged equivalent of a moisture stress index for mapping forest damage to coniferous stands on Camels Hump, Vermont (Rock et al., 1986). Spectral reflectance data in the ratio 1.65/1.23 μm or 1.65/0.83 μm correlated well with forest damage. Change detection analysis of high-elevation coniferous forests in August 1973 and 1984 MSS data from the Green Mountains of Vermont suggested that major reflectance decreases for the near-infrared bands were related to the change in canopy conditions (defoliation) associated with the forest decline process (Vogelmann, 1988). Color density slices of 750 nm and 950 nm band difference images were used to map the change. Ratios using Landsat (TM) bands TM 5/4

(1.65/0.83 μm) and TM 7/4 (2.22/0.83 μm) data of spruce/fir forest in the Green Mountains of Vermont and the White Mountains of New Hampshire correlated well with ground-based measurements of forest damage (Vogelmann and Rock, 1988). It is also important to note that NDVI did not prove useful in detecting spruce defoliation (Vogelmann and Rock, 1988). Both 1.65/0.83 μm and 2.22/0.83 μm band ratios quantified damage levels among individual mountains. Images displayed using the Landsat TM 5/4 (1.65/0.83 μm) ratio, the 1.65 μm band, and the 0.66 μm band were found to clearly distinguish between high and low damage areas to hardwood forests in southern Vermont and northwestern Massachusetts caused by pear thrips (Vogelmann and Rock, 1989).

Classification schemes using Landsat TM data detected three levels of canopy damage to Norway spruce stands in the Czech Republic (Lambert et al., 1995). TM1 (450 - 520 nm), TM2 (520 - 600 nm), TM3 (630 - 690 nm), and TM7 (2.08 - 2.35 μm) data were used to discriminate canopy damage in three categories (light, 5-25% defoliation; moderate, 25-50%; and heavy, > 50%). TM1 and TM2 discriminated moderate from light damage with 75-76% accuracy, TM3 discriminated moderate from heavy with 88% accuracy, and TM7 differentiated light from heavy with 87% accuracy (Lambert et al., 1995). Detection of more than three classes of damage to forest canopies using Landsat TM data may be limited by its inability to measure fine red edge features. TM's spectral resolution (band widths of approximately 100 nm) may contribute to these limitations.

Hyperspectral airborne platforms allow measurements of the red edge region with increased spectral resolution. An early attempt was made to acquire high quality imagery to detect changes in the vegetation red edge using Multispectral Electro-Optical Imaging

System/Scanner II (MEIS II), a 5-channel pushbroom imager (Hare et al., 1984). A methodology to analyze changes in red edge properties from 5-channel airborne multispectral imagery was introduced in which an analytical expression, Inverted-Gaussian Model (IG), represents vegetation reflectance in the region of the red edge. This made it possible for changes in red edge position and reflectance shoulder excursion to be detected (Hare et al., 1984; Miller et al., 1985; Rock et al., 1988). The IG model provides a quantitative representation of the vegetation red edge reflectance curve using four physically significant independent parameters (Miller et al., 1990). It provides an algorithm for airborne data acquired by the MEIS II (Miller et al., 1985; Rencz et al., 1986; Miller et al., 1988a) and by the airborne high-resolution imaging spectrometer, Fluorescence Line Imager (FLI) (Miller et al., 1988b; Rock et al., 1988), over sites of geobiotanical interest and forest decline. The FLI was used to detect the blue shift at the chlorophyll absorption maximum (chlorophyll well) for high-damage study sites in Vermont in 1985 (Rock et al., 1988). Measurement of fine red edge parameters and detection of blue shift with the hyperspectral (288 contiguous bands), high spectral-resolution (2.6 nm bandwidths), and high spatial-resolution (8 m to 10 m pixels) imaging spectrometer FLI are of considerable value in monitoring forest condition and state of health (Rock et al., 1988; Rock et al., 1991). A potential drawback to the IG model is that raw data from the red edge region is resampled in the process of being "fit" to a curve based on only 4 key parameters. Depending on the spectral resolution of the sensor, there could be as many as 50 bands of new data available in the red region. The IG method reduces the data into what are believed to be its key elements, but in the process some information is lost.

Field spectrometer data are also used for vegetation studies. Spectral reflectance measurements made using the VIRIS of sugar maple leaves variously affected by insects indicated consistent and diagnostic differences in the red edge region (680-750 nm) of the spectrum. The red edge inflection point (REIP), located at the wavelength at which the slope of the spectral signature is steepest in the red edge region, was used as an indicator of vegetation health (Moss and Rock, 1991; Vogelmann et al., 1993). In addition to REIP, two ratios provided diagnostic information: the ratio of reflectance at 740-720 nm (RE3/RE2) and the ratio of the first derivative values at 715-705 nm (D715/D705) (Vogelmann et al., 1993).

Using Medium Resolution Imaging Spectrometer (MERIS) for crop growth studies in The Netherlands, Clevers et al. (1999) developed a simplified method for deriving a red edge index that quantifies the red edge position - defined as the inflection point (or maximum slope) of the red/infrared slope. The reflectance spectra for MERIS bands located at 665, 705, 754, and 775 nm are used to approximate the slope of the red edge curve. The reflectance value at the midpoint of the line defined by the reflectance values of the four MERIS bands is used to approximate the reflectance value at the inflection point. The determination of the wavelength position of the inflection point – the red edge index – is described in the following way:

1. The reflectance at the inflection point (R_{re}):
$$R_{re} = (R_{665} + R_{775})/2 \quad (1)$$
2. The red edge wavelength (λ_{re}):
$$\lambda_{re} = 705 + 49 * ((R_{re} - R_{705})/(R_{754} - R_{705})) \quad (2)$$

R_{665}, R_{705}, R_{754}, R_{775} equal the reflectance values at 665, 705, 754, and 775 nm wavelength (λ), respectively. The constants 705 and 49 result from interpolation in the 705 – 754 nm interval.

It was determined that the "linear method" was more robust than the maximum second derivative method (red edge inflection point) for determining the red edge index.

Since the early findings of Horler et al. (1980, 1983) revealed the strong correlation between red edge features and chlorophyll content, remote sensing investigations have continued to seek the best method to utilize and quantify red edge features in order to assess vegetative health. In this study, levels of ice storm damage to hardwood canopies are detected using a normalized reflectance value at 714 nm (714nr) to represent blue shifts (Rock et al., 1988; Burnett 1999, 2001). The fine-feature red edge information provided by hyperspectral ASAS imagery is used to represent the blue shift. The effectiveness of this method is compared to traditional broadband measurements applying TM 5/4, NDVI, and VI to single scenes and in change detection studies.

Multiangle Viewing

In January 1997, the Workshop on Multiangular Remote Sensing for Environmental applications was held at the University of Maryland Conference Center to review research to date and to establish priorities for the future. It was concluded that the Earth's surface is non-Lambertian (solar radiance is not equally distributed by the Earth's surface). Terrestrial ecosystems are anisotropic, scattering solar radiance unevenly back into the atmosphere. The intensity and wavelength in which different land covers, and at lesser scales different vegetation types, reflect solar radiance from various solar azimuth and solar zenith angles is measured as the bidirectional reflectance distribution function (BRDF). Bidirectional reflectance measurements acquired with ASAS are used to study surface albedo, create scattering models, derive vegetation indices, and to create

algorithms for retrieving biophysical surface parameters (GSFC, 1998). Although BRDF is a concern to nadir-viewing sensors, it is particularly problematic to multiangle sensors. Future objectives seek to understand the radiative processes governing remote sensing and to quantify these processes. With the successful deployment of Terra by NASA in 1999 as the first phase of its Earth Observing System (EOS) satellite series and with the deployment of other satellites with multi-directional viewing capability, the natural resources remote sensing community is developing better methods to understand, interpret, and apply multiple viewing angle data.

Multiple view angle (MVA) sensors have been applied to forest canopy studies with three general objectives: to differentiate land cover types, to identify stand structures, and to take advantage of the *hotspot* phenomenon. MVA sensors were used to create land cover classification schemes (DeFries and Townsend, 1994). Nadir and off-nadir multispectral imagery revealed spectrally unique signatures for native and unmanaged grasses when compared to four other grass types (Dunham and Price, 1996). Classification of ASAS multiangle and multispectral measurements using artificial neural networks revealed that MVA data was effective in discriminating land cover types with 88% accuracy (Abuelgasim, et al. 1996). ASAS MVA data from the BOREAS project in Prince Albert, Saskatchewan and Thompson, Manitoba, Canada revealed that distinctions between three forest types (old aspen, old black spruce, and old jack pine) are best revealed in the visible red wavelength at the +26 degrees (backscatter) viewing angle. Reflectance in the red region was found to be view dependent, and angular effects on NDVI were high (Russell et al., 1993). Further study of the discriminating abilities of

using BRDF with MVA sensors shows that they improve traditional land cover algorithms to beyond 90% accuracy (Leroy et al., 1997).

Stand structure and BRDF are closely associated. Variations in structural geometry create differing scattering and shadowing effects, as solar radiance is absorbed and diffused by leaf and crown morphology. A hyperspectral bidirectional reflectance dataset of lawn grass and watercress canopies examined to demonstrate basic physical reflectance mechanisms of erectophile (grass- or needle-like) and planophile (broadleaf) canopy structures revealed that a strong influence of reflectance intensity on observed reflectance anisotropy is apparent for both canopies. Scattering effects within the canopies, as a function of canopy spectral absorption, explain this relationship (Sandimeier et al., 1998). The *hotspot* phenomenon has received much attention in the study of BRDF. The *hotspot* is the backscatter-viewing angle along the principle plane (sun directly behind the sensor) where at-sensor spectral reflectance is most intense. At this viewing angle shadowing is virtually eliminated and reflected solar radiance is greatest. The parallel or principle plane flight line (toward or away from the solar azimuth) was found to be optimal for NDVI sensitivity using AVHRR bands 1 (580 nm - 680 nm) and band 2 (730 nm - 1100 nm) when compared to the perpendicular plane (Kimes et al., 1984). The highest observed reflectance factors were recorded in the solar principle plane at the *hotspot* with viewing geometry approaching the antisolar direction (Ranson et al., 1994). A view-angle brightness gradient was revealed in AVIRIS forest canopy data that varied with wavelength consistent with BRDF predictions. The view-angle effect was associated with surface (canopy) structure and the inherent brightness of

the pixel (Kennedy et al., 1997). Multiangle, hyperspectral, and other new remote sensing technologies must overcome the complex challenges that BRDF studies have identified.

Change Detection Methods Applied to Satellite Imagery

Earth-orbiting satellites are well suited to change detection studies. Landsat Multispectral Scanner System (MSS) and Thematic Mapper (TM) platforms have collected spectral reflectance data in broad bands since the launch of Landsat 1 on July 23, 1972. For the last 30 years Landsat satellites have scanned the entire Earth's surface on a 16-day repeat cycle (Landsat 1- 3 on an 18-day repeat cycle). This unique archive of spectral data provides consistent coverage at short temporal intervals, and these are important ingredients for effective change detection studies.

Effective change detection also requires that changes in the phenomenon of interest (forest canopy condition) must be large enough to overcome detectable changes in radiance, emittance, or microwave backscatter values caused by other factors (Ingram et al., 1981; Singh, 1989; Oliver and Quegan, 1998). Images sensed at different times are exposed to various atmospheric conditions, solar radiance angles, conditions of soil (moisture levels), and seasonal vegetation phenology changes. These differences can be mitigated if scene changes are observed during the same time of the year and under similar atmospheric conditions.

The introduction of error is implicit in the image registration process. Two images must be force-fit during the rectification process, which involves warping and resampling the unregistered image onto a coordinate system. This procedure requires the collection of ground control points (GCPs) using a global positioning system (GPS) instrument.

Errors in field data collection of GCPs are magnified by the warping and resampling procedure. Most change detection studies are critically dependent on the accuracy of geometric registration of the two images (Townshend et al., 1992).

Ultimately, every change-detection methodology must determine what measure of difference (threshold) defines a true change in the spectral response of the same location in two separate images sensed at different times. Although much attention has been given to the accuracy of change detection methods (Congalton et al., 1983; Coppin and Bauer, 1994), the threshold decisions made by the end user can affect the accuracy of an investigation (Smits and Annoni, 2000) and should be made *a priori* of change detections results (Schowengerdt, 1983). The quality of the change detection methodology depends upon the quality of the image interpretation (Smits et al., 1999). The three major issues in this regard are the objectives and requirements of the change detection application, the methods to evaluate the results, and the change detection algorithms as such (Smits and Annoni, 2000).

Univeriate image differencing, or pixel-by-pixel subtraction, is the simplest and most widely used change detection method (Singh, 1984). The critical step is deciding where to place the threshold boundaries between change and no-change pixels plotted in a histogram. Threshold determination can be made on the basis of standard deviation in the *change* and no-change distributions (Stauffer and McKinney, 1978; Nelson, 1983; Singh, 1984) or by *t* test in comparing differencing of averaged images (Ingram et al., 1981). In this study pre- and post-event Landsat TM scenes are used for a change detection analysis of ice storm damage to forestland in the WMNF by applying the

univeriate image differencing or pixel-by-pixel subtraction method. Threshold decisions for this study were made through the supervised classification mapping process.

Accuracy Assessment and Fuzzy Rules

In order to evaluate the accuracy of ice damage classification maps, the overall,. user's, and producer's error are determined using the error matrix method (Congalton et al., 1983). The ground sites not used as training sites in the supervised classification method are used as reference data in the accuracy assessment. Each pixel within the forested area of the scene is classified into one of the ice damage classes of the classification scheme or is designated as unclassified and colored black on the map. These results are compared to the reference data sites, which are categorized by percent damage measurements of field data and represent the actual or true classification. The majority or mode of the pixels within a reference site must be categorized correctly for the individual reference site to represent an accurate classification. Unclassified pixels (black) are not counted in the accuracy assessment process.

Dividing the total number of correctly categorized sample units in all classes (along the error matrix diagonal) by the total number of reference data sites determines the overall accuracy of the classification map. The producer's accuracy is calculated by dividing the number of correctly classified sites in each classification category by the total number of reference sites in that category. Producer's errors are error of omission or exclusion: omitting a site from its proper category. The user's accuracy is derived by dividing the number of correctly classified sites in each classification category by the total number of sites classified in that category. User's errors are errors of commission or

inclusion: including a site in a category to which it does not belong. (Story and Congalton, 1986)

For this study all accuracy assessment results were evaluated. Fuzzy logic (Zadeh, 1965), using sliding class widths, will be applied to error matrix procedures if assessment results are marginally unacceptable, for example when an overall accuracy assessment of 40% is achieved (Gopal and Woodcock, 1994; Congalton and Green, 1999). Sliding class widths extend the boundary of correct categorization to include a fuzzy zone of, for example, 5% overlap into the range of categories on either side it in the error matrix. As applied to ice storm damage, the definition of the range of moderately damaged sites will be extended from a range of 25-49.9% canopy damage to a range of 20-54.9%. Similarly, lightly damaged sites will be extended from a range of 0-24.9% to a range of 5-29.9% and severely damaged sites from 50-100% to 45-100%. In effect, a reference site with 26% damage will be accurately categorized as lightly or moderately damaged.

CHAPTER II

ASAS HYPERSPECTRAL RED EDGE MEASUREMENTS

Introduction

During the summer following the January 1998 ice storm, ASAS datasets of 9 target areas in the WMNF were recorded for the purpose of detecting levels of ice damage to forest canopies. In this study the hyperspectral capability of ASAS is used to distinguish between the spectral fine-features of the red edge for quantifying differing levels of damaged forest canopies. The findings of Horler et al. (1980, 1983) showed that the position of the red-edge curve is directly correlated with leaf chlorophyll content and by extension, levels of green biomass. A shift in the wavelength position of the red edge curve in the direction of the blue region of the spectrum - the blue shift - is seen as an indication of reduced green biomass, one of the symptoms of ice storm damage to the forest canopy (Rock et al., 1988; Moss and Rock, 1991; Vogelmann et al., 1993). For this study, the blue shift was represented by measuring the reflectance value for normalized red edge (653 to 775 nm) values at ASAS 714 nm (714nr). The average value for *in situ* measurements of percent ice damage for study sites and the average 714nr for corresponding sites sensed remotely are used to map three levels of ice damage. For this study undamaged and lightly damaged sites are combined and referred to as the Light class, the other 2 classes are called Moderate and Severe.

The following hypotheses are tested:

2-1. Values of 714nr for nadir hyperspectral ASAS imagery of variously ice damaged hardwood sites (7.5 x 7.5 m sites, N = 210) can differentiate 3 levels of damage.

2-2. Values of 714nr for nadir hyperspectral ASAS imagery of variously ice damaged hardwood sites (7.5 x 7.5 m sites, N = 210) can be classified with greater than 80% overall accuracy.

The Advanced Solid-State Array Spectroradiometer (ASAS)

The airborne ASAS sensor has three features of potential use in improving the precision and accuracy of assessing hardwood canopy damage, such as that caused by ice storms. The ASAS sensor provides 1) hyperspatial (2.5- 4.5 m pixels) capabilities, 2) hyperspectral (62 contiguous narrow bands) capabilities, and 3) multiangle viewing capabilities. These features provide ASAS with the potential to detect and quantify spectral fine-features in reflectance data related to variations in canopy morphology (percent canopy damage to individual trees) and leaf condition (chlorophyll content) related to ice storm damage.

In this study the ability of nadir-viewing hyperspectral information to assess ice storm damage to hardwood forest canopies is investigated. Digital imagery is applied to a practical forestry problem – assessing levels of ice storm damage to hardwood forest canopies. Ice damage forms canopy gaps. Gaps expose materials other than the green leafy canopy layer, such as branches, stems, wood tissue, dead woody debris, groundcover, leaf litter, bare soil, and rocks. Vegetation indices are used to detect differences in green biomass amount in order to differentiate between non-vegetative

materials, containing less green biomass, from healthy canopy leaves. Hyperspectral ASAS imagery was used to detect and quantify spectral fine-features in reflectance data related to variations in canopy morphology (percent canopy damage to individual trees) and leaf condition (chlorophyll content) related to ice storm damage.

Materials and Methods

Study Area

Nine target areas (1 km x 1 km) were selected in the White Mountain National Forest (WMNF) of New Hampshire, representing various levels of damage to hardwood forest canopies resulting from the ice storm of January 1998 (Figure 2-1). The target areas are listed with level of ice damage in Table 2-1, below.

Table 2-1. Nine Target Areas in the WMNF with general/approximate level of damage, aspect, slope, elevation, and forest type.

SITE	DAMAGE	ASPECT	SLOPE	ELEV	FOR. TYPE
Hubbard Brook	Light	NE	15%	600m	Hardwood
Hubbard Brook	Moderate	NE	26%	810m	Hardwood
Hubbard Brook	Severe	NE	44%	695m	Hardwood
Bartlett	Light	NE	19%	319m	Hardwood
Bartlett	Severe	NW	18%	600m	Hardwood
Jefferson Notch	Moderate	SE	16%	573m	Hardwood
Killkenny	Light/Mod	NE	8%	540m	Hardwood
Black Mountain	Moderate	SW	20%	777m	Softwood
Pine Mountain	Severe	W	27%	606m	Hardwood

Hardwood stands at elevations from 550-1200 meters were most susceptible to damage. Areas dominated by hardwoods (> 60%) were selected for study. (Because field sampling revealed the hardwood composition at Black Mountain to be 31%, and the Killkenny ASAS scene missed the targeted area, these sites were not included in the

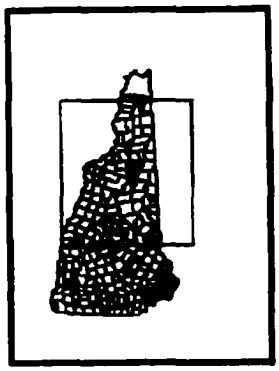

Figure 2-1
9 ASAS Target Areas
White Mt. National Forest
New Hampshire

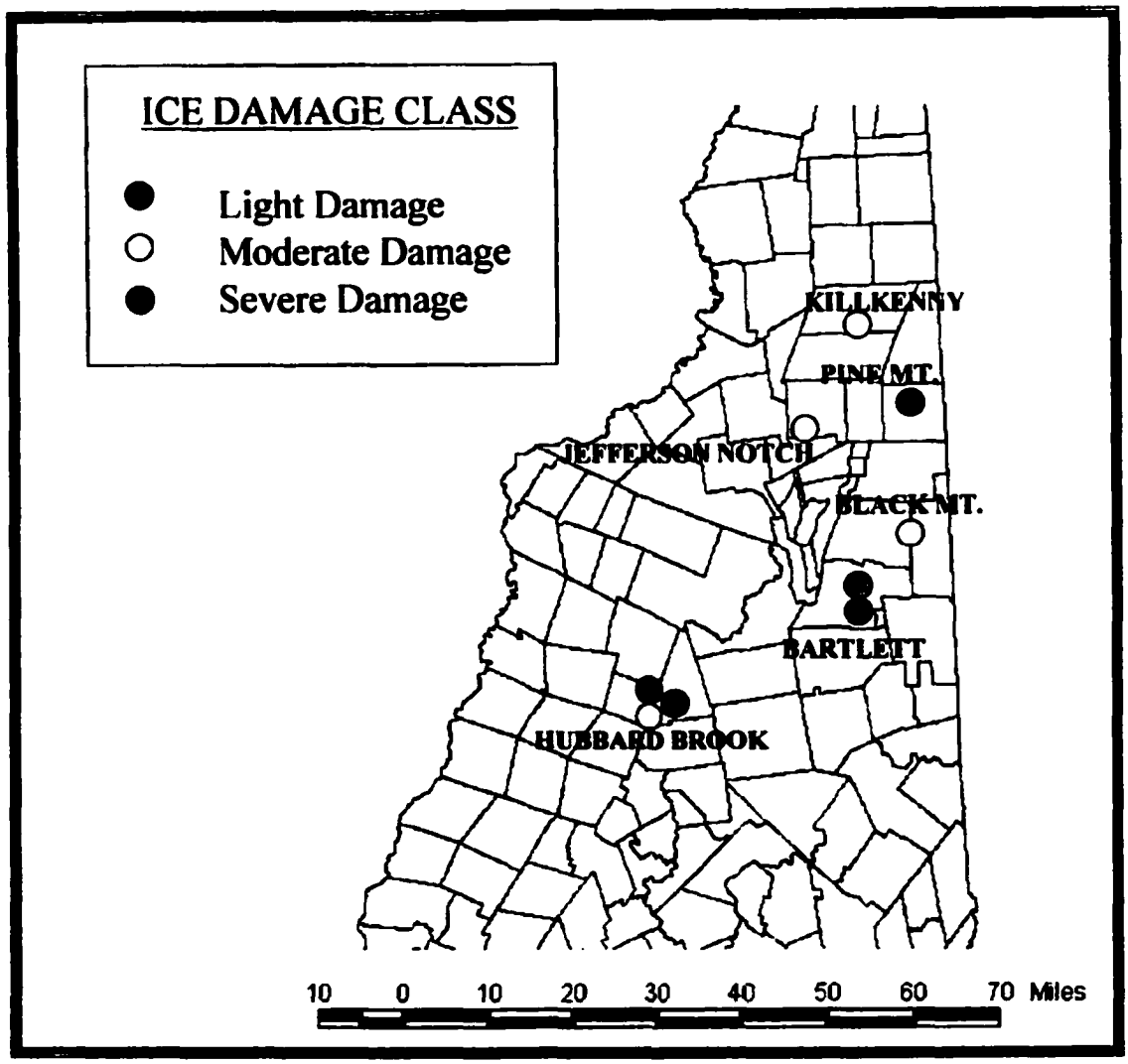

ASAS study.) USFS sketch maps of ice damage from the January 1998 storm were used to locate potential study areas. Site visits were made to confirm the general level of damage at each potential target area. The dominant hardwood (deciduous) species at the selected target areas included: red maple (*Acer rubrum*), paper birch (*Betula papyrifera*), sugar maple (*Acer saccharum*), beech (*Fagus grandifolia*), white ash (*Fraxinus Americana*), yellow birch (*Betula alleghaniensis*), and red oak (*Quercus rubra*).

Field Methods

Field data was collected for 288 sites from within the nine target areas. The area of each site is approximately 400 m^2 (experimental unit = 11.3-meter radius circle). Stratified random selection was used to determine sampling locations within designated target areas representing general categories of damage. All sites contained greater than 60% hardwood trees in the dominant or co-dominant crown position. For each target area, 24-48 sites were sampled. GPS points were recorded and differentially corrected for each sample site (+/- 2 m precision).

Three levels of ice storm damage were defined:

1. Light Damage: 0-24.9% damage
2. Moderate Damage: 25-49.9% damage
3. Severe Damage: 50-100% damage

Canopy trees were measured within an 11.3 m radius of the center of each plot. Trees within the circle plot were identified individually by species and measured for diameter at breast height (DBH) to the nearest 2" increment with a Biltmore stick and for percent ice storm damage to crown (0%, 25%, 50%, 75%, or 100%). Damage symptoms

were classified into four categories: stem or branches broken off, stem bent to approximately 45°, stem bent to approximately 60° or more, stem uprooted (Ciesla, 1998). Trained field-crew members classified the amount (percent of crown) and type of damage to each tree. In the case of bent stems, damage amount was based on a determination of the percent of the tree crown that would not likely recover from damage caused by the storm. Damage caused by the ice storm 6 months earlier was distinguishable from damage caused by other sources by the relatively unweathered, flesh color of the exposed wood tissue where breakage had occurred.

The average percent ice damage to the crowns of dominant and co-dominant trees in the canopy was calculated for each sample plot. The sizes of tree crowns varied and each represented a different fraction of the canopy for the plot. In order to account for variability in crown size within a plot, the fraction of the plot canopy that an individual crown represented was calculated based on the fraction of the total basal area (calculated from DBH measurements) for the plot contained in each tree. It was assumed that the fraction of the total basal area represented by one tree for a given plot approximated the fraction of the plot canopy area represented by its crown. Plot-level damage is calculated as a weighted mean based on the basal area and damage level for each tree within the plot (Table 2-2).

Table 2-2. Calculation of Average Percent Damage for a Sample Plot
BA = basal area, %DMG = percent damage

TREE	BA (FT^2)	%DMG	BA DMG (FT^2)
1.	1.0	50%	0.500
2.	0.5	25%	0.125
3.	0.5	25%	0.125
4.	0.5	25%	0.125
5.	0.5	25%	0.125
6.	0.5	25%	0.125
7.	0.5	25%	0.125
8.	0.5	25%	0.125
9.	0.5	25%	0.125
10.	0.5	25%	0.125
11.	0.5	25%	0.125
12.	0.5	25%	0.125
13.	0.5	25%	0.125
14.	0.5	25%	0.125
15.	0.5	25%	0.125
16.	0.5	25%	0.125
17.	0.5	25%	0.125
18.	0.5	25%	0.125
19.	0.5	25%	0.125
	10.0		2.750

2.750/10 = 0.275 or 27.5% damage

In addition to canopy damage measurements, data were collected for the following site characteristics: percent slope, aspect, forest type, canopy height, canopy cover type, canopy gap, midstory composition, and ground cover type.

Airborne Data Acquisition

A C-130 aircraft was flown by NASA at 10,000 feet over the study areas on July 14 and 15, 1998. Mounted on the underside of the plane, the ASAS sensor measured solar radiance reflected from the Earth's surface in pushbroom fashion. Spectral radiance data was recorded and converted to digital numbers (DNs) in 62 bands, 10 nanometers (nm) in

width, covering a spectral range from 400 nm to 1020 nm on the electromagnetic spectrum. The spatial resolution of the sensor varies with the altitude of the aircraft. At approximately 3,000 m, pixels are 2.5 x 2.5 m in size from the nadir view angle. One ASAS image, sensed at 3,000 m, represents a ground area of approximately 1 square kilometer (Irons et al., 1991; Russell et al., 1993; GSFC, 1998). Sunphotometer data were collected on the ground during overflights at two target area locations (Bartlett Experimental Forest and Hubbard Brook Experimental Forest). Microtops II sunphotometer data were collected at one-minute intervals while the aircraft was overhead and at least every 15 minutes during the entire overflight. Total atmospheric aerosol and water vapor measurements were recorded with each reading. The data were downloaded into a laptop computer and imported into Microsoft Excel format for entry into the atmospheric correction model, part of the digital imagery pre-processing routine (GSFC, 1998).

Table 2-3 lists times, aerosol optical thickness at 550 nm for ASAS data acquisition at the 9 target areas on July 14-15, 2002.

Table 2-3. ASAS Data Acquisition Information: Target name, data acquisition start and end time (GMT), aerosol optical thickness (AOT) at 550 nm, sunphotometer location (LOC), solar zenith angle (SZ), and solar azimuth (SA). (All data acquired on July 14, 2002 except Hubbard Brook Severe – July 15, 2002.)

TARGET	START	END	AOT	LOC	SZ	SA
Bartlett Severe	13:54:50	14:05:00	0.12	Bartlett	34.8°	240.4°
Bartlett Light	14:03:00	14:24:50	0.11	Bartlett	37.2°	244.7°
Hubbard Brook Mod	14:32:30	14:44:30	0.18	Hubbard	40.5°	250.0°
Hubbard Brook Light	14:47:40	14:57:20	0.12	Hubbard	43.0°	253.6°
Jeff Notch Moderate	15:10:30	15:34:00	0.17	Bartlett	48.3°	259.6°
Killkenny Light/Mod	15:39:30	15:48:00	0.19	Bartlett	52.6°	264.2°
Pine Mt. Severe	16:08:45	16:18:50	0.30	Bartlett	57.6°	269.4°
Black Mt. Moderate	16:24:30	16:33:20	0.25	Bartlett	60.9°	272.7°
Hubbard Brook Severe	15:00:00	15:30:00	0.29	Bartlett	47.1°	258.4°

Image Processing of ASAS Data

Raw datasets were pre-processed at Goddard Space Flight Center (GSFC). Instrument slew and non-coverage data were eliminated. Radiometric calibration gains were derived in the laboratory from integrating hemisphere lamp data and applied to each pixel. Pixel values were derived by applying the appropriate radiometric resolution factor, one for each band. Values represent at-sensor radiance (units = watts per square meter per steradian ($Wm^{-2}sr^{-1}nm$)). After the above pre-processing steps were completed by GSFC, the Second Simulation of the Satellite Signal in the Solar Spectrum (6S) radiative transfer/atmospheric correction model was applied to datasets to convert at-sensor radiance values to surface reflectance values on a scale of 0-1000 (Vermote et al., 1997). The model minimizes procedure iterations by subsetting pixels with similar view angles into small clusters and applying one correction algorithm to each cluster. Solar azimuth, solar zenith, and atmospheric path length are factored into each algorithm, a look-up-table (LUT) is created, and the appropriate correction factor is applied to each pixel cluster (GSFC, 1998).

Digital Orthographic Quads (DOQs) of the WMNF area were used to georeference nadir images. The DOQs, derived from a series of aerial photographs flown by the USDA Forest Service in May 1992, provided the necessary spatial precision for this purpose (1 x 1 m pixels). The accuracy of the DOQs was tested by matching GPS points of landmarks in the area of study sites to their corresponding landmarks in the imagery. The DOQs were determined to be accurate within approximately 5 m. Ground control points (GCPs) were selected manually and a first order polynomial transformation using nearest neighbor resampling was performed. The WMNF consists of rugged

terrain, but the slope and aspect ($\sigma < 17\%$ and $\sigma < 50^{\circ}$ respectively) were relatively consistent for any target area and it was assumed, therefore, that these factors did not significantly affect the spectral signatures within a given study site. A vector coverage of GPS points for each field site was overlaid on the rectified nadir images to locate field sites in the imagery.

Representation of Blue Shift – 714nr

For this study, the blue shift was quantified as the average normalized reflectance value for study sites at ASAS band 714 nm (714nr). Figure 2-2 shows a leftward shift in the position of the red edge curve in the direction of the blue region of the spectrum (blue shift) for successively more damaged sites. The blue shift is represented by the reflectance value at ASAS band 714 nm. The procedure normalizes atmospherically corrected ASAS reflectance values on a floating-point scale based on percent change within the range of values from 653 nm, the red chlorophyll absorption feature, to 775 nm, the infrared shoulder, on a pixel-by-pixel basis. The minimum value (ASAS band 653 nm) is subtracted from the digital value at each band and the difference is divided by the range (max – min) to obtain the normalized value. For example, the normalized reflectance values for the Hubbard Brook undamaged (HB-U) site were derived by finding the range of the red edge data for HB-U, i.e. 18 @ 653 nm to 337 @ 775 nm = 319 and dividing the difference between the ASAS reflectance value at each red edge band and the range minimum, 18, by the range, 319. For the normalization of the HB-U dataset, the reflectance value range (319) and minimum reflectance value (18) are

constant (Rock et al., 1988). The calculations of the normalized value for each of the 13 bands are demonstrated in Table 2-4.

Figure 2-2. 714nr - Blue Shift Representation

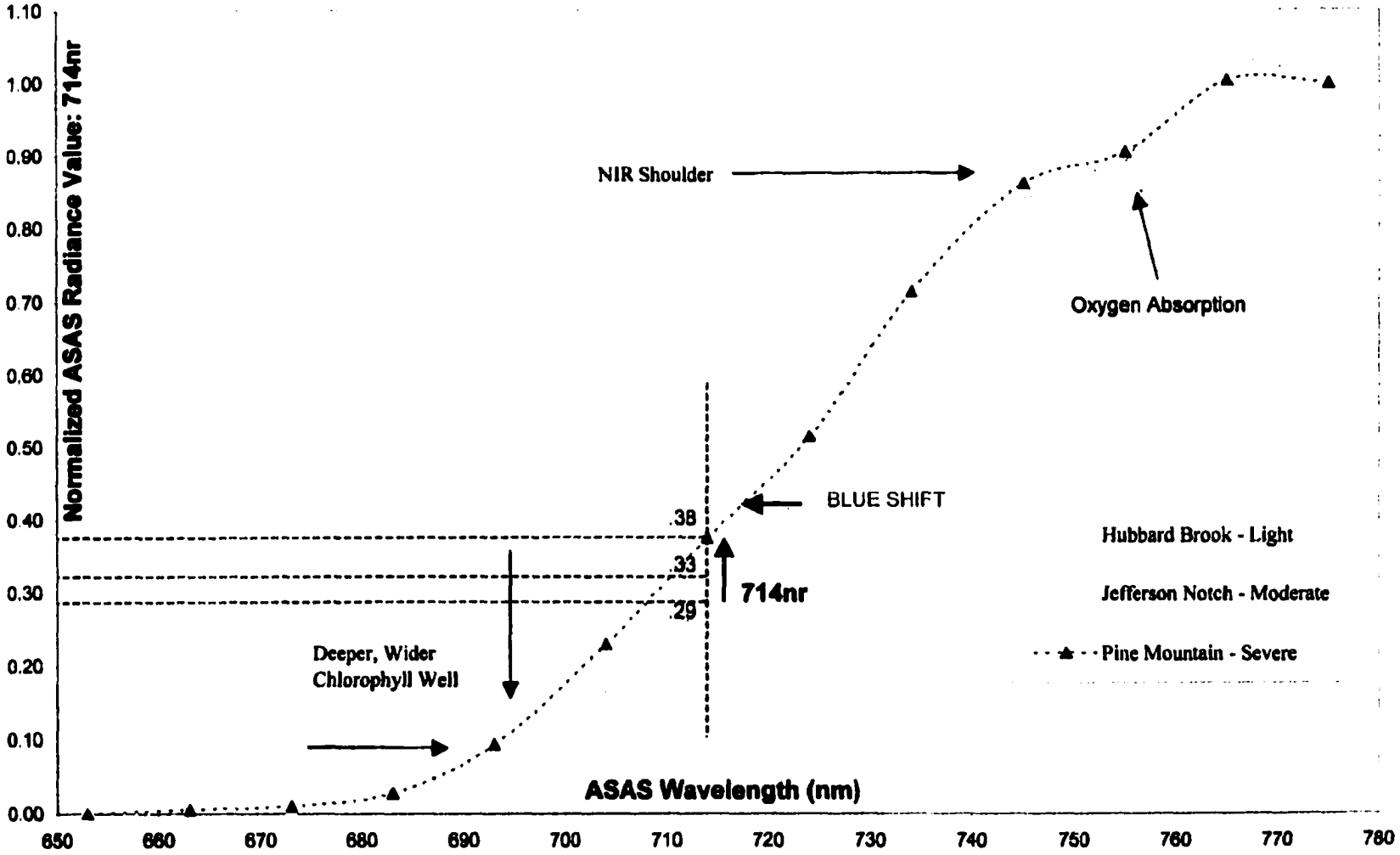

Table 2-4. Blue Shift Representation Example

Band 653 nm = reflectance value (18) - minimum value (18) / range (319) = 0
Band 663 nm = 18.7 – 18 / 319 = 0.002
Band 673 nm = 19.4 – 18 / 319 = 0.004
Band 683 nm = 23.0 – 18 / 319 = 0.157
Band 693 nm = 36.5 – 18 / 319 = 0.580
Band 704 nm = 68.6 – 18 / 319 = 0.159
Band 714 nm = 110.7 – 18 / 319 = 0.291 (.29 in Figure 2-2)
Band 724 nm = 162.3 – 18 / 319 = 0.452
Band 734 nm = 230.6 – 18 / 319 = 0.666
Band 745 nm = 284.9 – 18 / 319 = 0.837
Band 755 nm = 305.1 – 18 / 319 = 0.900
Band 765 nm = 345.5 – 18 / 319 = 1.027
Band 775 nm = 337.3 – 18 / 319 = 1.000

When red edge digital values from image datasets are normalized, on a pixel-by-pixel basis, as described above, the slope and wavelength position of the red edge curve, relative to curves of other pixels from within one image and relative to datasets from other images, are preserved. Due to the qualitatively invariant nature of these features, a shift in the wavelength position or change in slope of the red edge curve for one site in relation to another is a strong indication of a change in canopy condition, thus affecting chlorophyll content, as reported by Horler et al. (1980, 1983). As described above, the blue shift of the red edge represents a relative value for chlorophyll content and, by extension, green biomass. Increasing reflectance values at 714 nm correspond with shifts in the red edge curve toward the blue portion of the spectrum. It was hypothesized that increasing 714nr values for sites would correspond with increasing levels of canopy damage and, therefore, that a strong correlation between 714nr and percent damage from *in situ* measurements could be established.

ASAS Study Site Size and Sample Size

In situ measurements of percent canopy damage were collected from 288 study sites 400 m^2 in size from the 9 target areas (Table 2-1). Of the 288 sites, 210 met the qualification of having canopies consisting of at least 60% hardwood species and fell within the ASAS flight line coverage areas. It is important that sites are located accurately in the ASAS imagery so that the spectral signatures used represent the proper location. As mentioned above, GPS points were recorded at the center of each site *in situ* and differentially corrected to within 2 m accuracy and ASAS imagery was registered using DOQs to within 5 m accuracy. Study sites needed to be both large enough on the ground to contain a sufficient number of 2.5 x 2.5 m pixels in the imagery to spectrally characterize 3 levels of damage and small enough to have at least 50% of their ground area represented in a pixel kernel in the image. The effectiveness of 10 study site sizes ranging from approximately 7.5 x 7.5 m to 750 x 750 m on the ground and 3 x 3 to 300 x 300 pixels in the imagery was tested. ANOVA and the Tukey tests were used to determine the ability of 714nr values for the various site sizes to differentiate between 3 levels of damage – Light, Moderate, and Severe.

Effects of Ice Damage, Aspect, Slope, and Elevation on 714nr

In addition to *in situ* measurements of percent ice damage to hardwood canopies, field data were recorded for other study site characteristics that may affect 714nr values – aspect, slope, and elevation. These data were summarized in charts in order to show the relationship between levels of ice damage and these characteristics. Aspect, slope, and elevation demonstrated at least a moderate correlation to levels of ice damage. In order to

determine if any significant interaction existed among these factors affecting 714nr a multi-way ANOVA was performed.

In this test, the dependent variable was 714nr value (continuous data) and the independent variables were damage, aspect, slope, and elevation (categorical data). Three levels of damage were determined (Light, Moderate, Severe), 4 levels of aspect (North, East, South, West), 2 levels of slope (Gentle, Steep), and 2 levels of elevation (Low, High). The parameters of the treatment levels of these factors are listed in Table 2-5.

Table 2-5. Levels for Independent Variables in Multi-Way ANOVA of 714nr

FACTOR	LEVEL 1	LEVEL 2	LEVEL 3	LEVEL 4
Damage	Light	Moderate	Severe	
	0-24.9%	25-49.9%	50-100%	
Aspect	North	East	South	West
	315-44°	45-134°	135-224°	225-314°
Slope	Gentle	Steep		
	< 20%	> 20%		
Elevation	Low	High		
	< 580 m	>580 m		

Results

Field Study Site Characteristics Summarized

In situ field data were summarized and plotted to demonstrate how site characteristics may be associated with canopy damage caused by the ice storm. Figure 2-3 shows the canopy, midstory, and ground cover photographs of variously damaged sites. Site characteristics included, aspect, slope, and elevation. Sites with south and west aspects had higher average levels of ice storm damage than north and east (Figure 2-4). Average damage tended to increase with slope class (Figure 2-5). Ice damage was most severe between 600-750 m (Figure 2-6).

Figure 2-3. Ice Storm Damage Study Sites, White Mountain National Forest

Bartlett – Severe, July 1998

Bartlett – Light, July 1998

Jefferson Notch – Moderate, July 1998

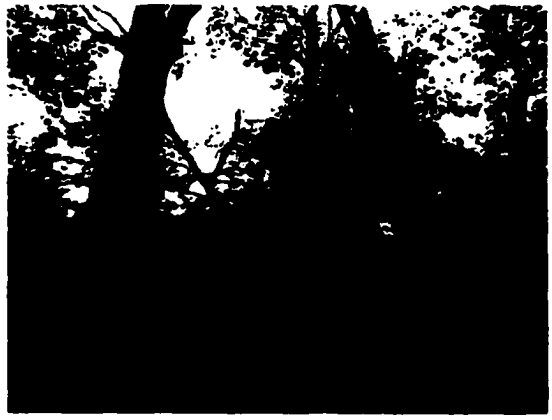

Hubbard Brook – Moderate, July 1998

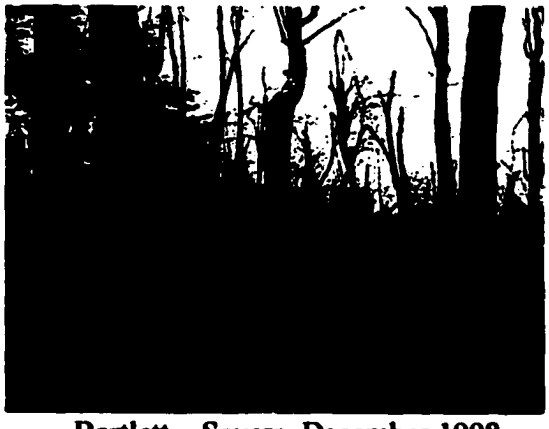

Bartlett – Severe, December 1998

Bartlett – Severe, July 1998

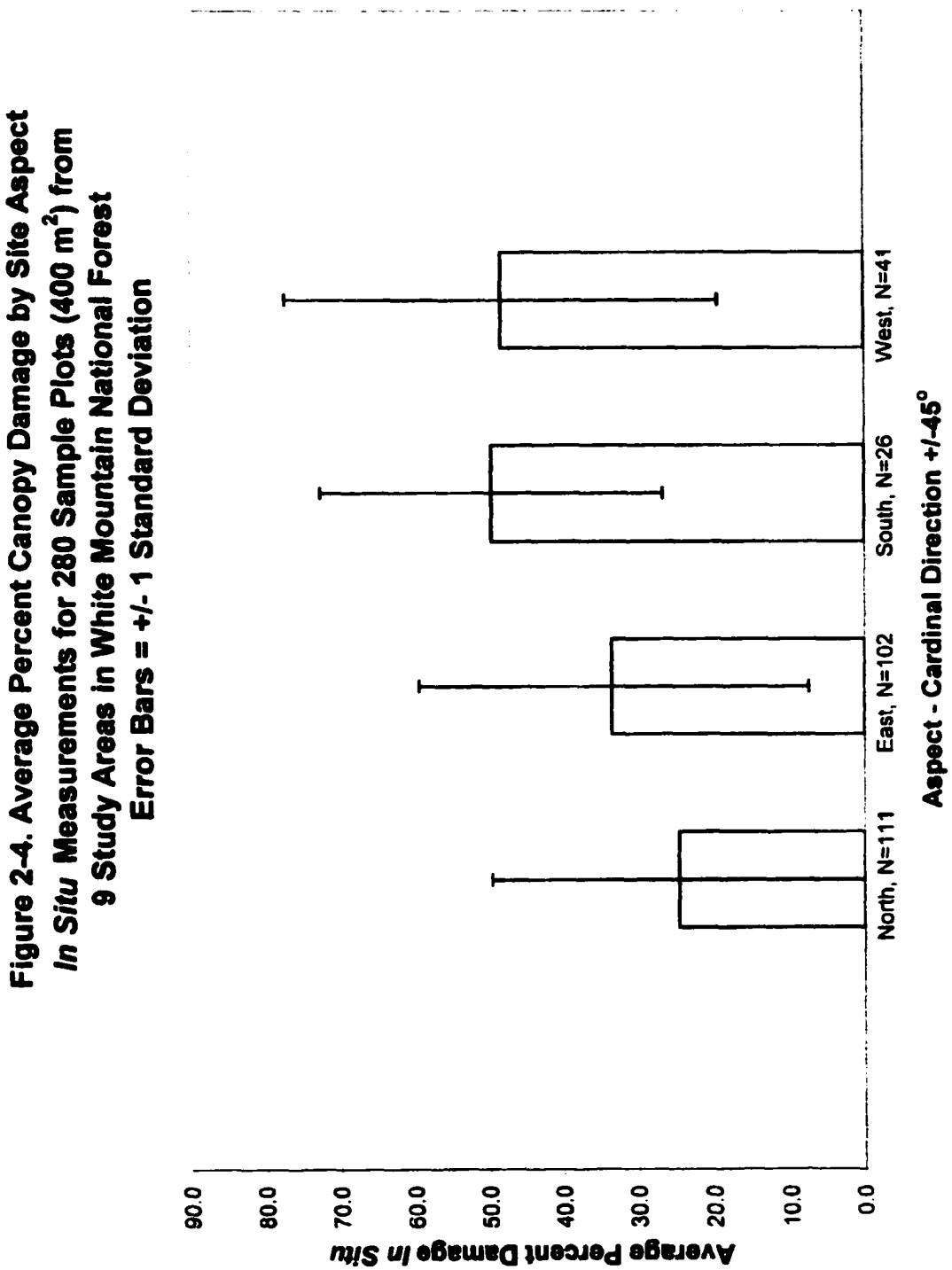

Figure 2-4. Average Percent Canopy Damage by Site Aspect *In Situ* Measurements for 280 Sample Plots (400 m^2) from 9 Study Areas in White Mountain National Forest Error Bars = +/- 1 Standard Deviation

Figure 2-5. Average Percent Canopy Damage by Slope Class *In Situ* Measurements for 280 Sample Plots (400 m^2) from 9 Study Areas in White Mountain National Forest Error Bars = +/- 1 Standard Deviation

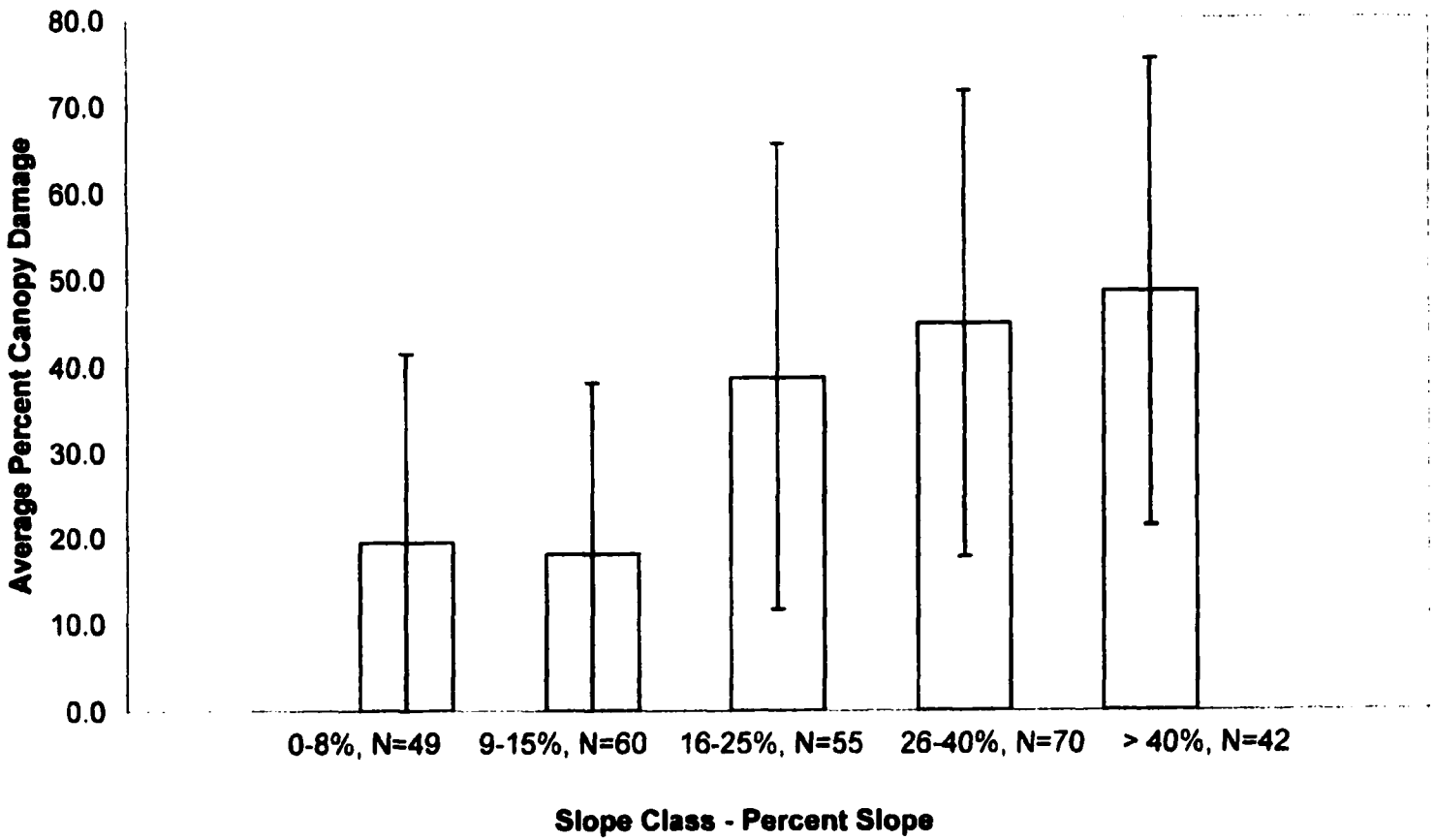

Figure 2-6. Average Percent Canopy Damage by Site Elevation Class *In Situ* Measurements for 280 Sample Plots (400 m2) from 9 Study Areas in White Mountain National Forest Error Bars = +/- 1 Standard Deviation

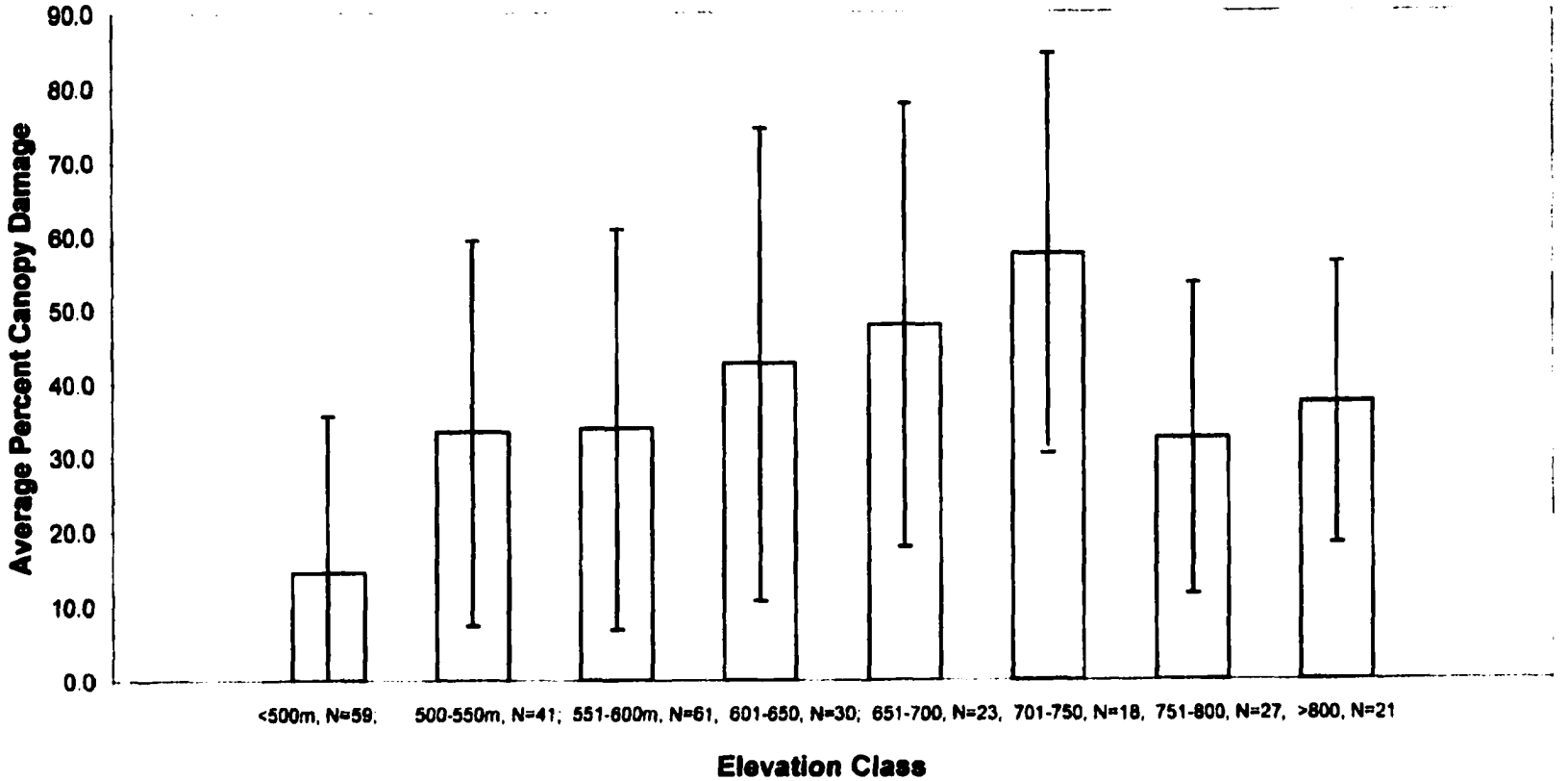

Carter Sensitivity Analysis

In order to verify that the red edge region was appropriate for ice damage differentiation, a sensitivity analysis was performed on ASAS data from variously damaged study sites using the method of Carter et al. (1992). These researchers developed a simple sensitivity analysis to identify the regions of greatest difference for the spectral reflectance signatures of a feature of interest, such as an ice damaged canopy, and the curve of a control feature, such as an undamaged canopy. The analysis reveals the areas of the spectrum (wavelengths) at which spectral differences, expressed as percent difference from the control area, are greatest. Application of the analysis separated damaged sites from the control feature most effectively in two spectral regions: the green peak (522 nm) and the middle portion of the visible red to the lower portion of the near infrared (NIR) region (663-734 nm – the red edge). Separation between the damaged canopy signatures and the control are at least partially stacked away from zero in rank order according to their damage class in these two regions. This is particularly evident at 522 nm and between 663-683 nm. In this study, the analysis flags the green peak (522 nm) and the section of the red edge region from 663-734 nm as best for ice damage assessment (Figure 2-7).

Figure 2-7. Carter Sensitivty Analysis. Two regions of greatest spectral difference - lower red edge and green peak - between control site and light, moderate, and severe ice storm damage (+/- 1 standard deviation).

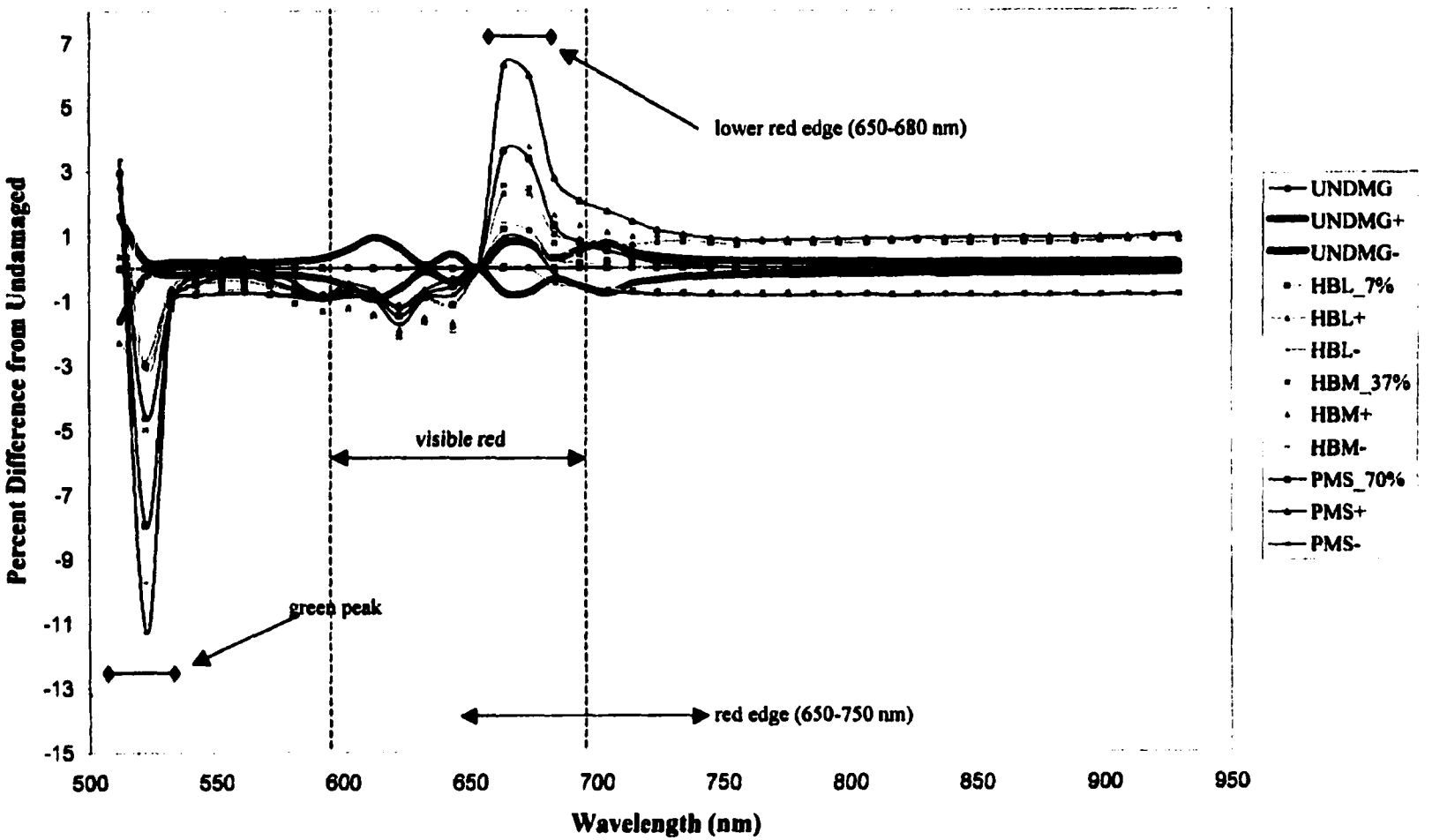

ASAS Study Site Size and Sample Size

Table 2-6 shows the results of the one-way ANOVA for 10 ASAS Study Site Sizes.

Table 2-6. Results of ASAS Study Site Size Analysis - 10 Site Sizes from 7.5 x 7.5 m to 750 x 750 m.

ASAS Site Size	Sample Size N=	ANOVA P-Value	Tukey Test Significantly Different Pairs
7.5 x 7.5 m	210	< 0.001	Severe-Mod, Severe-Light
12.5 x 12.5	208	< 0.001	Severe-Mod, Severe-Light
17.5 x 17.5	203	< 0.001	Severe-Mod, Severe-Light
27.5 x 27.5	203	< 0.001	Severe-Mod, Severe-Light
62.5 x 62.5	55	< 0.001	Severe-Mod, Severe-Light
92.5 x 92.5	53	< 0.001	Severe-Mod, Severe-Light
170 x 170	47	< 0.001	Severe-Mod, Severe-Light
250 x 250	34	0.002	Severe-Mod, Severe-Light
500 x 500	12	0.047	None
750 x 750	7	0.466	None

Note that the sample number is approximately 210 for study sites from 7.5 x 7.5 m to 27.5 x 27.5 m, but for larger study site sizes the sample size decreases. For sites larger than 27.5 x 27.5 m, the average percent damage for a cluster of reference sites contained within it determines its damage class. For example, the 92.5 x 92.5-m site size might have an average 714nr value of 0.32 and contain 4 reference sites with an average percent damage of 33%. This would place it in the Moderate class. The ANOVA analysis determines if the 714nr value means for each of the 3 damage classes are statistically the same. The statistical analysis considers the variances within and among groups (Zar, 1996). The Tukey Test goes one step beyond ANOVA to determine between which population means differences exist. This is also referred to as the Honestly Significant

Difference Test (HSD) (Tukey, 1953). For example, it determines if the Severe class can be statistically differentiated from the Light class.

It was determined that the smallest study site size (7.5 x 7.5 m) was the best size for this study for 3 reasons. 1. It differentiated levels of damage by 714nr as well or better than any other size. 2. Because 7.5 x 7.5 m (56 m^2) is smaller than the study areas measured on the ground (circular area with 11.3 m radius = 400 m^2), it allows for approximately +/-5 m error in image registration caused by topographic effects and +/- 2 m error for GPS points. This is within the spatial error of the DOQs. 3. Using smaller sites makes it possible to utilize a greater study site sample, N = 210.

Effects of Ice Damage, Aspect, Slope, and Elevation on 714nr

Multi-way ANOVA of the 714nr by the 4 factors was performed (N = 210, 7.5 x 7.5 m sites). A confidence level of $\alpha = 0.05$ (95%) was used. The multi-way ANOVA of the 714nr values to the 4 factors was significant ($P > 0.001$). This result is similar to the one-way ANOVA of the 714nr by damage determined above. The significance of the interactions among all 4 factors and pairs of factors was determined by the effect test (Table 2-7).

Table 2-7. Summary of Results of Multi-Way ANOVA Effect Test for Significant Interaction Among Damage, Aspect, Slope, and Elevation

Factors	Effect Test P-Value
Damage*Aspect*Slope*Elevation	P = 0.007
Damage*Aspect	P < 0.001
Damage*Slope	P = 0.009
Damage*Elevation	P = 0.017
Aspect*Slope	P = 0.994
Aspect*Elevation	P < 0.001
Slope*Elevation	P = 0.255

The test for interaction among all 4 factors was insignificant (P = 0.007). The tests for interaction between pairs of factors were significant for Damage and Aspect and Aspect and Elevation. This means that the effect of one is *not independent* of the presence of a particular level of another factor (Zar, 1996). For example, south aspect and severe damage are associated. Due to the known local characteristics of ice storms – that damage is often associated with certain aspects and elevations – these results are not unexpected.

To determine the significance of any one factor on 714nr, one-way ANOVAS were performed for 714nr by aspect, slope, and elevation, as it was for damage, Table 2-8.

Table 2-8. Summary of Results of One-Way ANOVA for 714nr by Damage, Aspect, Slope, and Elevation

Factor	P-Value
Damage	$P < 0.001$
Aspect	$P < 0.001$
Slope	$P = 0.699$
Elevation	$P = 0.047$

The ANOVA analysis shows that the 714nr means for the 3 damage classes and 4 aspects are not the same ($P < 0.001$). In all probability, aspect is associated with 714nr as a result of the particular local climatic conditions during the 3 days of the ice storm of January 1998 that made it more likely for severe ice damage to occur on slopes of specific aspects. In this way aspect is correlated with 714nr through its association with areas of severe ice damage, and not directly associated with 714nr. The one-way ANOVA results for aspect show that the West and South aspects were correlated with higher 714nr values, an indication of more severe damage. Figure 2-4, showing the average percent

damage by aspect, supports this finding. The field data (N = 210) are not intended to represent site features of damaged forested areas throughout the WMNF. Anecdotal evidence suggests that severe ice damage was associated with various aspects in different locations throughout the WMNF as a result of the storm. Therefore, any correlation between aspect and 714nr is indirect and specific to the January 1998 ice storm. This is an important distinction. Because ice damage is directly correlated to 714nr, after a subsequent ice storm it is expected that higher levels of 714nr would be associated with severe damage. It would not be expected, however, for the West and South aspects to be associated with severe damage after another ice event.

Differentiation of Ice Damage Using 714nr

Each study site consisted of variously damaged hardwood stands in a circular area 400 m^2 (11.3-m radius) measured on the ground. These study sites were located in rectified ASAS imagery using GPS data collected on the ground and represented in 3 x 3 pixel datasets (7.5 x 7.5 m). The target areas (as shown in Figure 2-1) are listed with the number of study sites by damage class in Table 2-9, below. The total sample size is 210.

Table 2-9. Target Areas and Number of Ground Sites by Damage Class (400 m^2 Sites)

	Ground Sites By Damage Class			
Target Area	Light	Moderate	Severe	Total
Bartlett - Light	43	3	1	47
Bartlett – Severe	1	6	16	23
Hubbard Brook - Light	24	0	0	24
Hubbard Brook - Moderate	4	17	5	26
Hubbard Brook - Severe	5	11	20	36
Jefferson Notch – Moderate	9	8	3	20
Pine Mountain - Severe	0	3	31	34
Total Sampling	86	48	76	210

In this study, the blue shift is represented as the average normalized red edge ASAS value at band 714 nm (for each study site. To provide reference data with which to compare the blue shift values, *in situ* measurements of percent damage to individual tree crowns located within a given study site (400 m^2) were averaged, as described above, to determine the mean percent canopy damage for the site.

Results of the ANOVA and Tukey tests for 714nr 3 x 3 pixel sites (7.5 x 7.5 m) are summarized in Figure 2-8. Detailed results are listed in the Appendix (Figure A-1).

Figure 2-8. ANOVA and Tukey Test results 714nr by Damage, 3 x 3 pixel sites, N = 210 The points represent 714nr values. Values of 714nr are grouped according to their corresponding percent canopy damage measured on the ground (0-24.9% = Light, 25-49.9% = Moderate, 50-100% = Severe). The box-and-whisker plots for each group of points indicate the level up to which 10% (lower line), 25% (bottom of box), 50% (center of box), 75% (top of box), and 90% (upper line) of the data fall. The circles for the Tukey-Kramer test are centered on the mean 714nr value for each damage class. The size of a circle is determined by the variance from the group mean at the 95% confidence level. Separation between circles indicates a statistical difference between their means.

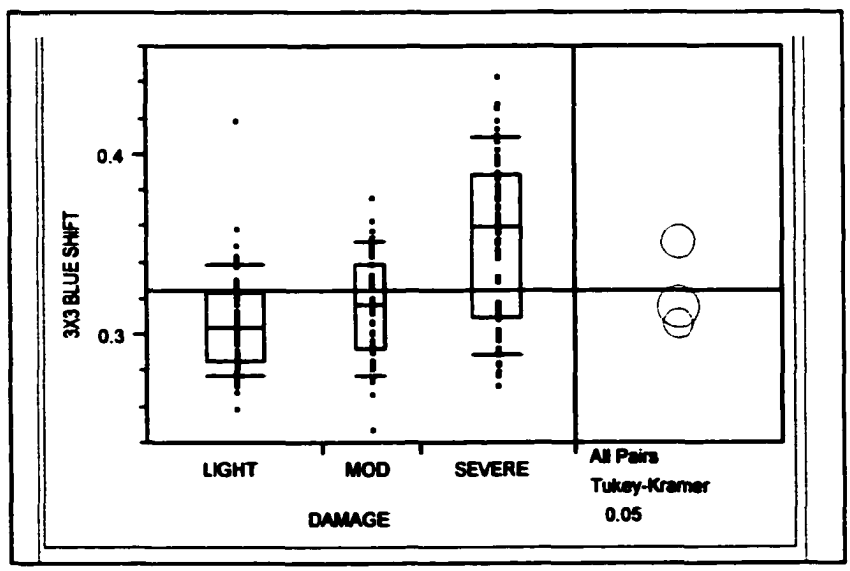

To the extent that 714nr represents blue shift, a lower value for 714nr suggests a higher level of green biomass within a site (less damage) and a higher value indicates a lower level of green biomass (more damage). The ANOVA analysis shows that the 714nr means for the 3 damage classes are not the same ($P < 0.001$). Further, the 714nr values successfully distinguish the Severe from the Moderate and Light damage classes but fail to differentiate between the Moderate and Light classes. The positive values in the Tukey Test matrix (also called Tukey-Kramer Test), the bottom chart in Figure A-1, indicate pairs of damage classes that are significantly different. The circles diagram at the right in Figure 2-8 demonstrates this separation visually. The Moderate and Light classes overlap and are, therefore, not statistically different. In the Tukey Test matrix the value describing this overlap is negative (-0.0053) but it is very close to being positive. That this value is close to being positive is an indication that some degree of difference exists between the two – the circles overlap partially.

These results suggest advantages and disadvantages of using hyperspectral ASAS data to detect levels of ice storm damage to forest canopies. On the one hand ASAS can detect fine-feature spectral changes by using many narrow bands of information within the red edge region. On other hand, because it is the nature of forest canopies to be spectrally heterogeneous rather than homogeneous – even undamaged closed canopies – and for the symptoms of ice storm damage to be a patchy mixture of spectral features, the spectral variability within even a 7.5 x 7.5 m study site is considerable. The average standard deviation of the 714nr value within the sites was approximately 0.025, while the Light damage mean was 0.307 and the Moderate mean was 0.317. Thus, the difference between the Light and Moderate means was less than one standard deviation for the data

for pixels within a site. This overlap of spectral variances is further demonstrated in the ANOVA results in Figure 2-8. The box-and-whisker plots define the quartiles of the 714nr for sites by damage class. Each data point on the chart represents the average 714nr value for 9 pixels within a 7.5 x 7.5 m site. In effect this averages or smoothes the data within a 3 x 3 pixel window (9 pixels) to one value. The box-and-whisker plots demonstrate the range of the smoothed data within each damage class. It is evident that there is considerable overlap between classes, as pointed out above, and particularly between the Light and Moderate classes. Thus, the high-resolution view (2.5 m pixels) magnifies the spectral heterogeneity of the canopy and, even when this variability is smoothed to a 7.5 x 7.5 m (3 x 3 pixel) study site, it persists. The study site size analysis, above, demonstrated that, at least for 714nr values, the spectral overlap between Light and Moderate remains significantly large even as site size increases. The 714nr-value changes between the Light and Moderate groups are not significant enough to separate them.

Classification Mapping and Accuracy Assessment of 714nr

Values of 714nr were used to classify 3 levels of ice damage by applying supervised thematic classification – classification mapping. A classification map, in this case to classify 3 levels of ice damage to forest canopies, is the product of a three-step procedure. 1. A spectral feature – the 714nr – is selected that distinguishes between clusters of pixels (polygons) within a digital scene. 2. Polygons from the scene, called training sites, are selected to represent and characterize distinct types of objects or materials – Light, Moderate, and Severe damage. A number of training sites are selected

to represent each type to be classified. 3. An iterative computer process scans the image pixel-by-pixel and classifies each pixel according to the relationship of its spectral value (714nr value) to its neighbors and then places it into the bin of the training site in which it is the best match. Training sites representing the same class are assigned a common color, for example pixels classified as severely damaged are colored red. Unclassified pixels are colored black. This is considered a supervised classification since the computer is trained or supervised in the classification process. The final product is an image with pixels classified into categories represented by different colors. The accuracy of the classified image is a test of the significance of the spectral feature used in the classification process. If 714nr values are an effective measure of levels of green biomass and if levels of green biomass are indicative of levels of ice damage to forest canopies, then the 714nr should classify damage successfully, with greater than 80% overall accuracy.

A supervised classification was applied to the 714nr from 210 sites (7.5 x 7.5 m) within 7 target areas. Pixels were classified into three comprehensive and mutually exclusive levels of ice damage – Light (0-24.9% damage), Moderate (25-49.9%), and Severe (50-100%).

Ten training sites were selected to represent each damage class. A systematic random selection process was used to determine which sites would be used as training sites. Reference sites were ranked by percent damage and the number of reference sites was divided by the number of training sites needed for each damage class (E.g. Light, 89/10 = 8.9). This quotient was rounded down (8.9 > 8) and then every 8^{th}, in this case, reference site was used to systematically select training sites from the ranked list. The 180 remaining sites were used as reference sites. Following the classification process the

reference sites were used to check the accuracy of the final product. The data were classified using the maximum likelihood resampling method in which pattern measurements or features of pixels are assigned by a decision rule to a class whose units are most likely to have given rise to such a feature (Jensen, 1996). For this study, the maximum likelihood decision rule was based on values from a single variable, 714nr.

Figures 2-9 to 2-15 show the classification maps for the 7 target areas. A visual inspection of the maps reveals a moderate correlation between the general known level of damage measured on the ground and the color of the majority of pixels in that area of the image for Bartlett Severe (Figure 2-10), Hubbard Brook Moderate (Figure 2-12), and Pine Mountain Sever (Figure 2-15). A thick black line represents the approximate area of the location of study sites within each target area scene.

Figure 2-9. Bartlett Light Supervised Classification Map
Ice Damage Levels: Gray = Light; Yellow = Moderate; Red = Severe
Black polygon outlines = extent of reference sites within target area.
Small black rectangles/dots = reference sites.

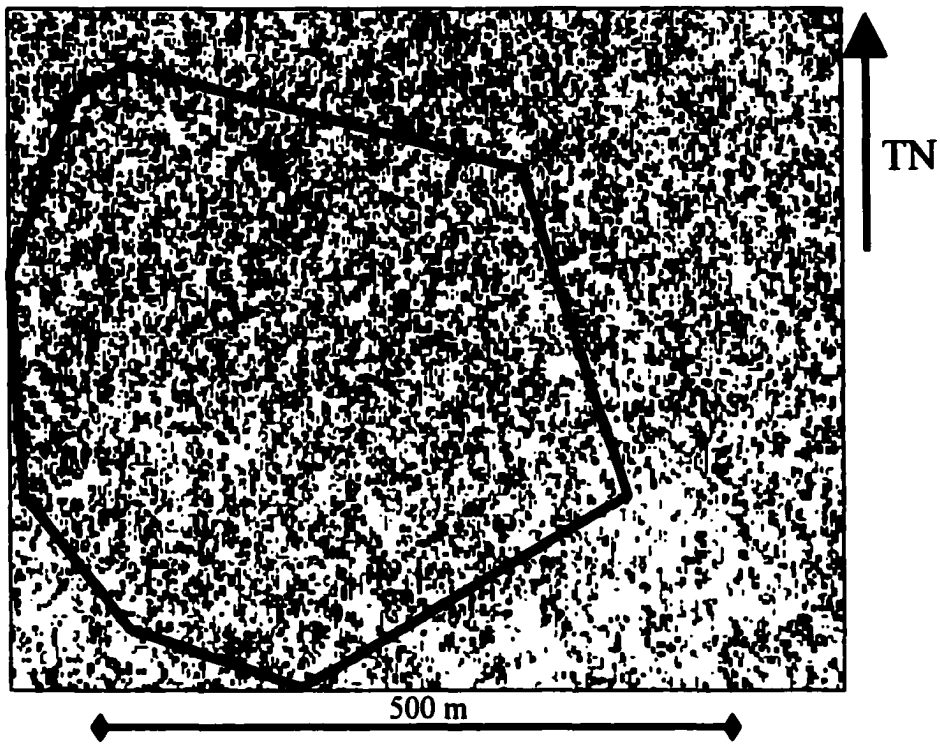

Figure 2-10. Bartlett Severe Supervised Classification Map
Ice Damage Levels: Gray = Light; Yellow = Moderate; Red = Severe

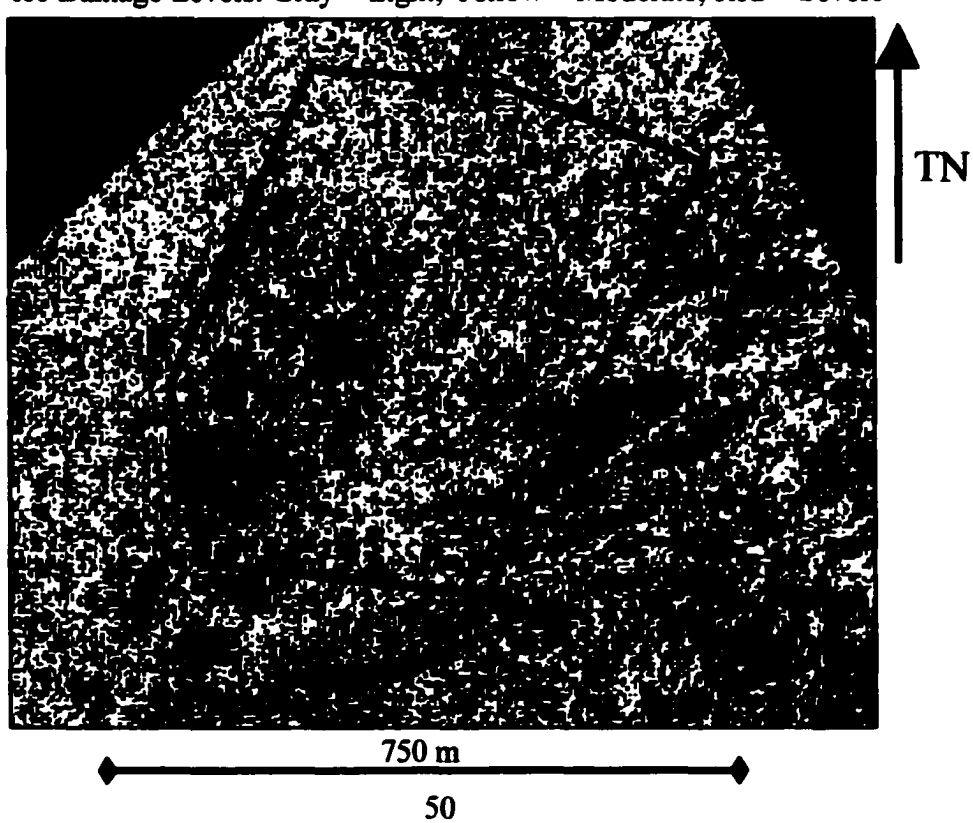

Figure 2-11. Hubbard Brook Light Supervised Classification Map
Ice Damage Levels: Gray = Light; Yellow = Moderate; Red = Severe

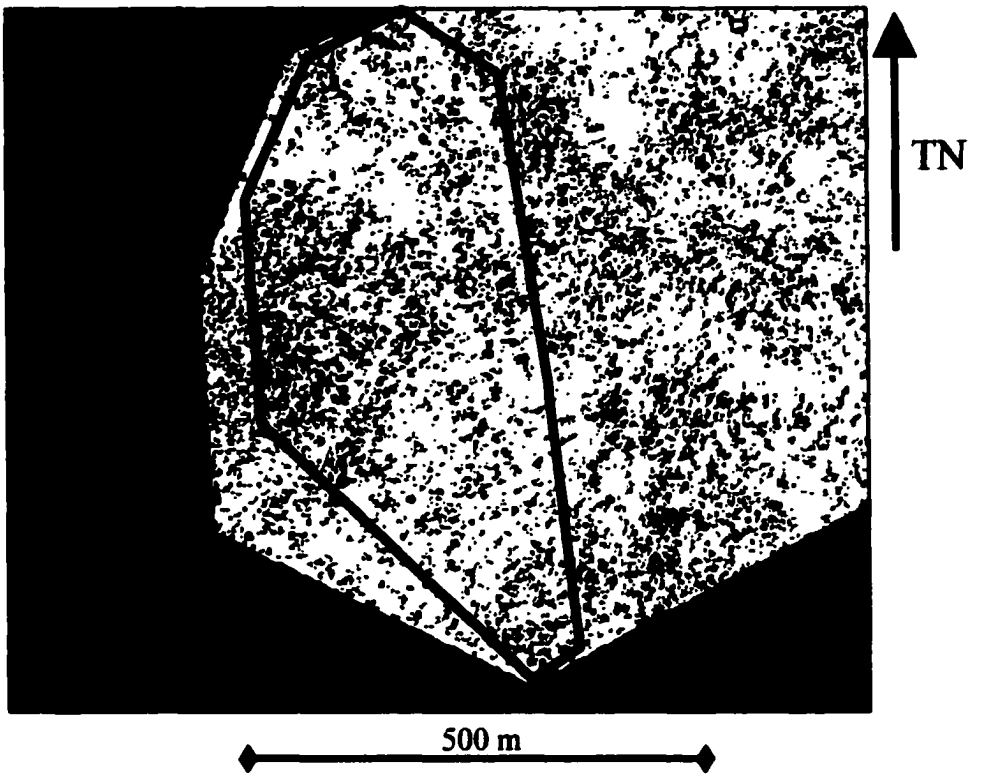

Figure 2-12. Hubbard Brook Moderate Supervised Classification Map
Ice Damage Levels: Gray = Light; Yellow = Moderate; Red = Severe

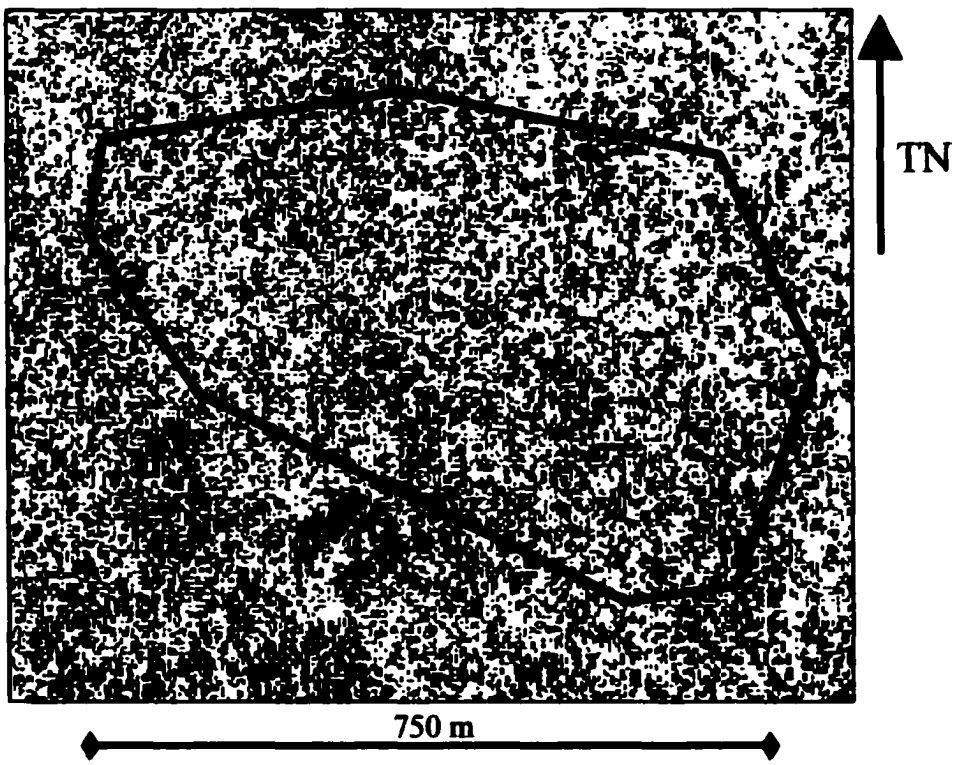

Figure 2-13. Hubbard Brook Severe Supervised Classification Map
Ice Damage Levels: Gray = Light; Yellow = Moderate; Red = Severe

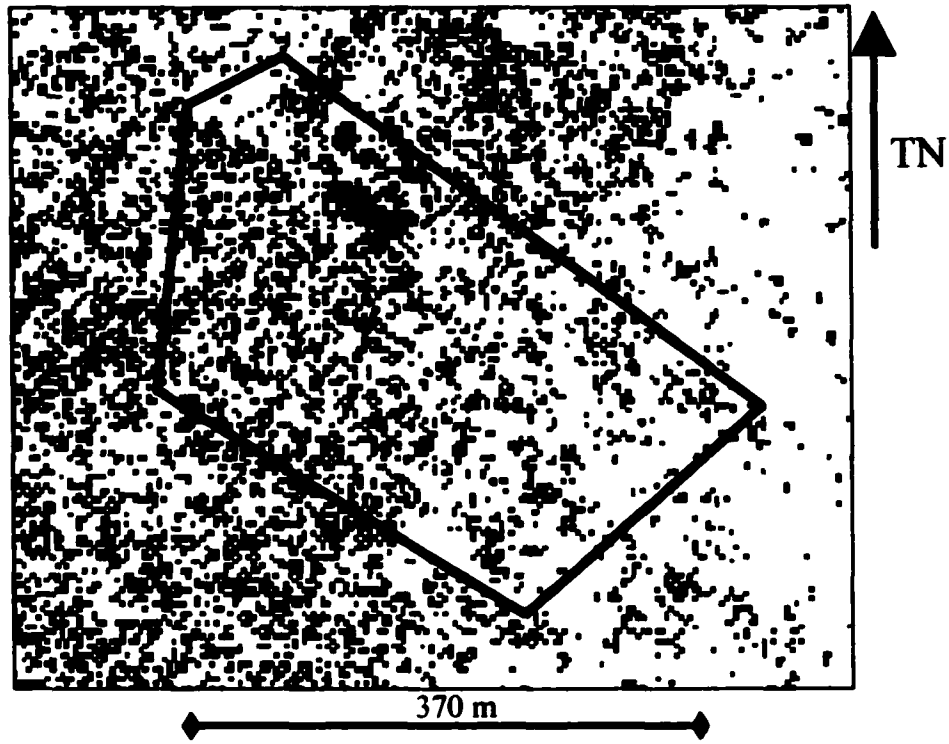

Figure 2-14. Jefferson Notch Moderate Supervised Classification Map
Ice Damage Levels: Gray = Light; Yellow = Moderate; Red = Severe

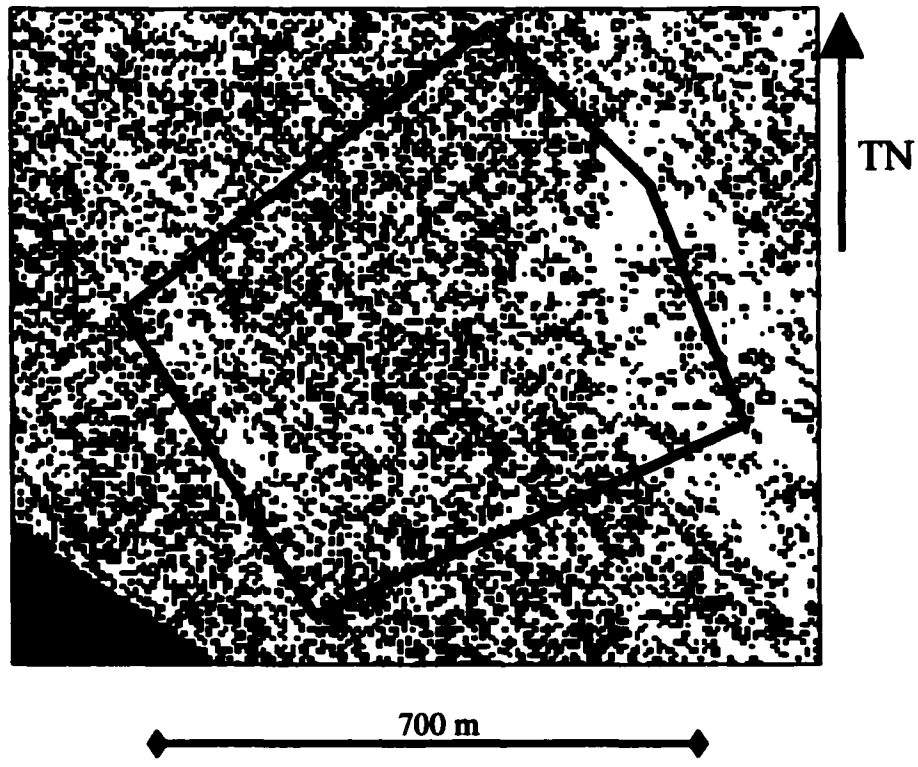

Figure 2-15. Pine Mountain Severe Supervised Classification Map
Ice Damage Levels: Gray = Light; Yellow = Moderate; Red = Severe

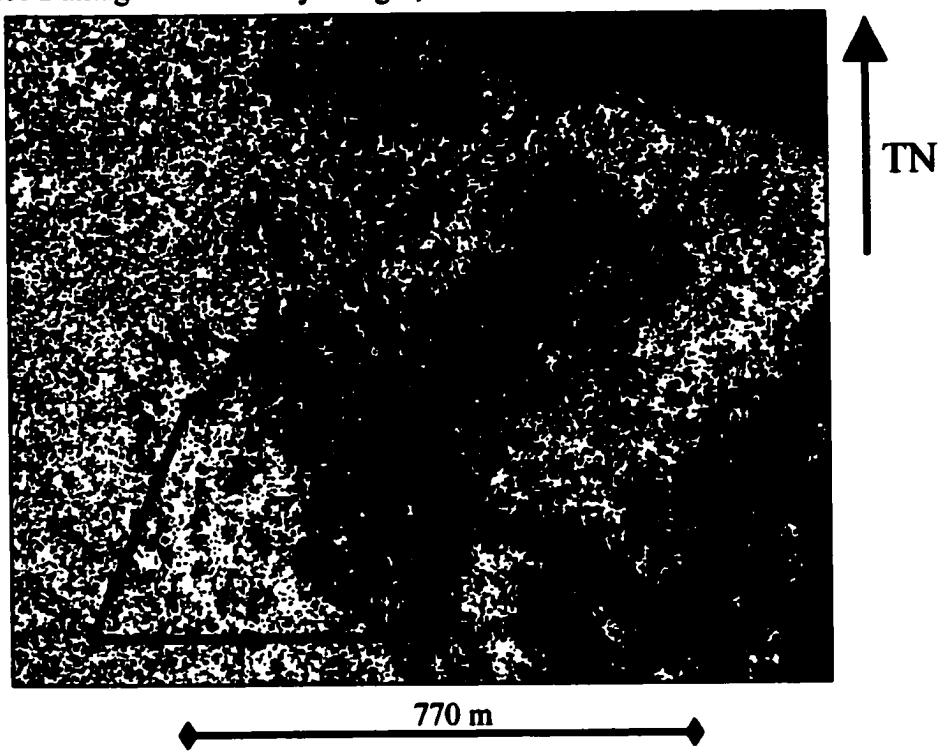

The error matrix accuracy assessment method was used to analyze these data more closely. In error matrix analysis, reference sites in the classification map are inspected to determine if they have been accurately classified. A modal rule was used for this determination: A reference site was correctly classified if more pixels of the corresponding class color (e.g. yellow for Moderate damage) are found within the site than any other class color. Unclassified pixels (black on the map) were not factored into the error matrix assessment.

Because ice storm damage is a matter of degree and does not occur in stepped categories, damage-class boundaries must be arbitrarily determined between classes. Ice damage at reference sites was measured on the ground as a percent of canopy damage from 0-100% and divided into 3 classes – Light (0-24.9%), Moderate (25-49.9%), and Severe (50-100%). To mitigate the problem of assigning stepped categories to continuous data, fuzzy boundaries were used in the error matrix process (Congalton and Green, 1999). A fuzzy boundary of +/- 5% was designated between damage classes. This fuzzy classification rule made it acceptable for a reference site to be classified as Moderately damaged, for example, if it was actually classified as Lightly damaged (by the modal rule) but its average percent damage was within 5% of the lower boundary of the Moderate class. For example, reference Site A was measured at 23% damage (within the Light class 0-24.9%), but classified as Moderate (25-49.9%). This classification is acceptable because the percent damage at Site A is within 5% of the Moderate class.

The results of the error matrix assessment for 714nr (7.5 x 7.5 m sites) are shown in Table 2-10.

Table 2-10. Error Matrix for 714nr for 1998 Post-Event Canopy Damage Classification Maps (7.5 x 7.5 m Study Sites)

		GROUND REFERENCE				
714nr		LIGHT	MODERATE	SEVERE	TOTAL	% USER'S ACCURACY
IMAGE CLASSIFICATION	LIGHT	29	5	10	44	66%
	MOD	30	27	15	72	38%
	SEVER	17	6	41	64	64%
		76	38	66	180	
PRODUCER'S ACCURACY		38%	71%	62%	**OVERALL ACCURACY**	**54%**

The overall accuracy of the 714nr classification map is 54%. In addition to the overall accuracy, user and producer's accuracies were determined for each damage class. User's accuracy calculates the percent of reference sites that are correctly classified from the total number of mapped (classified - rows in error matrix) sites in that class. For example, the user's accuracy of the Moderate class is only 38%. Twenty-seven of the 72 Moderate mapped sites were correctly classified and 45 represented committed errors, 30 were actually Light. This demonstrates that there was considerable confusion between the Moderate and the Light damage classes. The user's accuracies for the Light and Severe classes were better, 66% and 64% respectively. The producer's accuracy accounts for errors of omission. For example, 27 Moderate sites were correctly classified out of a total of 38 reference sites, 11 were mapped incorrectly. Thus, 27 of 38 sites classified as Moderate (71%) were mapped correctly and the remaining 29% represented errors of

omission. The producer's accuracy for the Moderate class is relatively high indicating that few sites (11) were mistaken as Light or Severe. The fuzzy classification rule was invoked 14 times out of 180 reference-site decisions or 8% of the time.

Conclusions

Nadir-viewing 714nr values are effective for differentiating Severe sites from Light and Moderate sites, but Light and Moderate sites are indistinguishable.

Hypothesis 2-1: That values of 714nr for nadir hyperspectral ASAS imagery of variously ice damaged hardwood sites (7.5 x 7.5 m sites, N = 210) can significantly separate 3 levels of damage is rejected.

Hypothesis 2-2: That values of 714nr for nadir hyperspectral ASAS imagery of variously ice damaged hardwood sites (7.5 x 7.5 m sites, N = 210) can be classified with greater than 80% overall accuracy is rejected.

Hyperspectral values of 714nr are effective for differentiating Severely damaged sites from Moderately and Lightly damaged sites. If the classification map error matrix were to combine the Light and Moderate damage classes and simply assess the ability of 714nr to distinguish between Severe damage and everything else, an overall accuracy of 73% would result. The 714nr is not able to differentiate Light from Moderate sites, however. That the 714nr can differentiate severely damaged canopy from other levels of damage is a significant finding. This suggests that the symptoms of severe damage – reduced green biomass and the exposure of greater amounts of spectrally distinct non-green materials and objects – can be detected using a single post-event ASAS scene and used for coarse regional assessments of ice storm damage. This method, involving many

ASAS overflights with specialized equipment, is an expensive alternative, however, and its effectiveness is only on par with methods using aerial photography.

CHAPTER III

ASAS NADIR VS. OFF-NADIR VIEWING

Introduction

The effectiveness of ASAS multiangle views to detect canopy damage is evaluated. ASAS datasets derived from various off-nadir view angles recorded during the summer following the January 1998 ice storm are used to measure spectral reflectance differences in sites with differing levels of ice storm damage to forest canopies. Prior to evaluating the ability of off-nadir views to detect levels of canopy damage, data for view angles +45°, +45°, nadir, –26°, and –45° off-nadir were evaluated to determine to what extent off-nadir viewing affects the slope and wavelength position of the red edge spectral features of an undamaged control site. When ASAS datasets are normalized for five view angles (+/-45, +/-26, and nadir) the red edge spectral signatures are qualitatively invariant: the shape, slope, and wavelength position of the red edge is not significantly changed. The effectiveness of the 714nr for off-nadir views to distinguish levels of ice damage to forest canopies is then compared to that of nadir data.

The following hypotheses are tested:

3-1. Red edge features of normalized ASAS datasets are not affected by sensor view angle.

3-2. Measurements of the 714nr for off-nadir hyperspectral ASAS imagery of variously ice damaged hardwood sites (90 x 90-meter sites, N = 50+/-) are

more effective than nadir imagery at differentiating 3 levels of ice damage to hardwood forest canopies.

The Advanced Solid-State Array Spectroradiometer (ASAS)

The airborne ASAS sensor has three features of potential use in improving the precision and accuracy of assessing hardwood canopy damage, such as that caused by ice storms: hyperspatial (2.5- 4.5-meter pixels) capabilities, hyperspectral (62 bands) capabilities, and multiangle viewing capabilities. These features provide ASAS with the potential to detect and quantify spectral fine-features in reflectance data related to variations in canopy morphology (percent canopy damage to individual trees) and leaf condition (chlorophyll content) related to ice storm damage.

In this study the effectiveness of off-nadir viewing to detect ice storm damage to hardwood forest canopies is investigated. Multiangle viewing technology is applied to a practical forestry problem - assessing levels of ice storm damage to hardwood forest canopies. Ice damage forms canopy gaps. Gaps expose materials other than the green leafy canopy layer, such as branches, stems, wood tissue, dead woody debris, groundcover, leaf litter, bare soil, and rocks. It is theorized that off-nadir views provide access to the sides of tree crowns and the edges of ice damage patches within the canopy exposing damage symptoms missed by nadir views. Vegetation indices are used to discriminate non-vegetative materials, containing less green biomass, from healthy canopy leaves.

Materials and Methods

Study Area and ASAS Data Acquisition

Nine target areas (1 km x 1 km) in the WMNF (Figure 2-1) were selected for study. The target areas and their known general level of ice damage are listed in Table 3-1.

Table 3-1. Nine Target Areas in the WMNF with general/approximate level of damage, aspect, slope, elevation, and forest type.

SITE	DAMAGE	ASPECT	SLOPE	ELEV	FOR. TYPE
Hubbard Brook	Light	NE	15%	600m	Hardwood
Hubbard Brook	Moderate	NE	26%	810m	Hardwood
Hubbard Brook	Severe	NE	44%	695m	Hardwood
Bartlett	Light	NE	19%	319m	Hardwood
Bartlett	Severe	NW	18%	600m	Hardwood
Jefferson Notch	Moderate	SE	16%	573m	Hardwood
Killkenny	Light/Mod	NE	8%	540m	Hardwood
Black Mountain	Moderate	SW	20%	777m	Softwood
Pine Mountain	Severe	W	27%	606m	Hardwood

A C-130 aircraft was flown by NASA at 3,000 m over the target areas on July 14 and 15, 1998. The ASAS sensor measured solar radiance reflected from the Earth's surface in pushbroom fashion. Spectral radiance data was sensed in 62 bands, 10 nanometers (nm) in width, covering a spectral range from 400 nm to 1020 nm on the electromagnetic spectrum. The spatial resolution of the sensor varies with the altitude of the aircraft. At 3,000 m, pixels are 2.5 meters in width across-track. Along-track pixel lengths increase with view angle. Pixels viewed at a 55° angle, for example, represent ground data collected within a pixel measuring approximately 4.5 meters along-track. The pivoting sensor mounting system allows viewing angles from +70° in the forward

direction to –55° backwards. One ASAS image, acquired at 10,000 feet, represents a ground area of approximately 1 square kilometer (Irons et al., 1991; Russell et al., 1993; GSFC, 1998). One flight line was flown along the parallel or principle plane (directly toward or away from the solar azimuth) and the other along an oblique flight line approximately 45° off the principle plane. Multiangle views were recorded at seven angles: +60° (forward direction), +45°, +26°, 0° (nadir), -26° (back-looking), -45°, and –55°. The result was two flight line series for each target area with seven images from each of seven view angles.

Image Processing of ASAS Data

Raw datasets of the off-nadir datasets were pre-processed at Goddard Space Flight Center (GSFC) by the same procedure used for the nadir ASAS datasets (see Chapter II). The Second Simulation of the Satellite Signal in the Solar Spectrum (6S) radiative transfer/atmospheric correction model was used to convert at-sensor radiance values to surface reflectance values on a scale of 0-1000 (Vermote et al., 1997). Rectified Digital Orthographic Quads (DOQs) were used to georeference the nadir image in each flight line. The WMNF consists of rugged terrain, but the variability of slope ($\sigma < 17\%$) and aspect ($\sigma < 50^{\circ}$) for any target area did not significantly affect the spectral signatures of a given study site within nadir images. Ground control points (GCPs) were selected manually and a first order polynomial transformation using nearest neighbor resampling was performed.

Off-nadir views were not georeferenced to DOQs because image smearing and ground area foreshortening made it impractical. Particularly at the larger view angles (+/-

45° and greater), pixel smearing resulting from aircraft instability (pitch, yaw, and roll) caused image distortions. In addition, large topographic features, such as ridgelines and steeper slopes, caused image foreshortening. If the target area lay on the backside of a ridge, for example, the pixels in the off-nadir view were elongated along-track, which caused a foreshortening of areas measured on the ground. Pixel width across-track also widened with view angle. Image distortion was particularly problematic for view angles greater than 45° and, therefore, the +60° and –55° views were not used for study.

For nadir views a vector coverage that included GPS points for each field site was overlaid on the rectified nadir images to locate field sites in the imagery. To avoid the misidentification of study sites in off-nadir views due to distortions, corresponding areas in off-nadir scenes were identified by matching similar pixel patterns created by shadowing that was visible in the crowns of the trees in the nadir image. The hyperspatial resolution of ASAS imagery (2.5-4.5 m pixels, 9-25 pixels per crown) made this method feasible even in undamaged stands containing homogenous canopy cover because shadow patterns were evident.

Distortions caused by smearing and foreshortening made it impractical to try to locate 7.5 x 7.5 m study sites in off-nadir scenes. For this study of off-nadir scenes, 90 x 90 m sites were used. At this spatial scale, corresponding sites could be located in off-nadir views by identifying pixel patterns from the nadir view for each scene. The number of pixels for a 90 x 90 m site in the nadir views of each target area was approximately 37 x 37 = 1369. The number of pixels in corresponding off-nadir scenes was reduced by foreshortening effects to about 900 pixels in many cases and to about 300 pixels in some cases. Some sites had to be eliminated because they were not identifiable in the image.

Despite the reduced pixel number of some sites, the spectral information was extracted from an area of canopy that corresponded to that of the nadir view and was, therefore, suitable for comparison.

Results

The Effect of View Angle on Red Edge Features

The effect of view angle on the slope and wavelength position of the red edge curve was investigated. It is well established that forest canopies are non-Lambertian, i.e. they do not scatter reflected radiance equally in all directions, and that the intensity of reflected radiance is greatest in the backscatter direction, where shadowing is minimized. As sensor view angle approaches the maximum backscatter position, the *hotspot* (view angle = solar zenith angle), the intensity of the reflected radiance increases incrementally. The slopes of the red edge curves for a series of view angles increase as the view angle approaches the *hotspot*. This step-by-step increase in red edge slopes for a view angle series is described as the brightness gradient (Kennedy et al., 1997). A normalization procedure was applied to ASAS multiple view angle datasets to eliminate the variability caused by backscatter effects (resulting in the brightness gradient) so that the view angle-independent spectral features of an object in one scene could be compared with those of the same object recorded from a different view angle.

The effectiveness of the normalization procedure was evaluated. An easily identifiable undamaged control site was selected from within the Hubbard Brook Light target area. The site contained an undamaged closed canopy surface area of approximately 18 x 18 m or the equivalent of approximately 3 hardwood crowns. Data

from 5 view angles (+/-45°, +/-26°, and nadir) for two flight lines were used for analysis. Charts of the spectral red edge signatures for the atmospherically corrected imagery and the normalized imagery are shown for the two flight lines (Figures 3-1 to 3-4). The parallel flight line was flown toward the sun (Figure 3-5). As a result intense backscatter reflectance is evident in the back-looking view angles, -45° and -26° of the parallel flight line (Figure 3-1). The oblique flight line was flown away from the sun and at an angle approximately 45° off the parallel plane (Figure 3-6). Intense backscatter is evident in the forward-looking views +26° and +45° and at nadir (Figure 3-3). The solar zenith angle was approximately 33° at the time the datasets were acquired, which explains why the -45° and -26° views from the parallel flight line and the +26° and +45° views from the oblique flight line – positioned near the *hotspot* – received the greatest backscatter effect. Figures 3-5 and 3-6 show the position of the sun, direction of the aircraft, and the reflectance values of 5 view angles for the two flight lines.

The dip in all the signatures at Band 755 nm (region of atmospheric oxygen absorption) reveals the inability of the atmospheric correction procedure to correctly model the known effect of atmospheric absorption at that wavelength (Figures 3-1 to 3-4). To avoid discrepancies caused by the oxygen absorption band (755 nm), ASAS bands from 663-744 nm were used for comparison of nadir to off-nadir red edge curves. The charts of the atmospherically corrected, but not normalized data (Figures 3-1 and 3-3), reveal the brightness gradient that is formed by more sharply increasing reflectance values at successively longer wavelengths along the red edge curve as the view angle approaches the *hotspot* view angle, +33° (solar zenith angle). The normalization

procedure removes variability caused by the backscatter effect, while preserving the shape and wavelength position of the red edge curve. In Figures 3-2 and 3-4 the

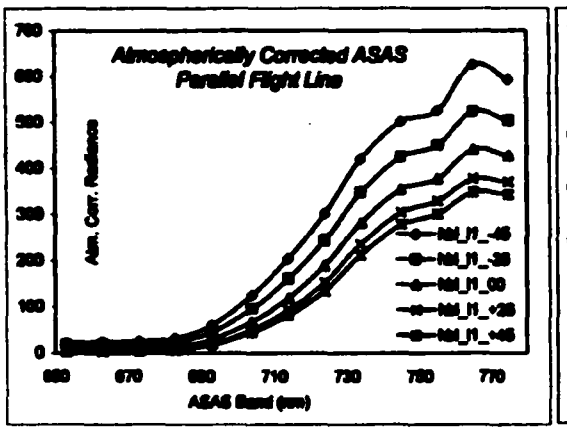

Figure 3-1. Red edge curves for 5 view angles. Atmospherically corrected, parallel ASAS flight line for undamaged site.

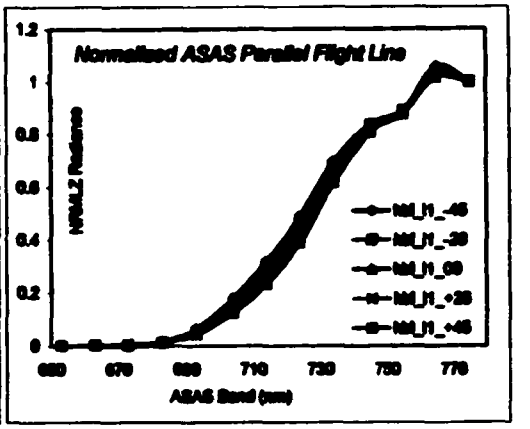

Figure 3-2. Red edge curves for 5 view angles. Normalised, parallel ASAS flight line for undamaged site.

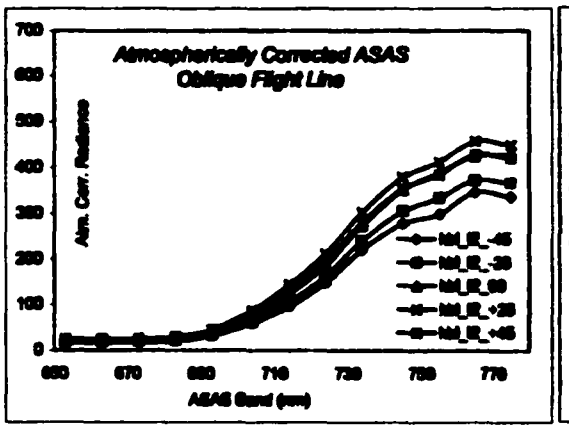

Figure 3-3. Red edge curves for 5 view angles. Atmospherically corrected, oblique ASAS flight line for undamaged site.

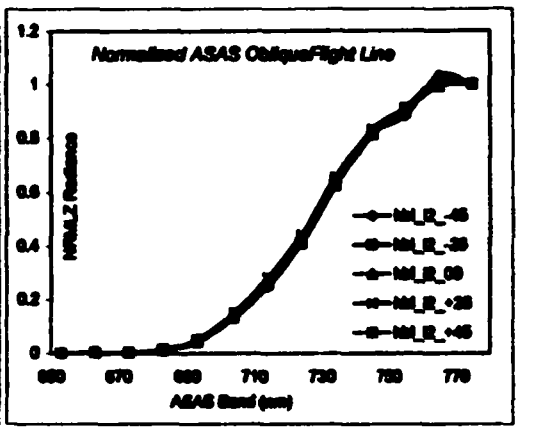

Figure 3-4. Red edge curves for 5 view angles. Normalised, oblique ASAS flight line for undamaged site.

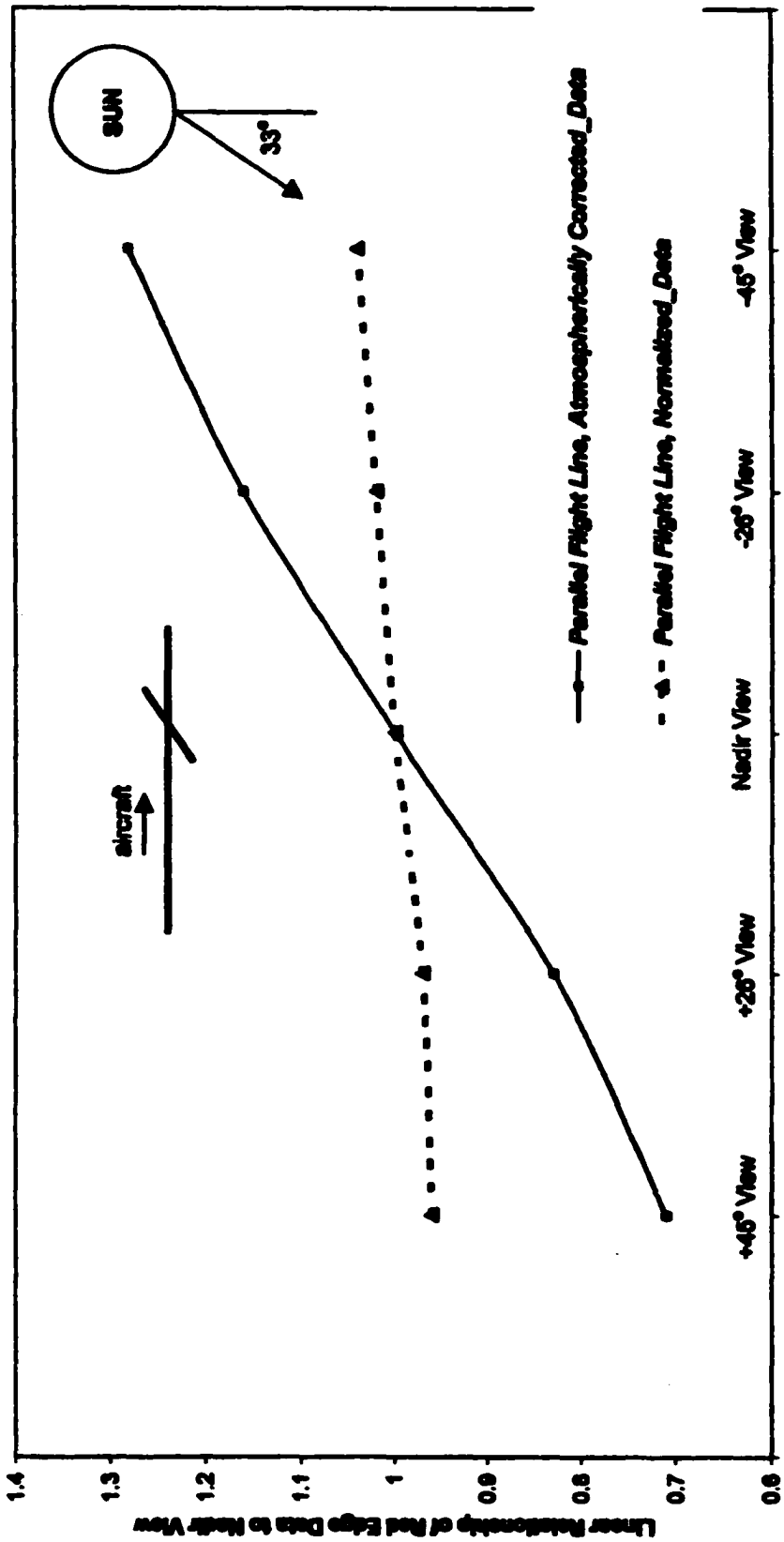

Figure 3-5. Backscatter Effect of Atmospherically Corrected and Normalized ASAS Data
Parallel Flight Line, Forward-Looking Views (+) in Backscatter Position
18m x 18m Undamaged Site

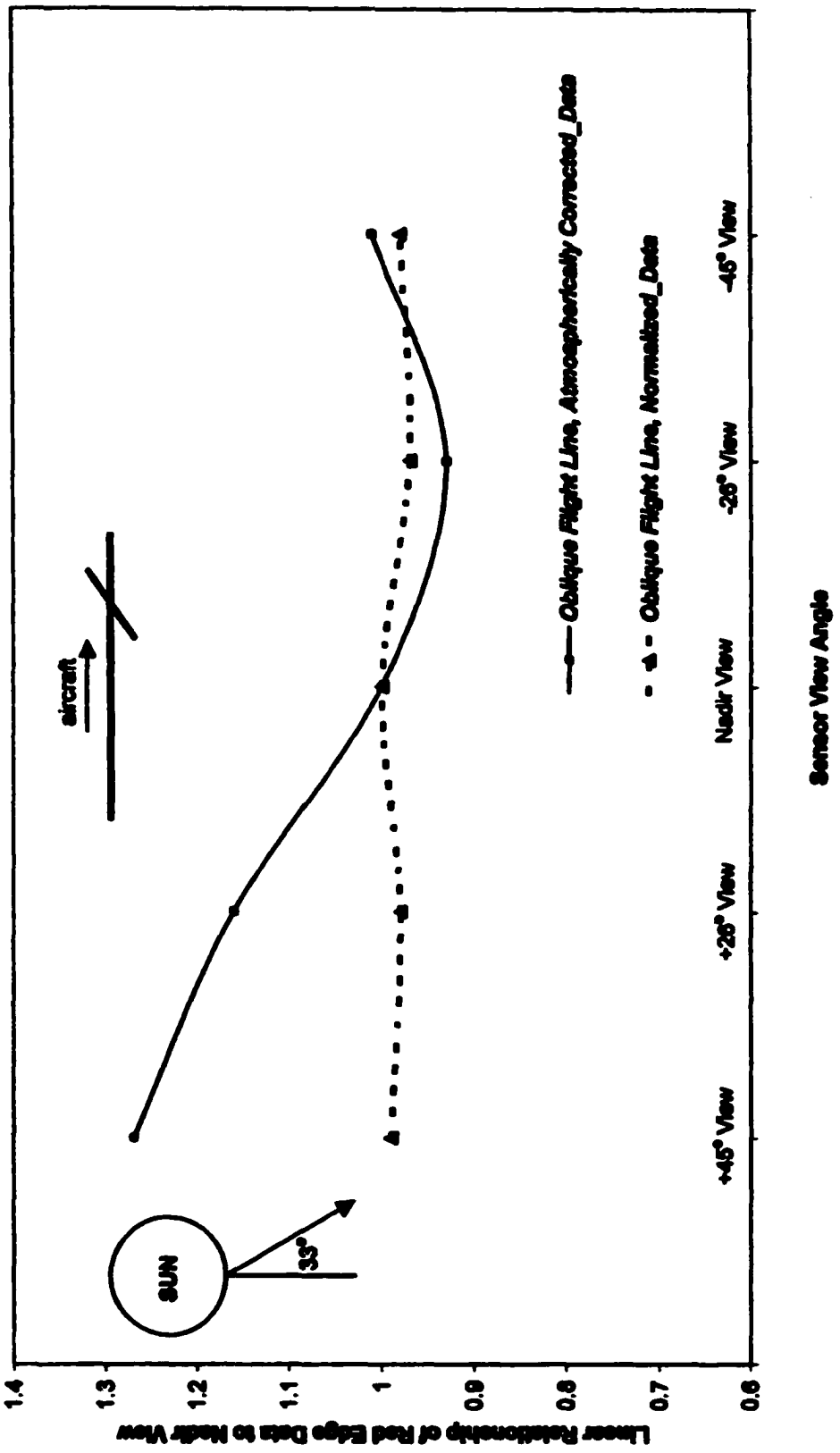

normalized curves are similar in shape and slope. Removing the backscatter effect does not eliminate all the variability resulting from multiangle viewing. Residual variability can be measured by regressing the red edge reflectance values or red edge curve data for a given off-nadir view to those of the nadir view, before and after the normalization procedure. The regression coefficient, or the slope of the best-fit regression line, (Zar, 1996) for pre- and post-normalization regressions vs. nadir, can be compared for each view angle in order to determine the amount of variability that is not explained by the backscatter effect. In Figures 3-5 and 3-6, red edge data sets are referred to in the y-axis label. Red edge data are the reflectance values by band wavelength for a view angle dataset that define the slope and shape of its red edge curve. These data are regressed against corresponding values for the nadir view and the resulting regression coefficient is the y-axis value for that view angle in the chart. A regression coefficient of 1 would indicate a 100% correction to nadir with removal of the backscatter effect. A slope greater or less than 1 indicates that other factors contributed to the variability between the normalized red edge values of the off-nadir and nadir datasets.

The results are depicted in Figures 3-5 and 3-6. The level of variability between off-nadir and nadir datasets is significantly reduced by the normalization procedure, as indicated by the relatively flat (dashed) curve that connects the values of the linear relationship between the normalized off-nadir vs. nadir views (which are all relatively close to 1) and the tilted solid curve connecting the un-normalized values. Table 3-2 lists the values of these relationships more precisely and the percent of the variability between off-nadir and nadir views that is explained by backscatter effect.

Table 3-2. Percent Variability of Off-Nadir from Nadir ASAS Datasets

Explained by Backscatter Effect for Parallel and Oblique Flight Lines

PARALLEL FLIGHT LINE View Angle	+45°	+26°	00°	-26°	-45°
Regression Coefficient to Nadir View Atm. Cor. Data	0.71	0.83	1	1.16	1.28
Regression Coefficient to Nadir View Nrmlz Data	0.96	0.97	1	1.02	1.04
% Variability Explained by Backscatter Effect	86%	82%		88%	86%
OBLIQUE FLIGHT LINE View Angle	+45°	+26°	00°	-26°	-45°
Regression Coefficient to Nadir View Atm. Cor. Data	1.27	1.16	1	0.93	1.01
Regression Coefficient to Nadir View Nrmlz Data	0.99	0.98	1	0.97	0.98
% Variability Explained by Backscatter Effect	96%	88%		57%	-100%

For example, the regression coefficient of the -26° parallel view to the nadir view is corrected from 1.16 to 1.02 or 88%. Overall, regression coefficients for normalized off-nadir datasets range from 1.04 to 0.96 (+/- 4%) from nadir datasets. Once the backscatter effect is removed, the slope, shape, and position of the red edge curves of spectral features of off-nadir datasets for undamaged hardwood canopies are not significantly different from those viewed at nadir.

It is noteworthy that the slope of the linear relationship (regression coefficient) between the red edge data for off-nadir and nadir views is related to the size of the phase angle created between the sun, target, and sensor: the smaller the phase angle, the more intense the backscatter effect, and the steeper the slope of the linear relationship. It is also significant that for all normalized view angle data (except two oblique flight line view angles, +26° and +45°), from 82-88% of the variability between the off-nadir and nadir datasets on the parallel flight line are explained by backscatter effect. In the case of the +26° view, its un-normalized red edge slope was very close to that of nadir, the regression coefficient to nadir = 0.93. Though the normalization corrected the slope of the curve to 0.97, this represented a small change, 57%, relative to other view angle corrections. In the case of the +45° view, it appears that the correction overcompensated for the backscatter effect and overcorrected the data. Overall, after the normalization procedure is performed on multiple angle red edge datasets, the difference in the regression coefficient between the off-nadir and nadir data is reduced to +/- 4% making it possible to compare the red edge features of variously damage study sites from multiple viewing angles.

As was demonstrated by Russell et al. (1993) un-normalized reflectance in the red region is view dependent and angular effects on NDVI are high. If datasets from various view angles are to be compared for variability in red edge features, it is best to normalize the data first. However, if the intention is to detect changes in reflectance in the red edge region due to variability in BRDF for a series of multiple angle views, it is best not to normalize the data. The variability provided from a series of un-normalized views can be

used as a set or composite to detect land cover types and features. The normalized approach was utilized for this study.

Nadir vs. Off-Nadir Viewing Damage Measurement Effectiveness

The effectiveness of normalized off-nadir red edge spectral features to measure ice storm damage was compared to normalized nadir datasets. ASAS scenes from both parallel and oblique flight lines are listed in Table 3-3:

Table 3-3. Flight Lines for Off-Nadir Analysis

Bartlett Light	Parallel
Bartlett Severe	Parallel
Hubbard Brook Light	Oblique
Hubbard Brook Moderate	Oblique
Hubbard Brook Severe	Parallel
Jefferson Notch Moderate	Oblique
Pine Mountain Severe	Oblique

Due to distortions in off-nadir scenes caused by pixel smearing and foreshortening, it was not practical to use 7.5 x 7.5 m study sites, as it was for the nadir view study (Chapter II). It was possible to represent corresponding sites from nadir images using 90 x 90 m study sites.

First, study sites (90 x 90 m) were located in georeferenced ASAS nadir imagery using a vector layer of GPS points collected at the field sites. Clusters of four 400 m^2 sites from within a 90 x 90 m area were averaged and used to represent the ice damage measured *in situ*. Sites were located in non-georeferenced +/-45° and +/-26° view angle images by identifying the corresponding tree crown and shadowing patterns of study sites

in the nadir image for a set of off-nadir images from a given flight line. The number of 90 x 90 m sites within each off-nadir scene varied depending on the quality and coverage of the imagery. The +45° view of Bartlett Light was defective and unusable. Table 3-4 shows the number of study sites for each target area and view angle.

Table 3-4. Number of Study Sites by Target Area and View Angle

View Angle	+45°	+26°	00°	-26°	-45°
Target Area					
Bartlett Light	0	13	12	7	6
Bartlett Severe	1	2	6	0	6
Hubbard Brook Light	6	7	6	7	7
Hubbard Brook Moderate	7	7	7	7	7
Hubbard Brook Severe	9	9	9	9	9
Jefferson Notch Moderate	2	6	6	6	6
Pine Mountain Severe	9	9	9	9	9
	34	53	55	45	50

When differentiating 3 levels of damage using ANOVA it is important to have a relatively balanced number of sites in each damage class (Zar, 1996). The Light class for +45° is the only category that falls short in this regard. As mentioned above, the Bartlett Light +45° image, which would have contributed 7 Light sites, was defective and unusable. Table 3-5 lists the number of study sites by damage class for each view angle.

Table 3-5. Number of Sites by Damage Class for Off-Nadir and Nadir Views

View Angle	Light	Moderate	Severe	N =
+45°	6	12	16	34
+26°	19	17	17	53
Nadir	19	17	19	55
-26°	15	14	16	45
-45°	14	17	19	50

Values of 714nr were used to differentiate 3 levels of damage – Light, Moderate, and Severe – and ANOVA and Tukey tests were applied as was done in the nadir study (see Chapter II). Nadir, -26°, and +45° views had unequal group means ($P < 0.001$), as shown in Table 3-6.

Table 3-6. Results of One-Way ANOVA for the 714nr by Damage in 3 Levels for 5 View Angles

View Angle	P-Value	R^2 =	N =
+45°	< 0.001	0.56	34
+26°	0.026	0.13	53
Nadir	< 0.001	0.31	55
-26°	< 0.001	0.29	45
-45°	0.005	0.20	50

In addition to having group means separate from the overall sample population, the 714nr for the +45° view had the strongest correlation with *in situ* measurements of damage, R^2

= 0.56. The Tukey test for significant difference between pairs of damage classes showed that the nadir and –26° views differentiated the Severe class from Light and Moderate classes. The +45° view was the only view able to distinguish all pairs of damage classes, including Light from Moderate. Figures 3-7, 3-8, and 3-9 show the summarized results of the Tukey Test for the nadir, -26°, and +45° views. Detailed results are for all view angles are listed in the Appendix (Figures A-2 to A-6).

The results of the nadir view using 90 x 90 m sites are similar to those for the nadir view using 210 sites (7.5 x 7.5 m) in Chapter II. The damage group means for the nadir view are not the same and the Severe class mean is significantly different from the Light and Moderate means. The general trend for the series of off-nadir views is to differentiate between classes more effectively as view angle approaches the nadir position, with the exception of the +45 view (see Table 3-6). If accepted as valid, this general trend of more effective differentiation between damage classes as the view angle approaches nadir would reject the working hypothesis that off-nadir views provide increased access to damage symptoms on the sides of tree crowns and on the edges of damaged canopy patches. There are a number of factors that should be considered before the positive results for the +45° view invalidate this trend.

One of the objectives of this study is to develop an ice damage detection scheme that is simple and practical to apply. The processing and analysis of off-nadir views adds complexity to the development of an ice damage detection tool. With each level of complexity and processing the opportunity for introducing errors that would affect results increases. There are 2 reasons why the results of the +45° view should be viewed with

Figure 3-7. ANOVA and Tukey Test Results for Nadir 714nr by Damage, 90 x 90 m Sites, N = 55 (From SAS Institute, Inc., 1997. *JMP IN*, Version 3.2.1.)

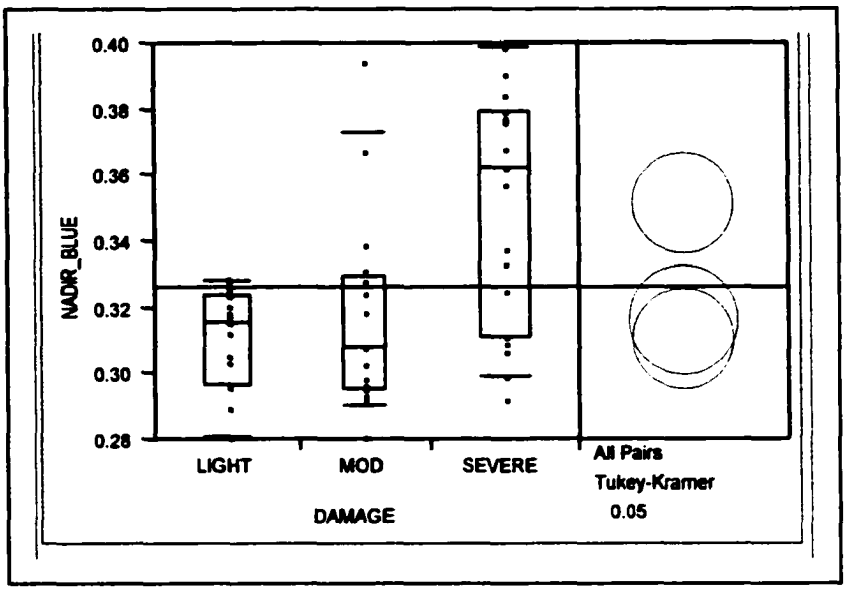

Figure 3-8. ANOVA and Tukey Test Results for ASAS -26° View 714nr by Damage, 90 x 90 m Sites, N = 45 (From SAS Institute, Inc., 1997. *JMP IN*, Version 3.2.1.)

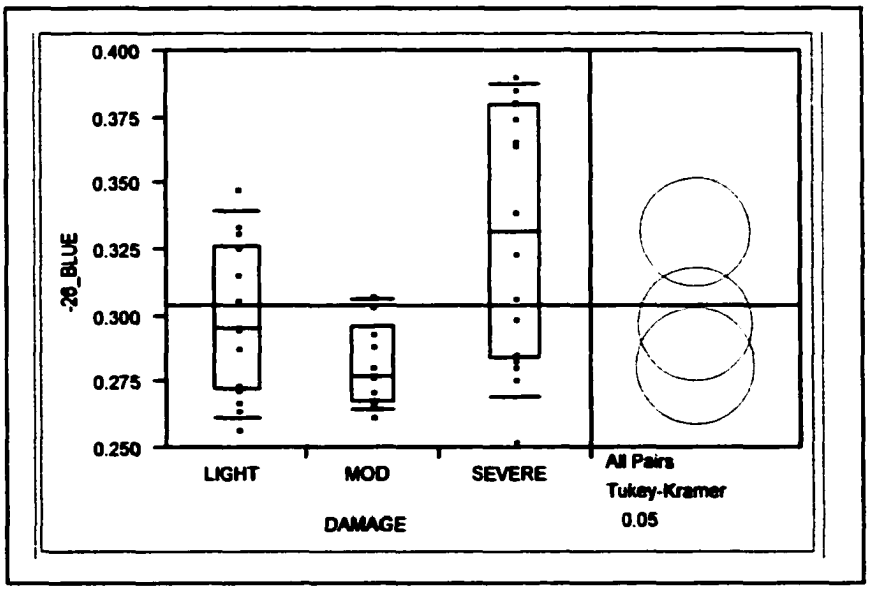

Figure 3-9. ANOVA and Tukey Test Results for ASAS +45° View 714nr by Damage, 90 x 90 m Sites, N = 34 (From SAS Institute, Inc., 1997. *JMP IN*, Version 3.2.1.)

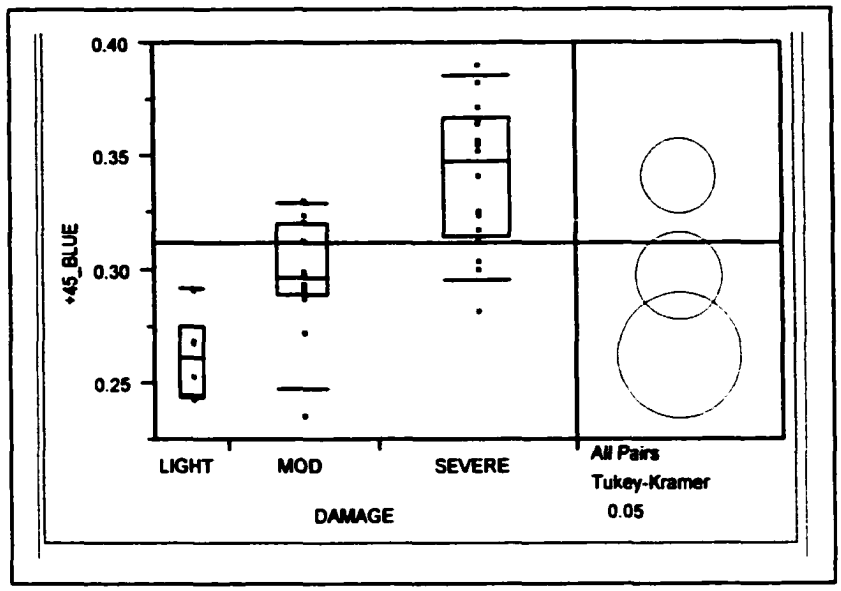

skepticism: the questionable accuracy of study site location for view angles +45° and greater and the small number (6) of study sites representing the Light class.

It was more difficult to locate study sites in scenes as view angle increased, particularly for the forward-looking (positive) views. The C-130 aircraft was equipped with a GPS-based instrument that located a given site on the ground (center of a target area) by its latitude and longitude on a screen in the cockpit. The pilot could then manually adjust the approach of the aircraft to fly over the center of the target area on a prescribed heading either parallel or oblique to the solar azimuth. Once this heading was established toward the target center, features of the actual site were identified visually in order to confirm the target area location. Because an effort was being made to verify the actual target center from visual clues on the approach to the target, it was more likely for

corrections to be made at the beginning of the approach during the sensing of wide-angle, forward-looking views. As any manual corrections were made to direct the aircraft toward the target, pixel smearing would occur leading to image distortions. Because the distance from the sensor to the target was greater at increased view angle, these distortions were magnified when any slight adjustment redirected the sensor. By contrast, at the nadir position the sensor was closer to the target area and more stable since the target center had been located and the flight line firmly established and the image was subject to less distortion. Distortions in +45° views made it more difficult to match a site location within the off-nadir scene with its corresponding site in the georeferenced nadir image. The opportunity for error in site location was greatest for the +45° view at each target area. In addition, some study sites in the +45° scenes were simply not visible in the image because they were hidden behind topographic features, such as ridges. This reduced the number of sites in the data sample.

The sample size for the +45° view was further reduced because the Bartlett Light scene was defective and unusable. This resulted in the Light class having only 6 study sites, while the Moderate and Severe classes had 12 and 16 respectively making the overall number of sites for the +45° view 34. This sample size is significantly less than the average sample size for the other views, an average of approximately 50.

It has been demonstrated that nadir values of 714nr do not differentiate the Light from the Moderate damage class effectively. Because the +45° view has fewer (6) Light reference sites to classify than the other views (14 to 19 Light sites), it can be assumed that by avoiding the more difficult task of having to classify more Light reference sites its overall ability to classify sites correctly is improved.

Application of ASAS imagery makes it possible to test the effectiveness of multiangle viewing to differentiate levels of damage caused by a severe canopy disturbance such as a major ice storm. It was hypothesized that off-nadir views could better detect damage to the sides of tree crowns from their side-looking perspective and detect ice damage symptoms that the nadir view would miss. The results of the study, however, demonstrate that the best view into canopy gaps is from the nadir perspective, from which materials other than healthy green vegetation can be detected and revealed by values of 714nr. This is especially true in the case of damaged hardwood stands. Ice accumulates on branches until the added weight snaps them off or, in the case of birch trees, bends them over. Woody debris accumulates on the ground below the gaps created in the tree crowns. The nadir-viewing sensor can view directly downward into gaps in the canopy and detect woody debris and other non-green vegetative materials symptomatic of ice damage that off-nadir views miss. Off-nadir views fail to detect the materials below the canopy and on the ground within gaps because they are hidden by remaining sections of the canopy that surround the gaps in all but the most severely damaged sites.

The normalization procedure does not provide a perfect correction for all sources of variability and differences between normalized off-nadir and nadir curves remain. Most of these differences can be attributed to sample error. It is not possible to select exactly the same surface area from each of 5 view angles. The ground area detected within a pixel changes increasingly as the view angle widens. Though the canopy at the undamaged site was technically closed, inevitably there are small gaps between leaves that expose other surface materials at certain view angles and not others. In addition, though care was taken to include only those pixels in the image that were included in the

undamaged crowns of a study site and though the spatial resolution of the imagery was very high (2.5 m), some pixels may have overlapped segments of crown edge and included reflectance signals from outside the study site. This is particularly hard to avoid at wider viewing angles.

Bi-directional reflectance distribution function (BRDF) is the measure of unique anisotrophy of a surface material and is a potential error-producing factor in spectral measurements viewed from various angles. BRDF varies with view angle and wavelength and is useful for identifying cover types. In all likelihood, BRDF did not contribute significantly to the spectral variability in this study because the BRDF for hardwood species in the study area is relatively consistent.

Conclusions

In light of past research on the *hotspot* phenomenon, it is not surprising that the normalization of the hyperspectral ASAS data to the red edge range from the chlorophyll well (653 nm) to the near infrared shoulder (775 nm) effectively removes the variability resulting from the backscatter effect. In this study, after normalizing the red edge features of off-nadir scenes, the difference in the regression coefficient between the off-nadir and nadir data is reduced to +/- 4% making it possible to compare the red edge features of variously damage study sites from multiple viewing angles.

Hypothesis 3-1: That red edge features of normalized ASAS datasets are not affected by sensor view angle is supported.

Though off-nadir viewing is useful for differentiating land cover types, stand structure, and in other applications that require more information pertinent to a

comprehensive spectral picture of canopy albedo, it is not as effective as nadir datasets for differentiating levels of ice storm damage to hardwood forest canopies using the 714nr as an indicator of damage symptoms. This study demonstrates that the nadir perspective is the simplest and most practical method for assessing ice storm damage. The nadir perspective is positioned to view directly into canopy gaps created by ice damage to hardwood crowns and to detect woody debris and other non-green vegetative materials within them.

Hypothesis 3-2: That measurements of the 714nr for off-nadir hyperspectral ASAS imagery of variously ice damaged hardwood sites (90 x 90-meter sites) are more effective than nadir imagery at differentiating 3 levels of ice damage to hardwood forest canopies is rejected.

CHAPTER IV

714nr VS. BROADBAND MEASUREMENTS

Introduction

In this study the ability of hyperspectral ASAS information to assess ice storm damage to hardwood forest canopies is compared to traditional broadband methods using Landsat TM imagery. First, VI, NDVI, and TM 5/4 indices are applied to study sites in a post-event (August 1998) TM image and these results are used to map 3 levels of damage. The accuracies of these classification maps are compared to the 714nr classification map results. Second, 714nr results are compared to TM VI, NDVI, and TM 5/4 change detection studies using pre- and post-event Landsat TM scenes to differentiate and map 3 levels of damage to forest canopies for corresponding study sites in the WMNF. Finally, the effectiveness and practicality of using Landsat imagery with and without change detection methods for differentiating 3 levels of ice damage is discussed.

The following hypotheses are tested:

4-1. Measurements of VI, NDVI, and TM 5/4 for a post-event Landsat TM scene (August 1998) of variously ice damaged hardwood sites (90 x 90 m sites, N = 66) are more effective than 714nr values (7.5 x 7.5 m sites, N = 210) for differentiating and mapping 3 levels of ice damage to hardwood forest canopies.

4-2. Measurements of VI, NDVI, and TM 5/4 applied to pre- and post-event Landsat TM scenes (August 1996 and 1998) of variously ice damaged hardwood sites (90 x 90 m sites, N = 66) using change detection are more

effective than nadir 714nr values (7.5 x 7.5 m sites, N = 210) at differentiating and mapping 3 levels of ice damage to hardwood forest canopies.

Materials and Methods

ASAS Data

The effectiveness of the 714nr to differentiate and map 3 levels of ice damage is compared to broadband methods using Landsat TM data. The results of one-way ANOVA and Tukey tests for the nadir 714nr and the accuracy of 714nr classification maps are used for comparison. The hyperspectral capability of the ASAS sensor was used to measure fine features of the red edge for representing blue shifts for 210 study sites (7.5 x 7.5 m) in the WMNF. It was determined that the 714nr can differentiate the Severe class from the Moderate and Light classes and map 3 levels of damage with an overall accuracy of 54%. These results are compared to similar tests of broadband methods.

Landsat TM Study Area

The 9 target areas (1 km x 1 km) selected in the WMNF for the ASAS study are all located within one Landsat TM scene, Path 13, Row 29. The inset map in Figure 2-1 depicts the coverage of this TM scene and the larger map in the figure shows the location of the target areas. The target areas are listed in Table 4-1 by damage class.

Table 4-1. Nine Target Areas in the WMNF with general/approximate level of damage, aspect, slope, elevation, and forest type.

SITE	DAMAGE	ASPECT	SLOPE	ELEV	FOR. TYPE
Hubbard Brook	Light	NE	15%	600m	Hardwood
Hubbard Brook	Moderate	NE	26%	810m	Hardwood
Hubbard Brook	Severe	NE	44%	695m	Hardwood
Bartlett	Light	NE	19%	319m	Hardwood
Bartlett	Severe	NW	18%	600m	Hardwood
Jefferson Notch	Moderate	SE	16%	573m	Hardwood
Killkenny	Light/Mod	NE	8%	540m	Hardwood
Black Mountain	Moderate	SW	20%	777m	Softwood
Pine Mountain	Severe	W	27%	606m	Hardwood

Landsat TM Data Acquisition

Change detection studies can be limited in their effectiveness if care is not taken in acquiring appropriate imagery. Not only are pre- and post-event datasets required, but also atmospheric conditions at the time of acquisition should be similar for scenes that are compared. Solar radiance is scattered and absorbed by gases and aerosols on its path from the sun to the Earth's surface and back up to the sensor. Spectral signals are affected differently as atmospheric conditions change. Scenes used in change detection of forest canopy should be acquired during the same period of the growing season. Spectral reflectance signals vary, particularly in the NIR, as plants begin their seasonal growth, flush out, and approach senescence. In order to compare signals from two scenes, a minimal amount of spectral change should have occurred between the reflectance responses of surface materials that were unaltered during the time period between data acquisition. In addition, it is important to be sure that images are coregistered accurately and precisely (+/- <1 pixel).

For this study Landsat TM scenes (Path 13, Row 29) were obtained that cover northern New Hampshire and include all 9 target areas, which represented the forest canopy conditions prior to and following the January 1998 ice storm. Both scenes were acquired by Landsat 5 during the same seasonal period (August 30, 1996 and August 20, 1998) and under similar atmospheric conditions, with 0% cloud cover and minimal haze over the target areas. It is therefore assumed that the vegetation was phenologically similar for the two scenes.

Image Processing for Landsat TM Data

Landsat 5 scenes were obtained as Level I products - radiometrically and geometrically corrected. The bands that were used in this study were TM band 3 (0.63 - 0.69 μ), TM band 4 (0.76 - 0.90 μ), and TM band 5 (1.55 - 1.75 μ). A coregistration procedure was performed utilizing a series of ground control points. It was determined that the 1998 scene was coregistered to the 1996 scene with a residual mean square (RMS) of less than 1.0 pixel (30 x 30 m pixels). Because the WMNF contains diverse topography including rugged terrain that can make the georeferencing process problematic, DOQs (1 x 1 m pixels) were also used to check the accuracy of the TM registration, particularly in the target areas. The accuracy for the target areas was determined to be within 1.0 pixel. Because cloud cover existed in the northwest section of both scenes, which did not include the target areas, scene subsets were clipped from the full-size image to eliminate the clouds in this section of both scenes. Subsets of the 1998 and 1996 scenes were matched pixel-for-pixel (by corresponding coordinates) to ensure precise change detection analysis.

Reflectance values from the 1998 scene were normalized against the 1996 scene using clusters of pixels (polygons) from a series of four ground objects ranging in brightness from light to dark. Vogelmann and Rock (1989) applied this method effectively in a TM band differencing study of forest canopy damage caused by pear thrips. A total of approximately 1,000 pixels from areas of rock outcrops (light), undamaged deciduous stands (intermediate light), undamaged conifer stands (intermediate dark), and deep-water lakes (dark) were selected. Target objects were selected that appeared to have undergone minimal amounts of reflectance change. The mean reflectance value from each cover type for the 1998 scene was determined and regressed against corresponding 1996 values for TM bands 3, 4, and 5. The result defined a linear relationship between the reflectance values for the two scenes with a very strong correlation ($R^2 = 0.99$) for all three bands. The function defined by the linear relationship was applied to the 1998 reflectance values on a pixel-by-pixel and band-by-band basis, completing the normalization process. Following normalization, 3 vegetation indices were applied to the data, VI, NDVI, and TM 5/4, then univeriate image differencing (pixel-by-pixel subtraction) was used to measure changes that occurred during the two years between the acquisitions of the two scenes. No tree harvests were carried out by the Forest Service and no major disturbances, other than the 1998 ice storm, are known to have affected the forest canopy in any of the study areas (sites where *in situ* measurements were collected and from which image data were analyzed) during the two-year period.

Since TM5 measures leaf tissue moisture, it is important that general moisture levels are approximately the same at the time when different scenes are acquired for

change detection analysis. A false positive signal for ice storm damage could occur if the post-disturbance image was acquired during a very dry period (relative to the pre-disturbance image) or if the pre-disturbance scene was acquired during a very wet period (relative to the post-disturbance image). Measurements of precipitation recorded at Hubbard Brook Experimental Forest indicated that the total precipitation amounts for January-August 1996 and 1998 were approximately 46" and 41" respectively. For the purpose of this study, it is assumed that the forestland moisture conditions in the study area were not significantly different in late August of 1996 and 1998.

Broadband Vegetation Indices

Vegetation indices have been applied to landcover studies using broadband sensors since the early 1970s, with the advent of the Landsat MSS program. Since sensors, such as Landsat MSS and TM, do not acquire narrow-band (10+/- nm), red edge spectral data, the broadband (100+/- nm) Vegetation Index (VI) and NDVI, have been used to monitor crop conditions and to determine vegetation condition. These indices exploit spectral information from TM3 (630-690 nm) and TM4 (760-900 nm). Similar to the 714nr but on a coarser spectral scale, VI and NDVI are used to measure levels of green biomass. Both indices describe the relationship between amounts of absorbed radiance in the red band (TM3) and reflected radiance in the NIR band (TM4). Higher values for VI (TM4 / TM3) indicate higher levels of green biomass. NDVI (TM4 – TM3 / TM4 + TM3) applies values for a similar ratio of TM4 and TM3 but on a normalized scale from 0 to 1.

TM 5/4 (TM5 = 1,550-1,750 nm; TM4 = 760-900 nm) was used as a vegetation index in the 1980s. An assessment of the Visible/Infrared Intelligent Spectrometer (VIRIS) and the NS-001 Thematic Mapper Simulator (TMS) data acquired in field and laboratory studies led to development of an imaged equivalent of a moisture stress index for mapping forest damage to coniferous stands on Camels Hump, Vermont (Rock et al., 1986). Spectral reflectance data in the ratio 1.65/1.23 μm or 1.65/0.83 μm correlated well with forest damage. Images displayed using the Landsat TM 5/4 (1.65/0.83 μm) ratio, the 1.65 μm band, and the 0.66 μm band were found to clearly distinguish between high and low damage areas to high elevation softwood forests in Vermont and New Hampshire (Vogelmann and Rock, 1988) and hardwood forests in southern Vermont and northwestern Massachusetts caused by pear thrips (Vogelmann and Rock, 1989).

Field Methods

Field data collected for the ASAS study at 288 sites from within the nine target areas was used for the Landsat TM study. In the ASAS study one site (400 m^2) represented a study site on the ground. For the TM studies a cluster of 4 ASAS sites (7.5 x 7.5 m) within a 90 x 90 m area on the ground represented a study site. The average percent canopy damage for the 4 smaller sites within the 90 x 90 m area was used to represent the amount of damage in the larger study site. In the ASAS study 210 smaller sites were within the ASAS coverage. In the TM studies 66 larger sites were within the TM scene.

Results

Differentiating Canopy Damage Using Post-Event Scenes - 714nr vs. TM Vegetation Indices

The effectiveness of the 714nr method to measure ice damage was compared to Landsat TM data using a single post-event image to which VI, NDVI, and TM 5/4 were applied. The target areas and number of sites by damage class are listed in Table 4-2 for the TM study. The sample size is 66.

Table 4-2. Target Areas and Number of TM Sites by Damage Class

	Sites By Damage Class			
Target Area	Light	Moderate	Severe	Total
Bartlett - Light	11	2	0	13
Bartlett – Severe	0	3	3	6
Hubbard Brook - Light	7	1	0	8
Hubbard Brook - Moderate	0	7	0	7
Hubbard Brook - Severe	0	4	5	9
Jefferson Notch – Moderate	2	2	2	6
Kilkenny – Light/Moderate	5	2	1	8
Pine Mountain - Severe	0	0	9	9
Total Sampling	25	21	20	66

Each study site (90 x 90 m) was located within the TM scene using GPS points collected on the ground and represented by a 3 x 3-pixel window. Thirteen study sites not contained by ASAS imagery were covered by the TM scene and were included in the study. The average value for the 9 TM pixels (30 x 30 m) in each study site from the 1998 TM scene was determined for each of the 3 vegetation indices. One-way ANOVA and Tukey tests were applied to these data to determine the effectiveness of each index to differentiate three levels of canopy damage in the same fashion as applied to the 714nr.

As an added basis for comparison the 714nr for 90 x 90 m study sites (N = 53) were also determined and their effectiveness for differentiating canopy was tested. For this study, the 714nr for each 90 x 90 m site was determined as the average 714nr value for a 36 x 36-pixel window or approximately 1,300 pixels.

Figures 4-1 to Figure 4-4 summarize the results of the one-way ANOVA and Tukey tests for the 714nr (90 x 90 m) and TM VI, NDVI, and TM 5/4 indices (90 x 90 m). Detailed ANOVA and Tukey Test results are listed in the Appendix (Figures A-7 to A-10).

Figure 4-1. One-Way ANOVA and Tukey Test Results for the 714nr by Damage 90 x 90 m Sites, N = 53. The points represent 714nr values (vegetation indices values in subsequent charts). Values of 714nr are grouped according to their corresponding percent canopy damage measured on the ground (0-24.9% = Light, 25-49.9% = Moderate, 50-100% = Severe). The box-and-whisker plots for each group of points indicate the level up to which 10% (lower line), 25% (bottom of box), 50% (center of box), 75% (top of box), and 90% (upper line) of the data fall. The circles for the Tukey-Kramer test are centered on the mean 714nr value for each damage class. The size of a circle is determined by the variance from the group mean at the 95% confidence level. Separation between circles indicates a statistical difference between their means.

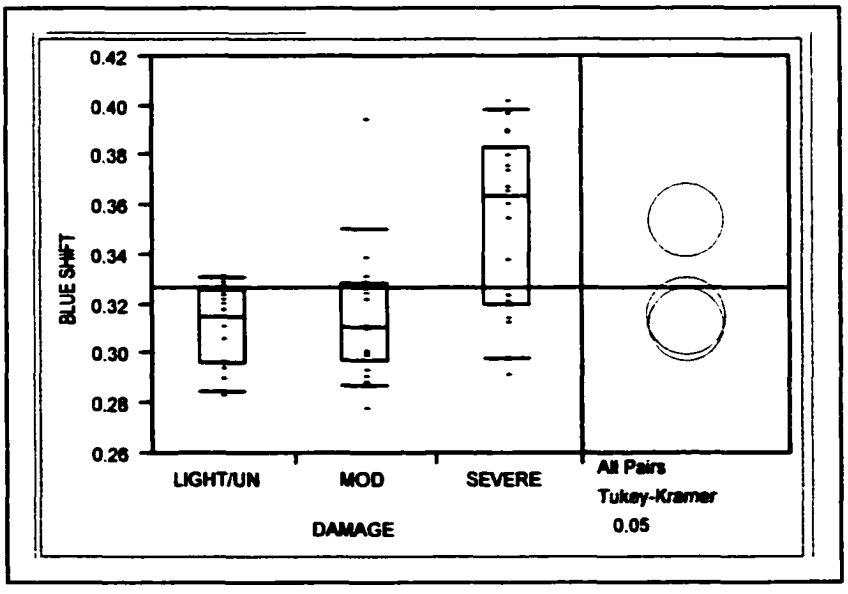

Figure 4-2. One-Way ANOVA and Tukey Test Results for TM VI by Damage 90 x 90 m Sites, N = 66

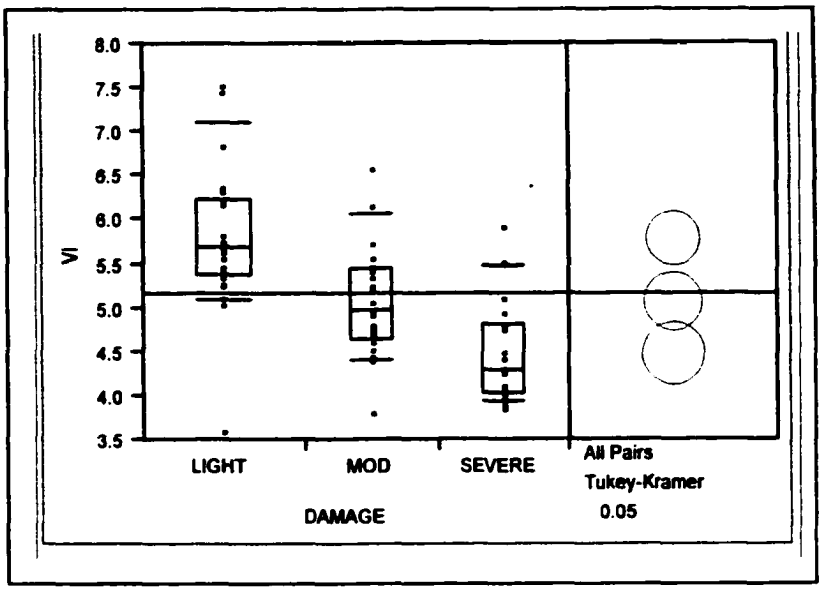

Figure 4-3. One-Way ANOVA and Tukey Test Results for TM NDVI by Damage 90 x 90 m Sites, N = 66

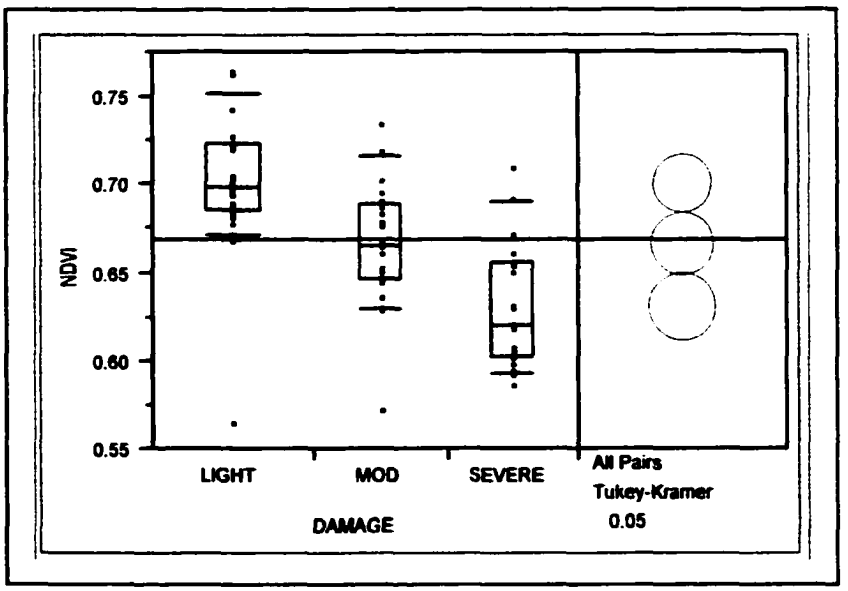

Figure 4-4. One-Way ANOVA and Tukey Test Results for TM 5/4 by Damage 90 x 90 m Sites, N = 66

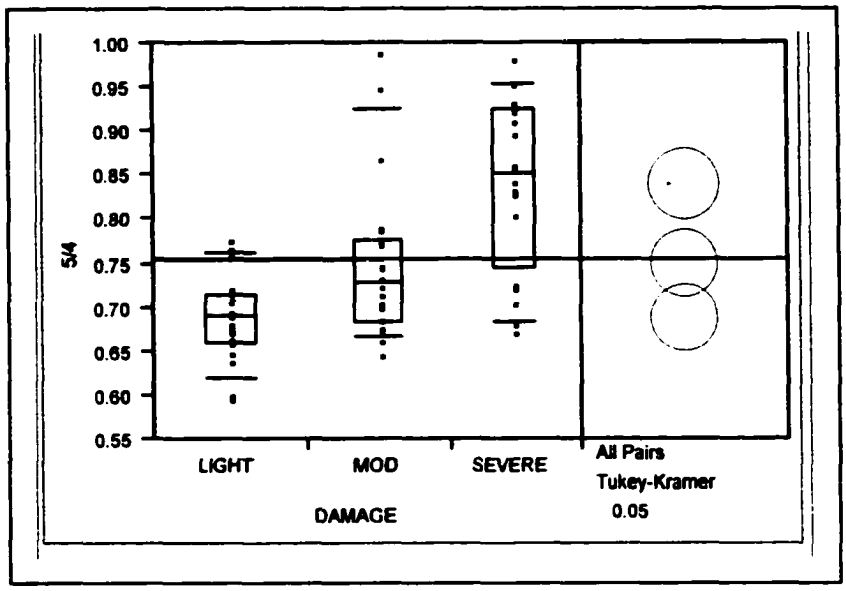

Similar to the 714nr results for 7.5 x 7.5 m study sites, the group means of 3 damage levels (Light, Moderate, and Severe) of the 714nr for 90 x 90 m study sites were not the same ($P < 0.001$) and the mean for the Severe damage class was significantly different from the mean for the Moderate and Light classes. The correlation between the 714nr and percent damage values or "goodness of fit" test, was stronger but not significantly different for the larger study sites than for the smaller sites, $R^2 = 0.35$ and $R^2 = 0.26$, respectively. The group means for all 3 TM indices were not the same ($P < 0.001$) and all pairs of damage class means were significantly different, including means for the Light and Moderate classes. The significant difference between damage classes is demonstrated visually by the degree of separation of the circles representing the 3 damage levels at the right in Figures 4-1 to 4-4 and by the positive separation values for

the groups in the chart at the bottom of Figures A-7 to A-10. It is possible for circles to overlap slightly, as they do for the Light and Moderate groups in Figure 4-4, and for their means to still be significantly different. The summary of these results is listed in Table 4-3.

Table 4-3. Results of One-Way ANOVA and Tukey Tests for the 714nr and TM VI, NDVI, and TM 5/4 (90 x 90 m Study Sites)

			Damage Level Differentiation L = Light, M = Moderate, S = Severe		
INDEX	P-VALUE	R^2 =	L from M	L from S	M from S
714nr	P < 0.001	0.35	No	Yes	Yes
TM VI	P < 0.001	0.40	Yes	Yes	Yes
TM NDVI	P < 0.001	0.40	Yes	Yes	Yes
TM 5/4	P < 0.001	0.40	Yes	Yes	Yes

Classification Mapping Using Post-Event Scenes – 714nr vs. TM Vegetation Indices

Results of the classification map differentiating 3 levels of canopy damage using the 714nr for a post-event ASAS scenes were compared to classification maps derived by applying 3 TM vegetation indices, VI, NDVI, and 5/4 to a post-event Landsat TM scene. A similar supervised classification procedure was applied to the TM vegetation indices images as was applied to the 714nr image. For the TM mapping, as for the ANOVA analysis above, study sites were 90 x 90 m in size. A 3 x 3-pixel window in the imagery (90 x 90 m) represented each study site on the ground. The percent damage for each site on the ground was determined as the average of 4 smaller study sites (7.5 x 7.5 m)

contained within its 90 x 90 m area. As listed in Table 4-1, there were 66 sites available for training or reference sites for the supervised classification procedure.

A supervised classification was applied to TM VI, NDVI, and 5/4 measurements for 66 sites (90 x 90 m) from 8 target areas. Pixels were classified into three comprehensive and mutually exclusive levels of ice damage – Light (0-24.9% damage), Moderate (25-49.9%), and Severe (50-100%). Six training sites were selected, using the systematic random method, to represent the Light class and 5 each to represent the Moderate and Severe classes. The 50 remaining sites were used as reference sites. Following the classification process the reference sites were used to check the accuracy of the classification map. The data were classified using the maximum likelihood resampling method.

Figures 4-5 to 4-13 show close-ups of the classification maps for the target areas for the 3 indices. These maps reveal a strong correlation between the known general level of damage for each target area and its corresponding classification group. Bold black circles identify the target areas in the maps and small black rectangles/dots represent sample plots (400 m^2).

Figure 4-5. **VI 1998** - Bartlett Light and Severe Supervised Classification Map
Ice Damage Levels: Gray = Light; Yellow = Moderate; Red = Severe
Black circle outlines = extent of reference sites within target area.
Small black rectangles/dots = reference sites.

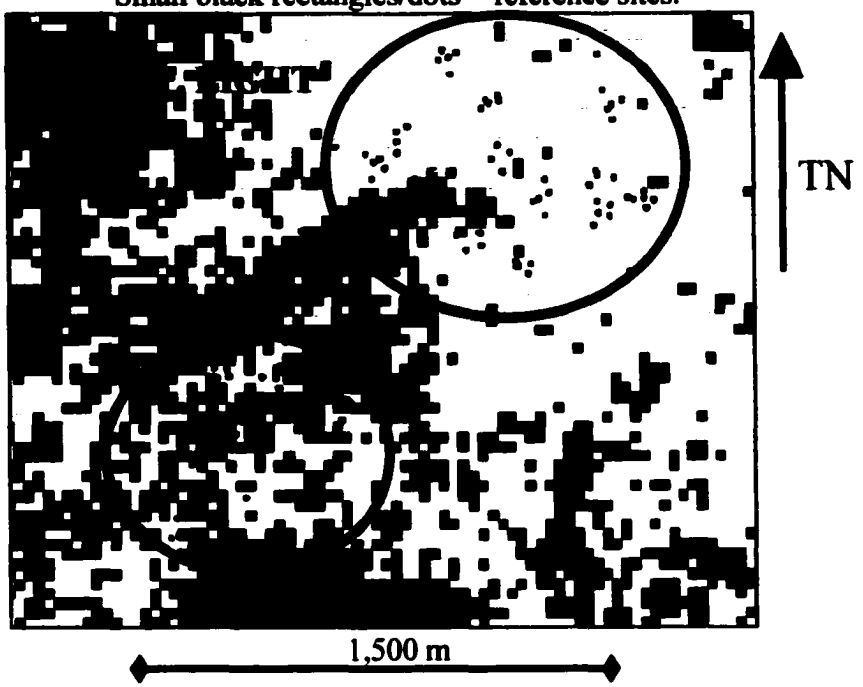

Figure 4-6. **VI 1998** - Hubbard Brook, Light, Moderate, and Severe
Supervised Classification Map Ice
Damage Levels: Gray = Light; Yellow = Moderate; Red = Severe

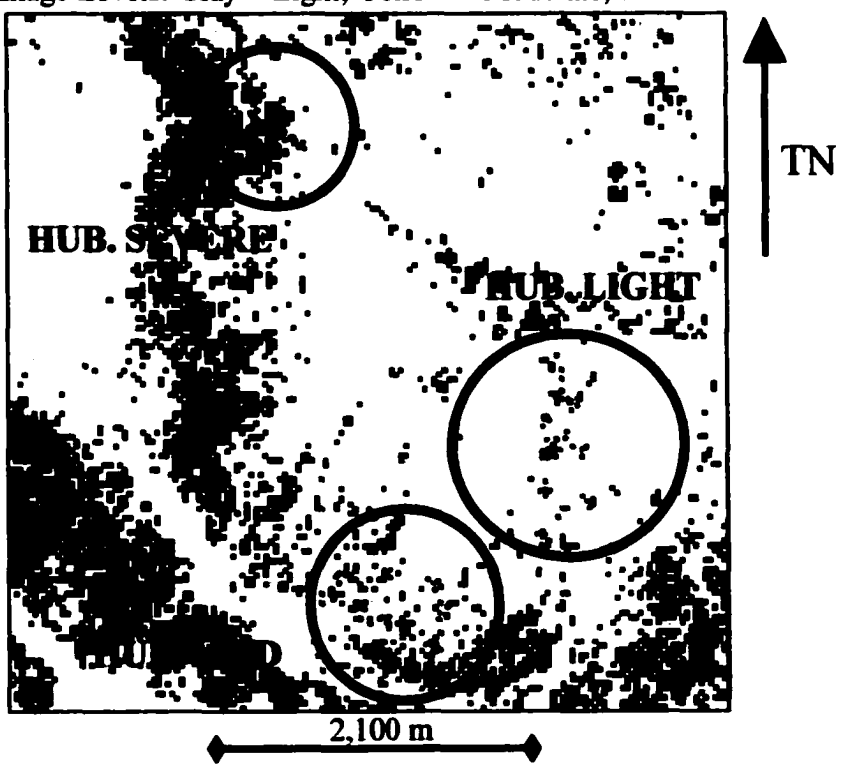

Figure 4-7. **VI 1998** - Jefferson Notch Moderate, Kilkenny Moderate, and Pine Mountain Severe Supervised Classification Map
Ice Damage Levels: Gray = Light; Yellow = Moderate; Red = Severe

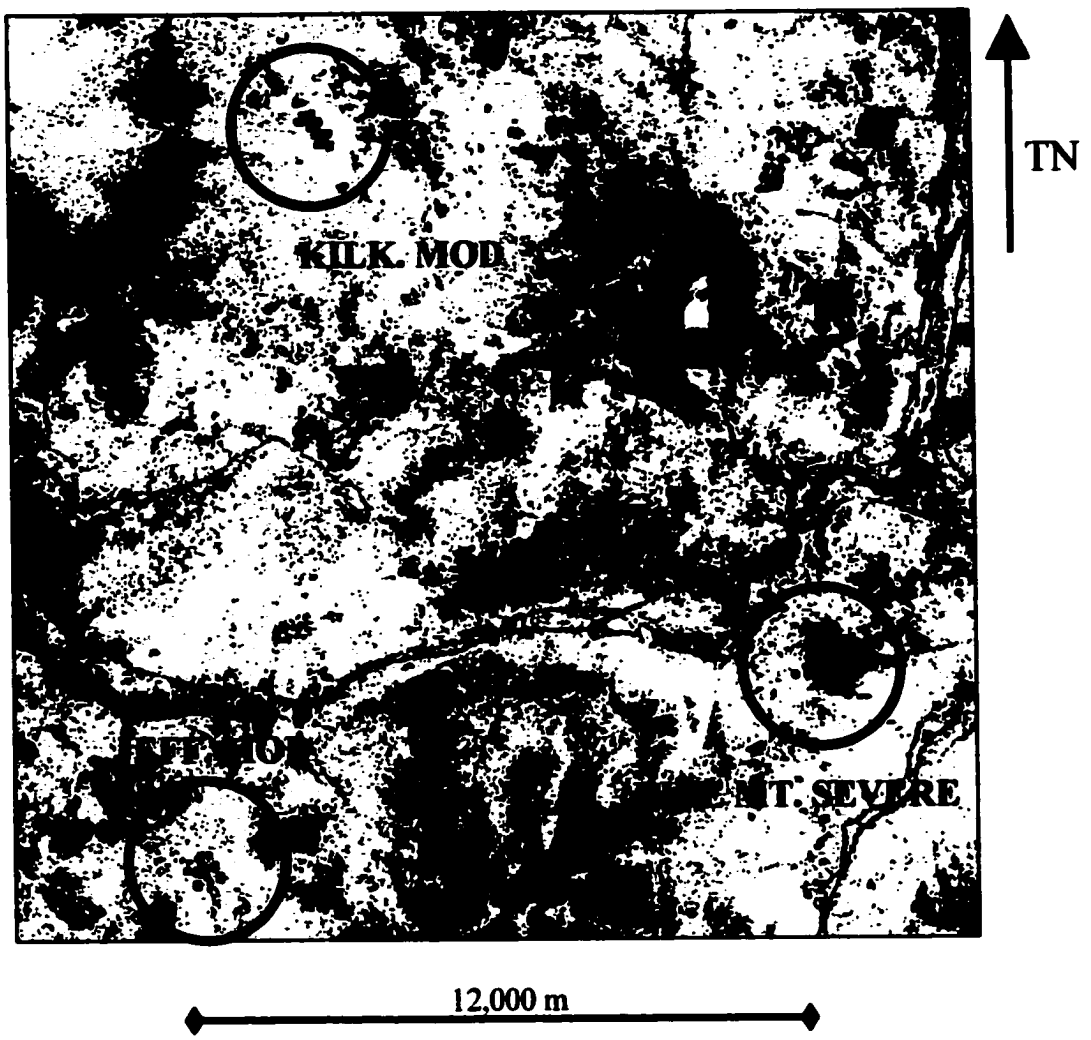

Figure 4-8. **NDVI 1998** - Bartlett Light and Severe Supervised Classification Map
Ice Damage Levels: Gray = Light; Yellow = Moderate; Red = Severe

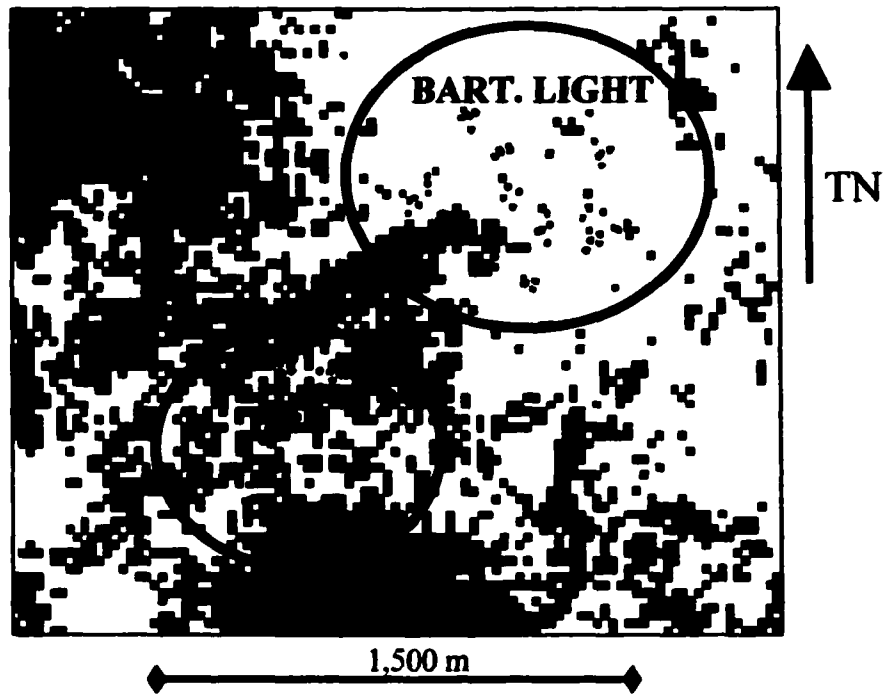

Figure 4-9. **NDVI 1998** - Hubbard Brook, Light, Moderate, and Severe
Supervised Classification Map Ice
Damage Levels: Gray = Light; Yellow = Moderate; Red = Severe

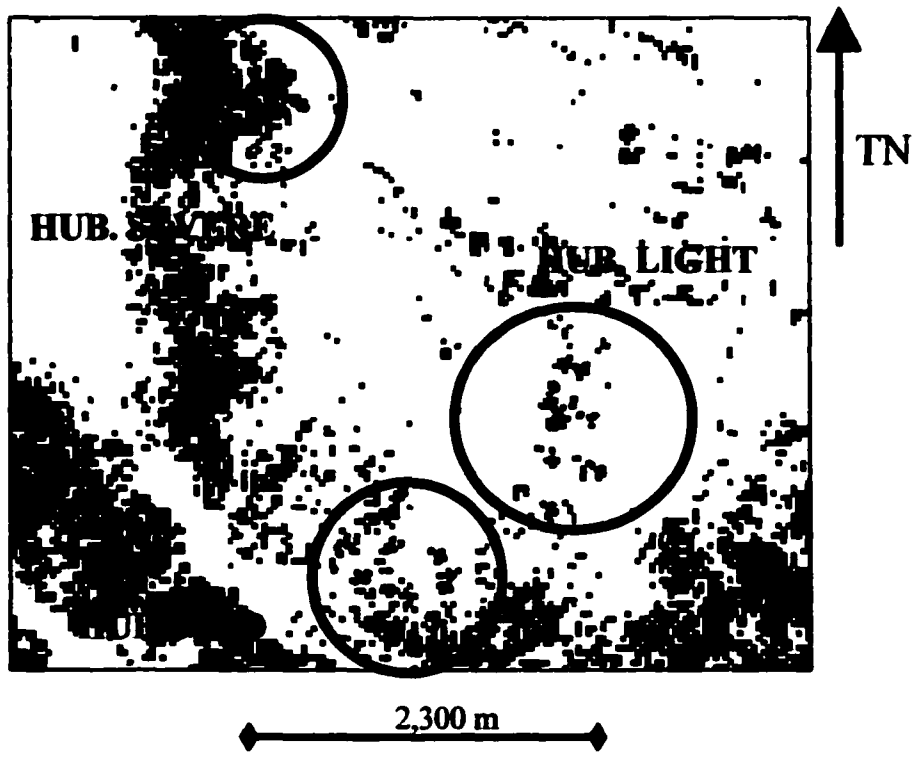

Figure 4-10. **NDVI 1998** - Jefferson Notch Moderate, Kilkenny Moderate, and Pine Mountain Severe Supervised Classification Map
Ice Damage Levels: Gray = Light; Yellow = Moderate; Red = Severe

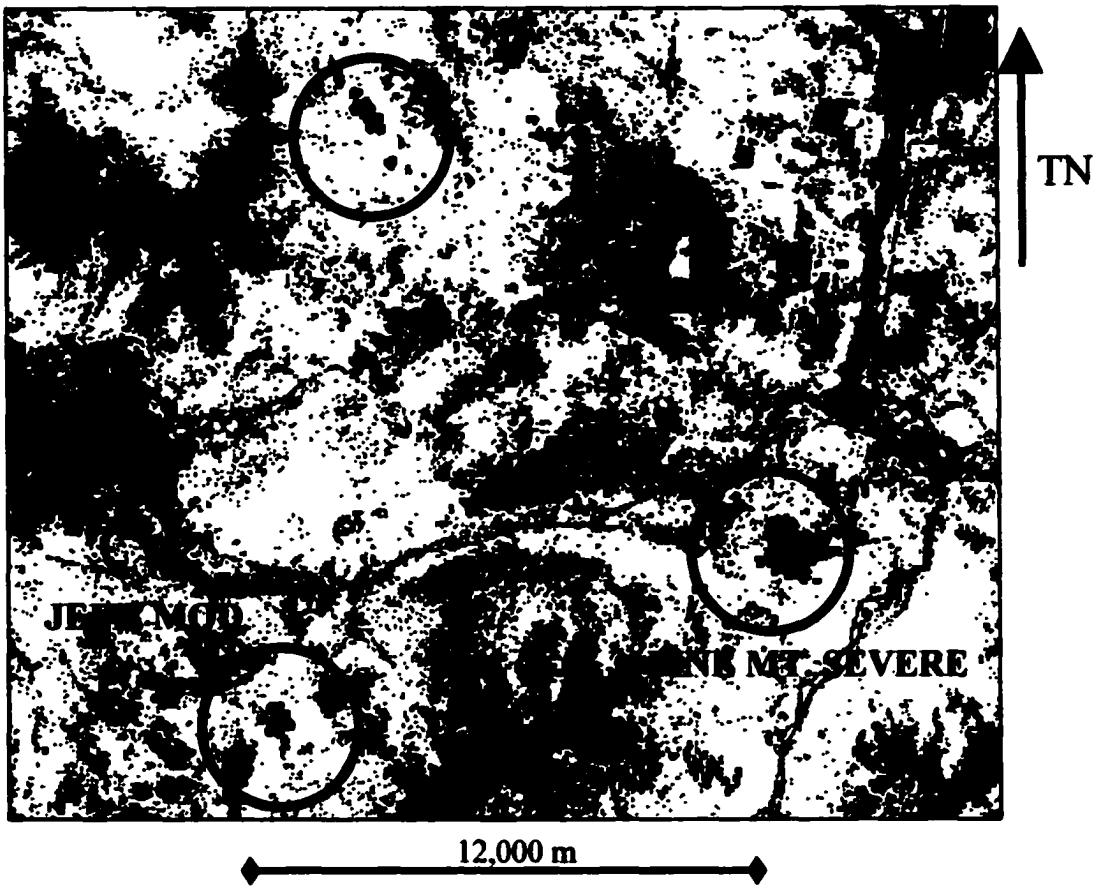

Figure 4-11. **TM 5/4 1998** - Bartlett Light and Severe Supervised Classification Map
Ice Damage Levels: Gray = Light; Yellow = Moderate; Red = Severe

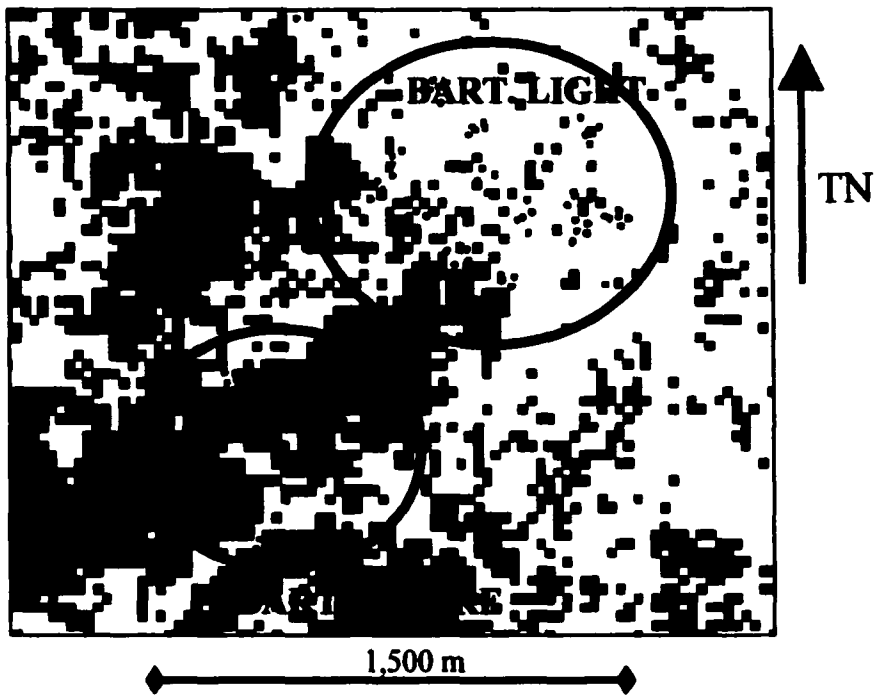

Figure 4-12. **TM 5/4 1998** - Hubbard Brook, Light, Moderate, and Severe
Supervised Classification Map Ice
Damage Levels: Gray = Light; Yellow = Moderate; Red = Severe

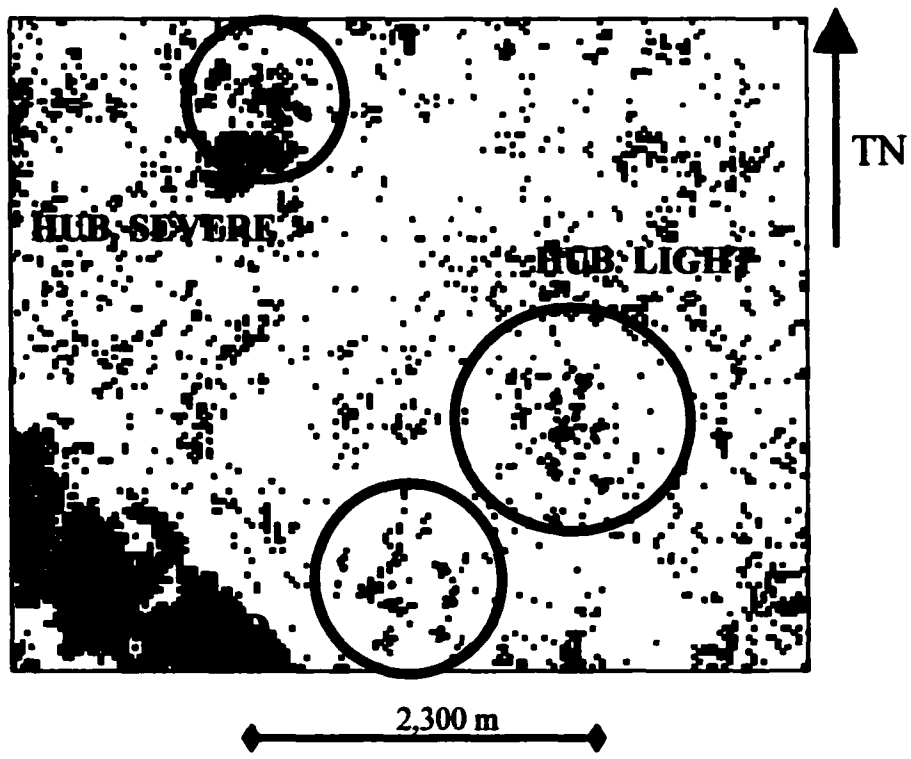

Figure 4-13. **TM 5/4 1998** - Jefferson Notch Moderate, Kilkenny Moderate, and Pine Mountain Severe Supervised Classification Map
Ice Damage Levels: Gray = Light; Yellow = Moderate; Red = Severe

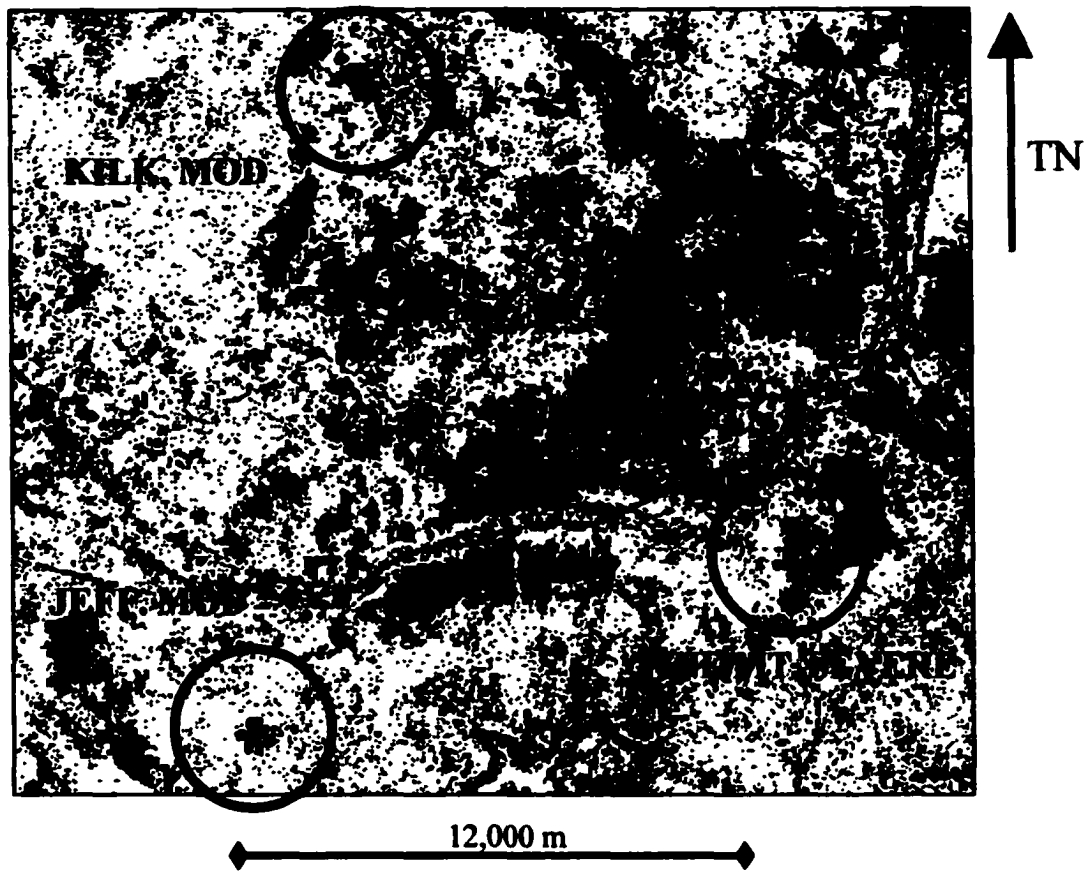

The error matrix accuracy assessment method was used to analyze these data more closely. Similar procedures were used in the error matrix analysis as were used for the 714nr classification map, including application of the modal and fuzzy classification rules (see Chapter II). The results of the error matrix assessment are shown in Table 4-4, below.

Table 4-4. Error Matrices for TM Vegetation Indices for 1998 Post-Event Canopy Damage Classification Maps (90 x 90 m Study Sites)

GROUND REFERENCE

VI INDEX		LIGHT	MODERATE	SEVERE	TOTAL	% USER'S ACCURACY
IMAGE CLASSIFICATION	LIGHT	13	6	1	20	65%
	MOD	5	10	3	18	56%
	SEVER	1	0	11	12	92%
		19	16	15	50	
PRODUCER'S ACCURACY		68%	63%	73%	OVERALL ACCURACY	68%

GROUND REFERENCE

NDVI INDEX		LIGHT	MODERATE	SEVERE	TOTAL	% USER'S ACCURACY
IMAGE CLASSIFICATION	LIGHT	16	5	3	24	67%
	MOD	2	10	2	14	71%
	SEVER	1	1	10	12	83%
		19	16	15	50	
PRODUCER'S ACCURACY		84%	63%	67%	OVERALL ACCURACY	72%

GROUND REFERENCE

5/4 INDEX		LIGHT	MODERATE	SEVERE	TOTAL	% USER'S ACCURACY
IMAGE CLASSIFICATION	LIGHT	17	6	4	27	63%
	MOD	0	10	0	10	100%
	SEVER	2	0	11	13	85%
		19	16	15	50	
PRODUCER'S ACCURACY		89%	63%	73%	OVERALL ACCURACY	76%

The overall accuracy of the 714nr post-event classification map was 54% (Chapter II). The error matrix results for all 3 TM indices demonstrate better overall accuracies than the 714nr: VI = 68%, NDVI = 72%, and 5/4 = 76%. That all 3 broadband indices classify levels of damage with greater accuracy for a single post-event scene than hyperspectral red edge features suggests that coarse resolution spatial and spectral information is better suited for differentiating levels of canopy damage symptoms caused by ice storms than hyperspatial and hyperspectral data. It is clear that the ability of broadband indices to distinguish Light from Moderate damage is the most important factor in its classification superiority. This is most apparent in the producer's accuracies (based on errors of omission) for the Light damage class for NDVI and 5/4, 84% and 89% respectively, as compared to 38% for the 714nr. Whereas TM indices were able to correctly classify Light sites approximately 85% of the time, the 714nr correctly classified Light sites less than half as well.

Differentiating Canopy Damage Using Pre- and Post-Event Scenes – 714nr vs. TM Vegetation Indices

The effectiveness of the 714nr method and the TM vegetation indices to differentiate levels of damage from single post-event scenes was compared to the results of a change detection study using pre- and post-event TM scenes to which VI, NDVI, and TM 5/4 were applied. As described in more detail above, the change detection image was created by normalizing the 1998 scene to the 1996 scene, applying 1 of the TM vegetation indices to the pre-event and post-event scenes, and subtracting, pixel-by-pixel, the index values for the 2 co-registered images.

The target areas and number of sites by damage class are the same as those listed in Table 4-2 for the post-event TM study. The sample size is 66. Study sites (90 x 90 m) were located and their values determined as in the post-event study. One-way ANOVA and Tukey tests were applied to these data to determine the effectiveness of each method to differentiate three levels of canopy damage with change detection.

Figures 4-14 to 4-16 show the summarized results of the one-way ANOVA and Tukey tests for change detection values for TM VI, NDVI, and TM 5/4 indices. Detailed results are listed in the Appendix (Figure A-11 to A-13). The plot charts showing the quartiles of the damage classes for the change detection analyses at the top of Figures 4-14 to 4-16 require explanation. In Figure 4-14 and 4-15, sites damaged more severely by the ice storm show a greater reduction in VI and NDVI values. This difference is plotted as a negative value. Thus, high negative values of change indicate more severe damage for VI and NDVI. In Figure 4-16, sites damaged more severely show an increase in 5/4 value. This change is plotted as a positive value. Thus, high positive values of change indicate more severe damage for 5/4.

Figure 4-14. One-Way ANOVA and Tukey Test Results for TM VI 1998-1996 Change Detection by Damage, 90 x 90 m Sites, N = 66

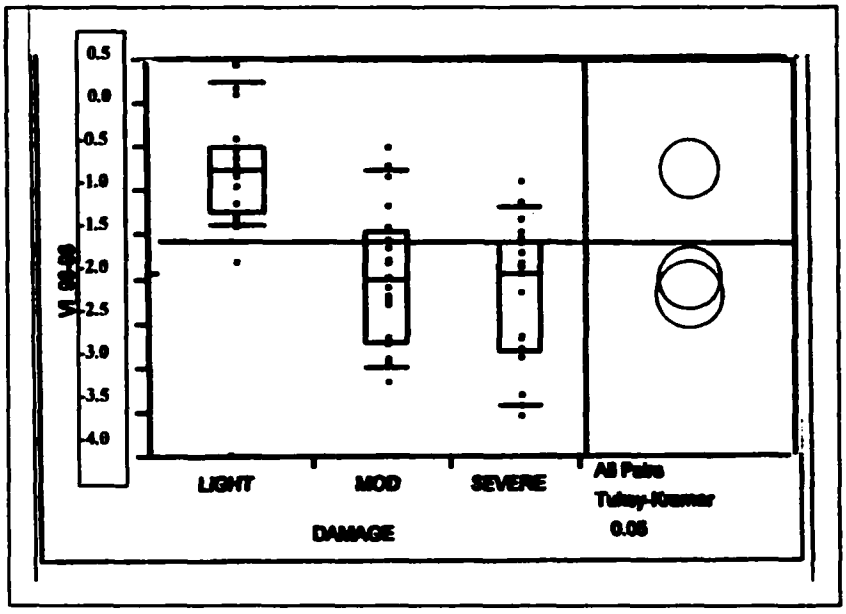

Figure 4-15. One-Way ANOVA and Tukey Test Results for TM NDVI 1998-1996 Change Detection by Damage, 90 x 90 m Sites, N = 66

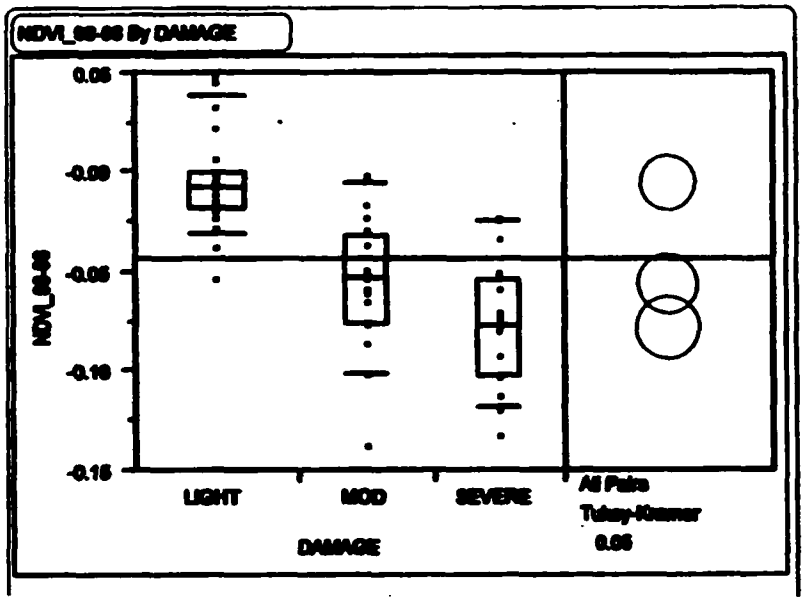

Figure 4-16. One-Way ANOVA and Tukey Test for TM 5/4 1998-1996 Change Detection by Damage, 90 x 90 m Sites, N = 66

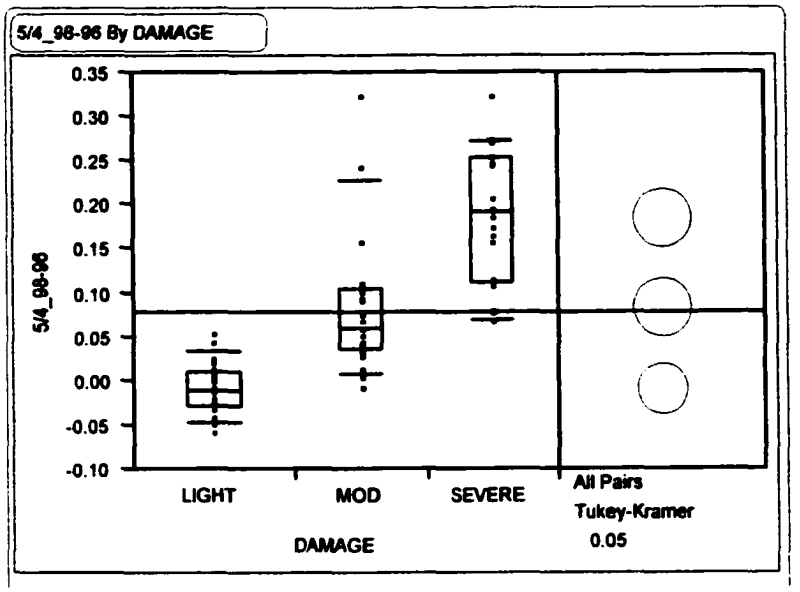

The group means of the 3 damage classes for each of the change detection studies for the 3 TM indices were determined by ANOVA to be different and all pairs of damage class means were found to be significantly different, except the means for the Severe and Moderate classes in the VI change detection study. The degree of significant difference between damage classes is demonstrated visually by the degree of separation of the circles representing the 3 damage-level groups at the right in Figures 4-14 to 4-16 and by the positive separation values for the groups in the chart at the bottom of Figures A-11 to A-14. The separation of the circles for the 3 damage classes in the 5/4 change detection study is the most significant. A summary of these results as listed in Table 4-5.

Table 4-5. Results of One-Way ANOVA and Tukey Tests for Change Detection Studies Using TM VI, NDVI, and 5/4 (90 x 90 m Study Sites)

			Damage Level Differentiation L = Light, M = Moderate, S = Severe		
INDEX	P-VALUE	R^2 =	L from M	L from S	M from S
TM VI	P < 0.001	0.47	Yes	Yes	No
TM NDVI	P < 0.001	0.54	Yes	Yes	Yes
TM 5/4	P < 0.001	0.62	Yes	Yes	Yes

Change detection methods improve the correlation of the change values to the percent damage of sites in all cases: For VI from $R^2 = 0.40$ to 0.47, for NDVI from $R^2 = 0.40$ to 0.54, and for 5/4 from $R^2 = 0.40$ to 0.62. This improvement is particularly evident in the steady positive progression of the means for the change values of the 3 levels of damage in the 5/4 study, Figure A-14. The effectiveness of VI to differentiate levels of damage is reduced in change detection results. This is also the case, though to a lesser degree, for NDVI. This suggests that TM5 (an indicator of green vegetation moisture amount) is more sensitive to changes in green biomass amount when used in a ratio with TM4 than TM3 (an indicator of chlorophyll absorption). TM 5/4 exploits data from the SWIR, which includes a spectral range of 1.0-2.5 μm. Specifically, TM5 utilizes the midrange of the SWIR region (1.55-1.75 μm). Values in the 1.65 μm and 2.20 μm regions of the SWIR have been shown to provide an accurate indication of leaf water content (Rohde and Olson, 1971; Tucker, 1980) and forest damage (Rock et al., 1986; Vogelmann and Rock, 1988, 1989). As mentioned above, previous studies have successfully utilized the TM 5/4 ratio to detect levels of damage to hardwood canopies

(Vogelmann and Rock, 1989). The successful differentiation of levels of ice damage by change detection methods using TM 5/4 ratio demonstrates not only that change detection studies can measure canopy damage more effectively than single post event images, but also that leaf water content, expressed in the TM 5/4 ratio, is highly correlated to canopy disturbance, such as ice damage. .

Classification Mapping Using Change Detection Values for TM Vegetation Indices

Results of the classification map differentiating 3 levels of canopy damage using pre- and post-event TM scenes were compared to classification maps derived from a single post-event TM scenes. The same supervised classification procedure was applied to the change detection values as was applied to the post-event-only TM indices values. The same study site size and study sample, and corresponding training sites and reference data were also used.

Figures 4-17 to 4-25 show the classification maps for the change detection studies. As with the previous maps, these classification maps reveal a strong correlation between the known general level of damage for each target area and its corresponding classification group. Bold circles indicate the extent of the reference sites within the target areas.

Figure 4-17. **VI 1998-96** - Bartlett Light and Severe Supervised Classification Map
Ice Damage Levels: Gray = Light; Yellow = Moderate; Red = Severe

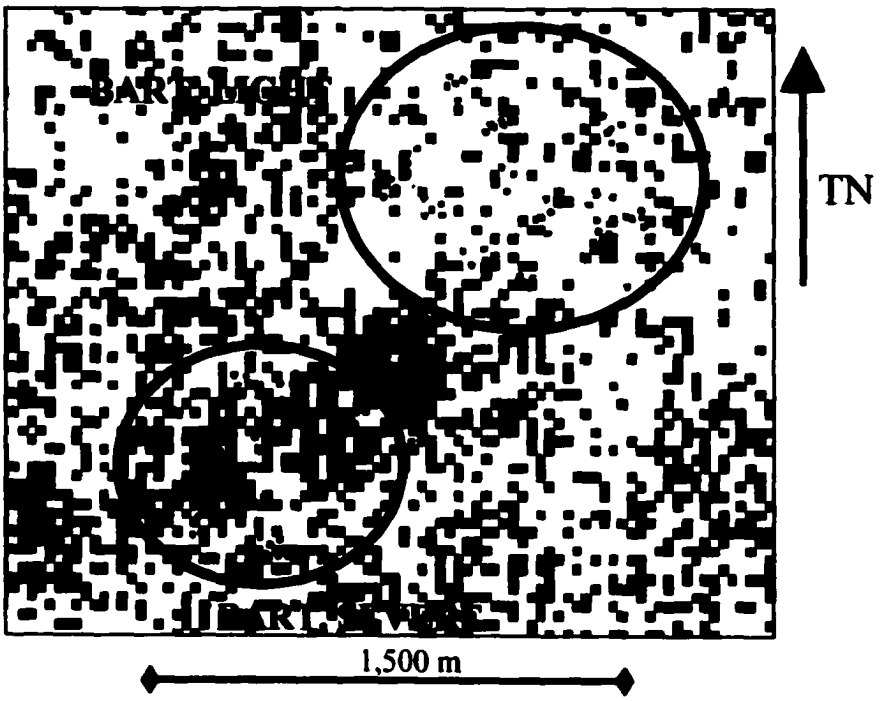

Figure 4-18. **VI 1998-96** - Hubbard Brook, Light, Moderate, and Severe
Supervised Classification Map Ice
Damage Levels: Gray = Light; Yellow = Moderate; Red = Severe

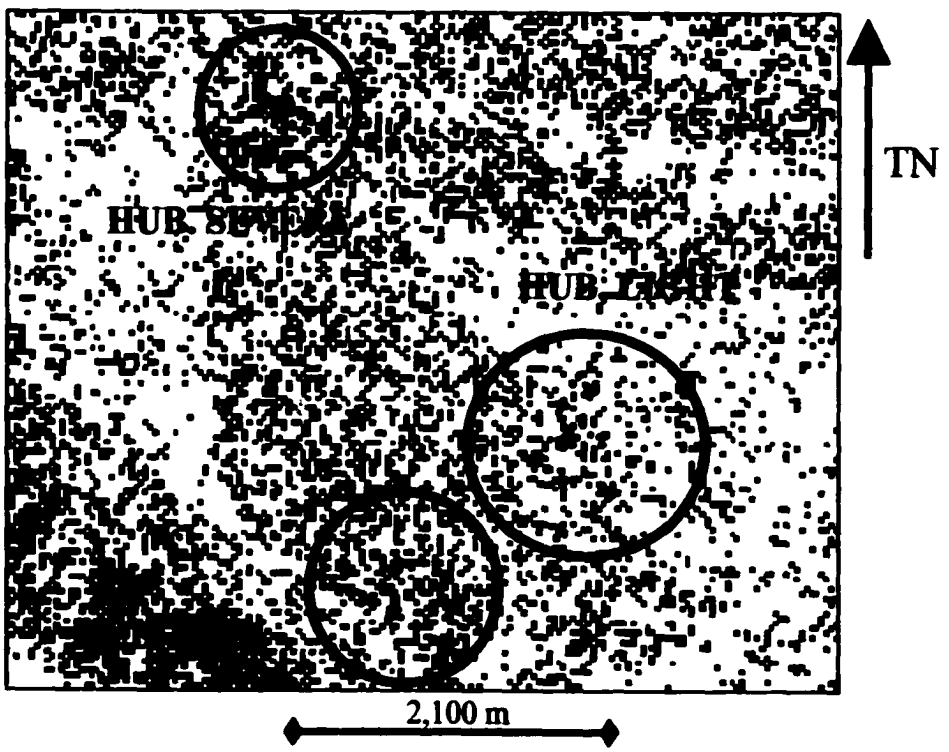

Figure 4-19. VI 1998-96 - Jefferson Notch Moderate, Kilkenny Moderate, and Pine Mountain Severe Supervised Classification Map
Ice Damage Levels: Gray = Light; Yellow = Moderate; Red = Severe

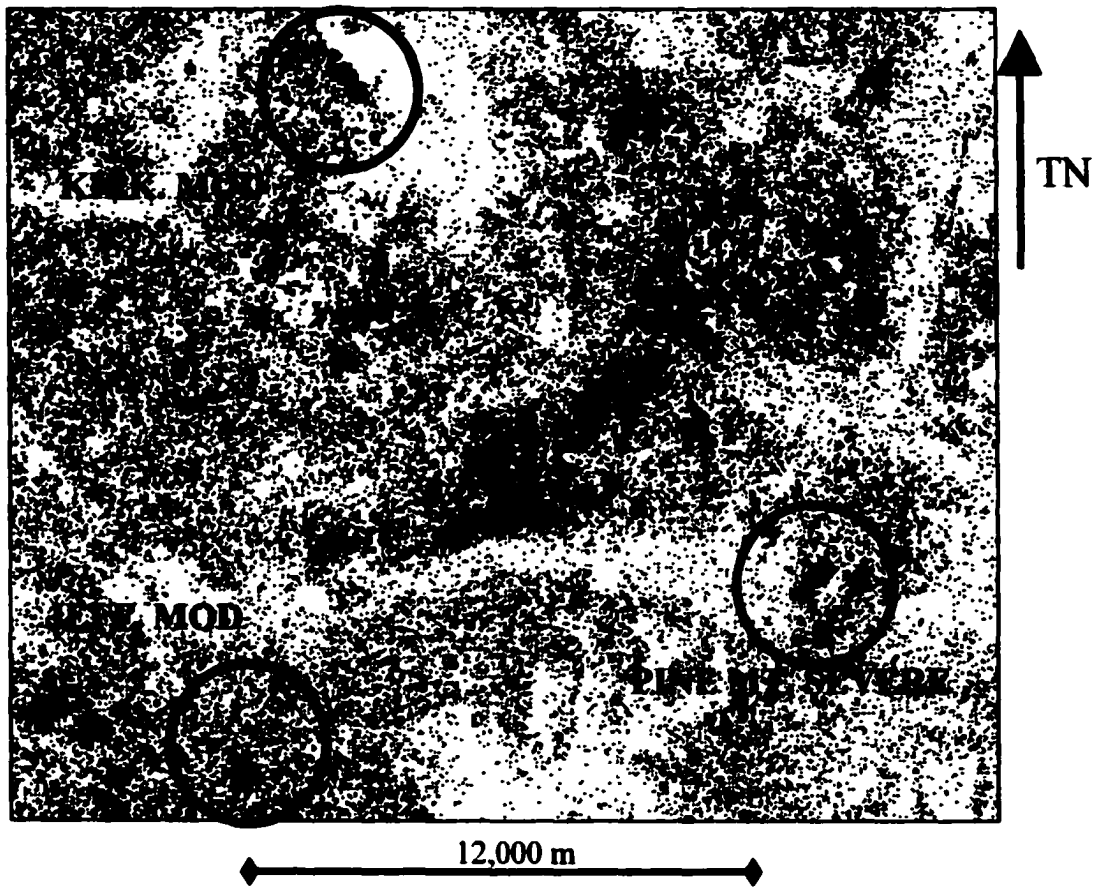

Figure 4-20. **NDVI 1998-96** - Bartlett Light and Severe Supervised Classification Map
Ice Damage Levels: Gray = Light; Yellow = Moderate; Red = Severe

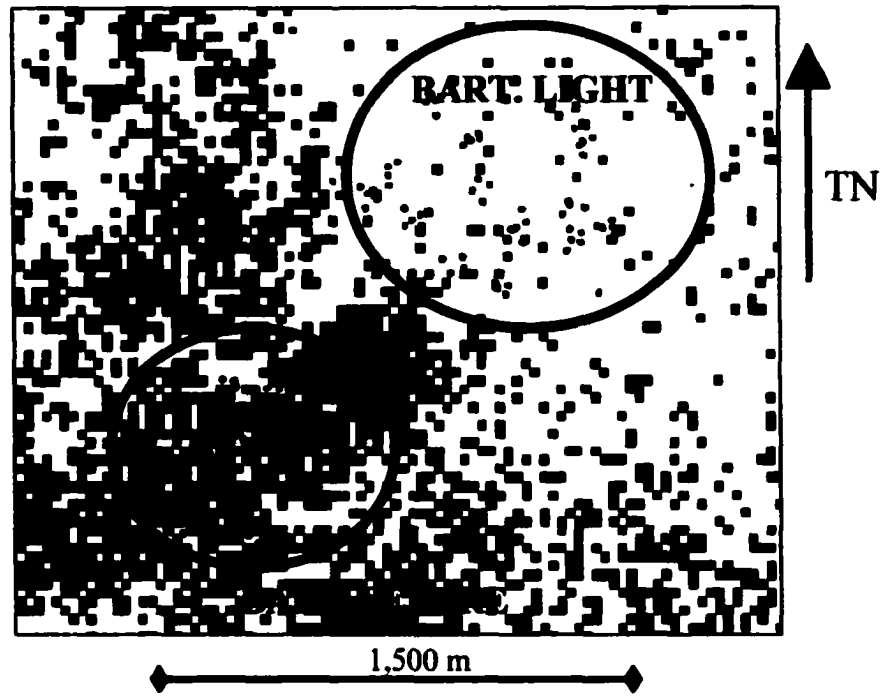

Figure 4-21. **NDVI 1998-96** - Hubbard Brook, Light, Moderate, and Severe
Supervised Classification Map Ice
Damage Levels: Gray = Light; Yellow = Moderate; Red = Severe

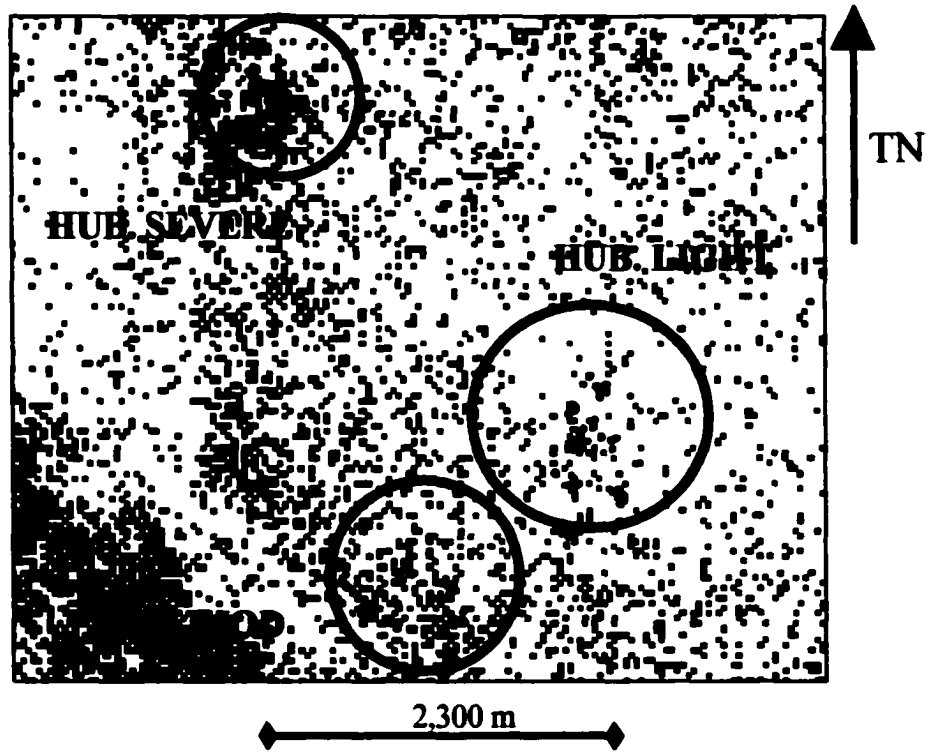

Figure 4-22. **NDVI 1998-96** - Jefferson Notch Moderate, Kilkenny Moderate, and Pine Mountain Severe Supervised Classification Map
Ice Damage Levels: Gray = Light; Yellow = Moderate; Red = Severe

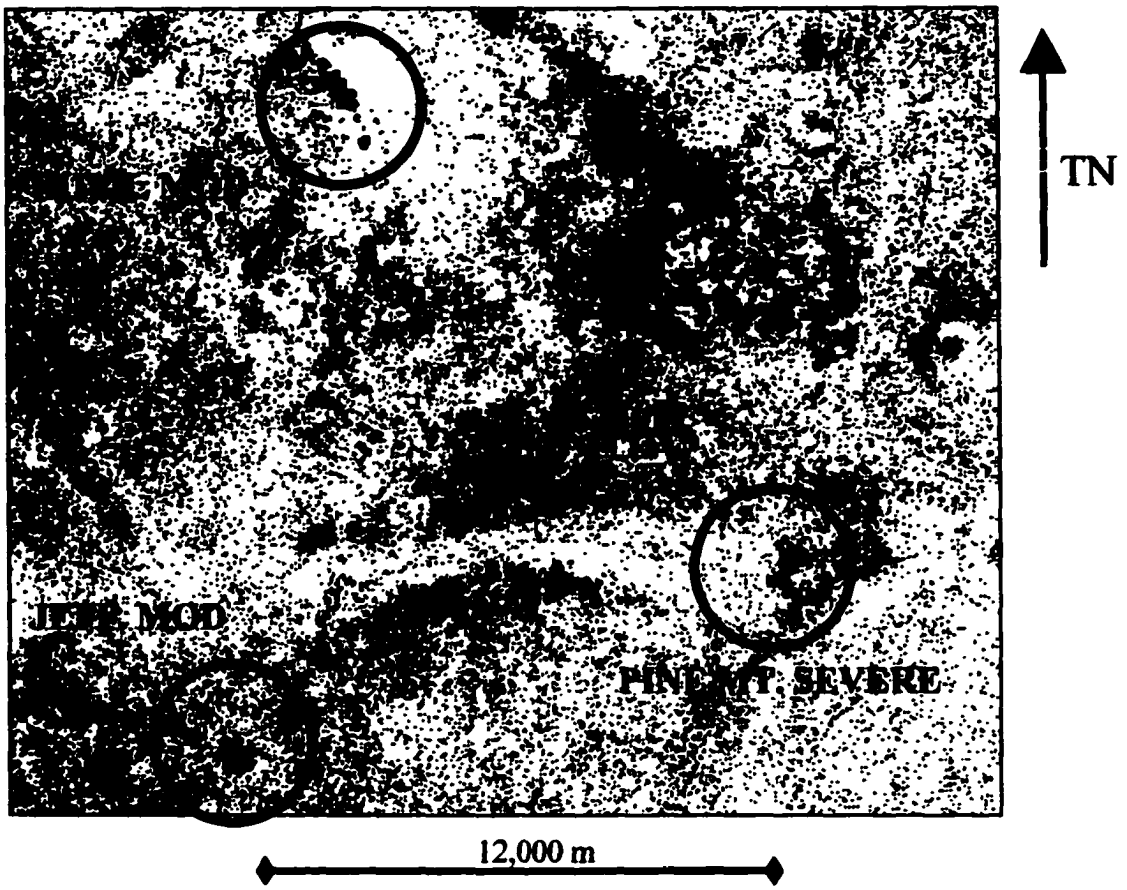

Figure 4-23. **TM 5/4 1998-96** - Bartlett Light and Severe Supervised Classification Map
Ice Damage Levels: Gray = Light; Yellow = Moderate; Red = Severe

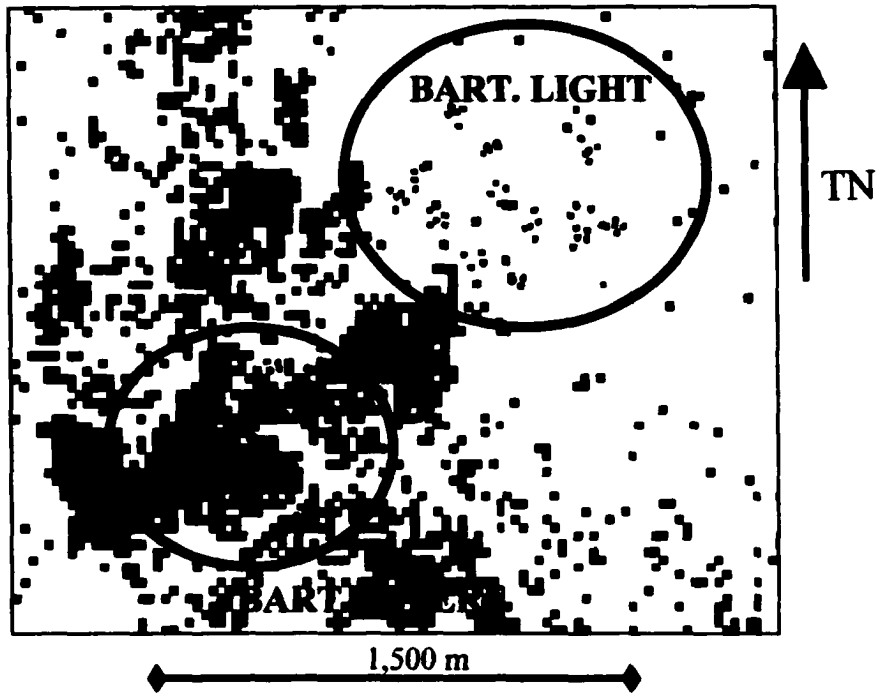

Figure 4-24. **TM 5/4 1998-96** - Hubbard Brook, Light, Moderate, and Severe
Supervised Classification Map Ice
Damage Levels: Gray = Light; Yellow = Moderate; Red = Severe

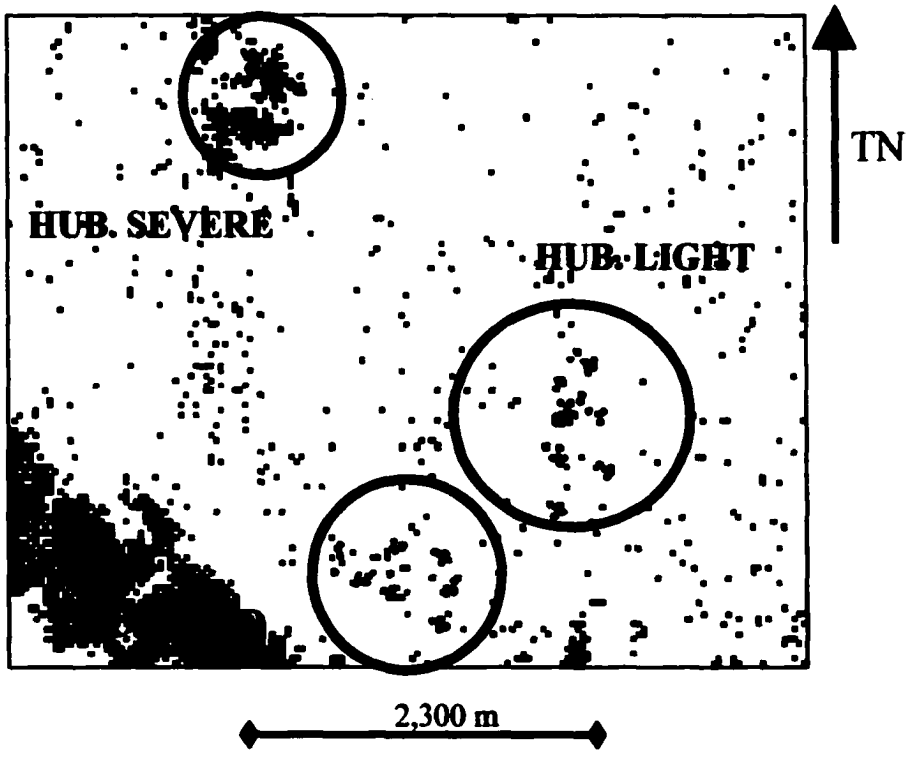

Figure 4-25. **TM 5/4 1998-96** - Jefferson Notch Moderate, Kilkenny Moderate, and Pine Mountain Severe Supervised Classification Map
Ice Damage Levels: Gray = Light; Yellow = Moderate; Red = Severe

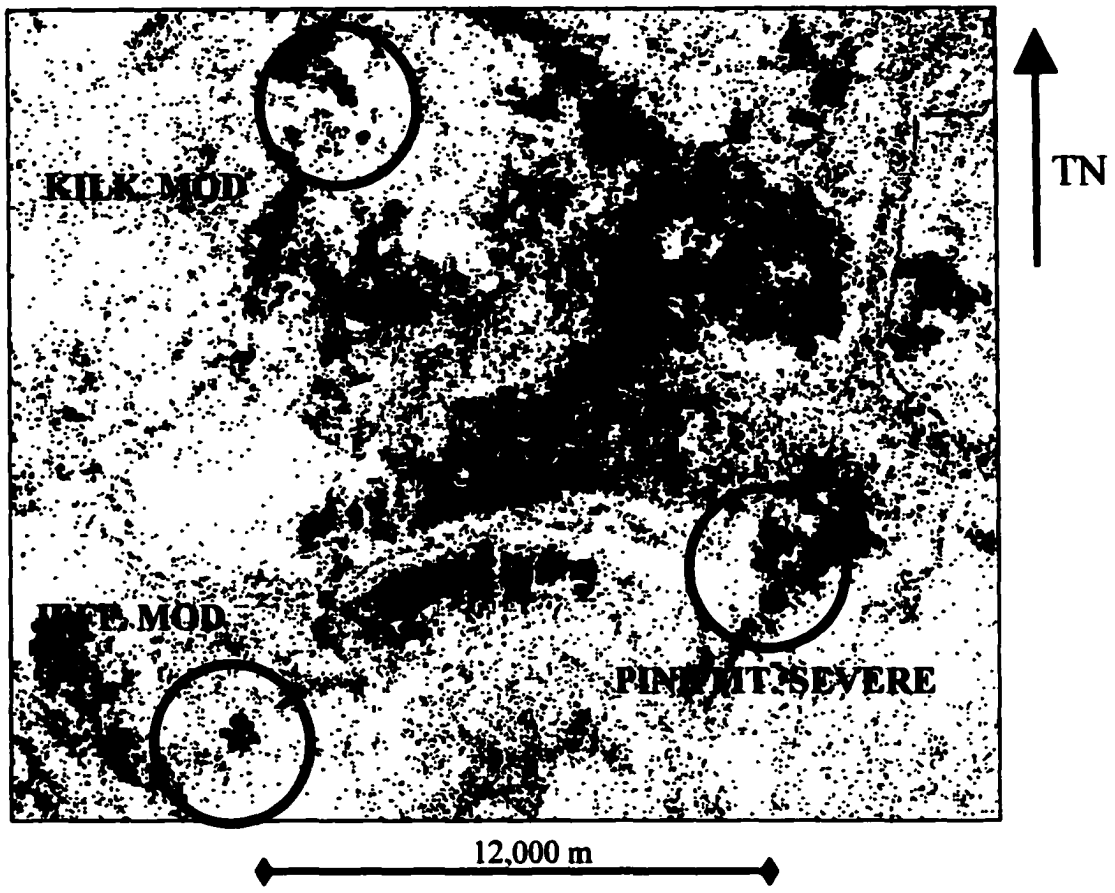

The same error matrix accuracy assessment method was used to analyze these data more closely, as well, including application of the modal and fuzzy classification rules. The results of the error matrix assessment are shown in Table 4-6, below.

Table 4-6. Error Matrices for TM Vegetation Indices Change Detection Studies (1998-1996 TM Scenes) for Canopy Damage Classification Maps (90 x 90 m Study Sites)

GROUND REFERENCE

VI 1998-1996		LIGHT	MODERATE	SEVERE	TOTAL	% USER'S ACCURACY
IMAGE CLASSIFICATION	LIGHT	18	1	0	19	95%
	MOD	0	12	6	18	67%
	SEVER	1	3	9	13	69%
		19	16	15	50	
PRODUCER'S ACCURACY		95%	75%	60%	OVERALL ACCURACY	78%

GROUND REFERENCE

NDVI 1998-1996		LIGHT	MODERATE	SEVERE	TOTAL	% USER'S ACCURACY
IMAGE CLASSIFICATION	LIGHT	16	1	0	17	94%
	MOD	3	13	3	19	68%
	SEVER	0	2	12	14	86%
		19	16	15	50	
PRODUCER'S ACCURACY		84%	81%	80%	OVERALL ACCURACY	82%

GROUND REFERENCE

5/4 1998-1996		LIGHT	MODERATE	SEVERE	TOTAL	% USER'S ACCURACY
IMAGE CLASSIFICATION	LIGHT	19	4	1	24	79%
	MOD	0	12	6	18	67%
	SEVER	0	0	8	8	100%
		19	16	15	50	
PRODUCER'S ACCURACY		100%	75%	53%	OVERALL ACCURACY	78%

The overall accuracy of the 714nr post-event classification map was 54% (Chapter II). The error matrix results for all 3 TM change detection studies demonstrate better overall accuracies than the 714nr and than the 3 TM post-event-only vegetation indices: VI change detection to post-event-only, 78% to 68%; NDVI, 78% to 72%, and TM 5/4, 82% to 76%. It is noteworthy that despite the improvements in classification accuracy, the Tukey tests (numerical results and circle charts) demonstrate that damage-class means are not as well separated as they are for the 3 post-event-only scenes. The degree of improvement in classification accuracy for any of the 3 indices in the change detection studies was not statistically significant, however. It is determined that TM VI, NDVI, and 5/4 values for post-event-only TM scenes and TM VI, NDVI, and 5/4 derived by change detection differencing for pre- and post-event TM scenes are more effective for differentiating 3 levels of damage to hardwood canopies than the 714nr for post-event-only ASAS scenes.

Conclusions

Traditional broadband Landsat TM methods are more effective than the 714nr for differentiating 3 levels of damage to forest canopies. The superiority of TM data over that of ASAS was demonstrated by two comparison analyses using ANOVA and Tukey tests and by comparing the overall accuracies of classification maps based on broadband TM and hyperspectral ASAS scenes.

The effectiveness of the 714nr to differentiate levels of damage from single post-event ASAS scenes was compared to those of 3 vegetation indices, TM VI, NDVI, and 5/4, for single post-event TM scenes. It was determined that the 714nr differentiated the

Severe damage class from Light and Moderate classes, but could not differentiate the Light and Moderate classes effectively, while all 3 TM indices successfully differentiated all damage classes. In addition it was determined that the overall accuracy of the error matrix assessments of classification maps derived from all 3 TM indices were superior to that of the 714nr. The overall accuracies were 68% for TM VI, 72% for TM NDVI, 76% for TM 5/4, and 54% for the 714nr.

Hypothesis 4-1: That measurements of TM 5/4, NDVI, and VI for a post-event Landsat TM scene (August 1998) of variously ice damaged hardwood sites (90 x 90-meter sites, N =66) are more effective than the nadir 714nr (7.5 x 7.5-meter sites, N=210) for differentiating and mapping 3 levels of ice damage to hardwood forest canopies is supported.

In the second analysis the effectiveness of the 714nr to differentiate levels of damage from single post-event scenes was compared to those of 3 vegetation indices, TM VI, NDVI, and 5/4, in a change detection study using pre- and post-event TM scenes. All 3 TM indices change detection studies successfully differentiated all damage classes, except VI, which could not differentiate the Moderate from Severe class. In addition it was determined that the overall accuracies of the error matrix assessments of classification maps derived from all 3 TM change detection studies were superior to the overall accuracy of the 714nr for a single post-event ASAS scene. The overall accuracies were 78% for TM VI, 82% for TM NDVI, 78% for TM 5/4, and 54% for the 714nr.

Hypothesis 4-2: That measurements of TM 5/4, NDVI, and VI applied to pre- and post-event Landsat TM scenes (August 1996 and 1998) of variously ice damaged hardwood sites (90 x 90-meter sites, N = 66) using change detection are more effective

than the nadir 714nr (7.5 x 7.5-meter sites, N=210) at differentiating and mapping 3 levels of ice damage to hardwood forest canopies is supported.

When the effectiveness of ASAS ice damage detection methods is compared to that of TM imagery used in change detection analysis comparing data from pre- and post-event scenes, traditional methods out-perform the 714nr for two reasons. First, it is apparent that change detection, utilizing pre- and post-event data, is better suited to ice damage assessment. Ice damage from a major storm such as that of January 1998, create gaps (changes) in the canopy that are detectable with broadband spectral information and lower spatial resolution than the 714nr. The ability of TM NDVI to detect differing levels of damage increased significantly when change detection analysis was used.

The second reason for the success of traditional broadband methods stems from the use of the extended spectral coverage of the TM 5/4 ratio. As was found in previous studies of canopy damage to forest canopies, the TM 5/4 ratio is a sensitive indicator of plant condition (Rock et al., 1986; Vogelmann, 1988; Vogelmann and Rock, 1989). The ratio measures the relationship between spectral reflectance in the NIR (TM4), which is sensitive to green biomass amount, and reflectance in the SWIR (TM5), which is sensitive to canopy water content. The combination of high reflectance in the NIR and high absorption in the SWIR is an indication of healthy green vegetation. Decreases in reflectance in the NIR or increased reflectance in the SWIR correlate with decreasing plant health. Ratios indicating decreased plant health can be triggered by defoliation or ice damage, such as broken branches and stems. Both damage conditions expose non-green vegetation and dead or inorganic materials (woody debris, leaf litter, bare soil, and rocks) to the sensor overhead. The exposure of materials other than healthy green canopy

increases the 5/4 ratio, indicating decreased health, by either decreasing reflectance in the NIR or decreasing absorption (increasing reflectance) in the SWIR, or both.

Landsat TM methods are not only more effective for detecting ice damage, they are simpler and more cost-effective to apply. Change detection requires pre- and post-event TM scenes and added procedures, due to the necessity of carefully matching spectral, temporal, and registration factors, all of which introduce errors. Single post-event scenes simplify data and image processing and produce accurate results. Because the cost of TM scenes has been reduced to a current price of approximately $600 per scene and because scenes are regional in scale (175 x 175 km), regional studies can be cost effective.

CHAPTER V

CONCLUSION

The objective of this study was to evaluate the ability of two special features of the airborne sensor ASAS – hyperspectral resolution and off-nadir viewing – to detect levels of ice damage to hardwood canopies and to compare the overall effectiveness of the 714nr to detect damage to that of traditional Landsat TM broadband methods. This evaluation was carried out in three steps.

1. The hyperspectral capability of ASAS was used to distinguish between the fine-features of the red edge curve for differing levels of damaged forest canopies. It was determined that the blue shift can be represented by measuring the reflectance value for normalized red edge (653 to 775 nm) values at ASAS band 714 nm. Hyperspectral ASAS data are utilized to measure the 714nr and, in turn, measure 3 levels of damage to hardwood canopies. The 714nr was effective in differentiating Severe from Light and Moderate levels of damage and classified 3 levels of damage with an overall accuracy of 54%.

2. The off-nadir viewing capability of ASAS was used to measure spectral reflectance differences for study sites with differing levels of ice storm damage to forest canopies in order to determine whether the additional spectral information provided by off-nadir views improved the effectiveness of ice damage assessments. It was theorized that the off-nadir view would detect ice damage symptoms on the sides of tree crowns that were inaccessible to the nadir perspective. First, it was determined that data for view angles from +45° to –45° off-nadir do not significantly affect the slope and wavelength

position of the red edge spectral features of an undamaged canopy site. After red edge datasets (653 to 775 nm) were normalized for five view angles (+/-45, +/-26, and nadir), it was determined that the shape, slope, and wavelength position of the red edge curves were not significantly changed. The ability of off-nadir views, from $+45^{0}$ to -45^{0} off-nadir, to distinguish levels of ice damage to forest canopies using the 714nr was then compared to that of nadir datasets. It was determined that nadir data were more effective at distinguishing levels of damage than any of the off-nadir view angles. It was concluded that the nadir view provides the best perspective from which to detect the spectral signals of materials other than green vegetation exposed within and on the forest floor of gaps caused by ice storm damage. Off-nadir views have access to the sides of crowns but, in most cases, do not have access to materials, such as woody debris, within and on the ground in gaps. Nadir is, thus, the best perspective for measuring the percent of green biomass associated with variously damaged and undamaged sites.

3. The ability of hyperspectral ASAS data to detect levels of ice storm damage was compared to Landsat TM traditional broadband approaches. Broadband vegetation indices were applied to single post-event TM scenes and to change detection (univariate image subtraction) for pre- and post-event TM scenes to detect levels of damage to forest canopies. The effectiveness of three traditional vegetation indices, VI, NDVI, and TM 5/4, to differentiate 3 levels of damage and to classify them was compared to the 714nr. The Tukey test results demonstrate the significant difference between damage classes and the overall accuracies of error matrix assessments of classification maps. Both broadband methods out-performed the 714nr method using all 3 vegetation indices. The range of the 6 overall accuracies for the 3 indices using both single post-event and change detection

methods was from 68-82%, as compared to 54% for the 714nr. The best overall accuracy was achieved by change detection using NDVI, 82%.

In the final analysis, the special features of ASAS (hyperspatial, hyperspectral, multiangle viewing) did not enhance its ability to detect ice storm damage to hardwood canopies. The traditional broadband approach using Landsat TM provided sufficient spatial, spectral, and view-angle capability for the task at hand. In addition, conditions of acquisition related to sun-target-sensor geometry were constant for each TM scene. The TM experiment was simplified and more controlled as a result. A stated objective of this study was to keep detection methods as simple and practical as possible. The special features of ASAS added complexity to image processing that, in turn, introduced errors and added costs. Using satellite imagery, such as Landsat TM, with 175 x 175 km scenes can greatly reduce costs for regional ice damage assessment studies.

Were ASAS applied to a task that specifically required its special capabilities, complexity would be unavoidable but necessary and the outcome would have justified the extra time and effort. The hyperspectral subtleties of red edge features are more appropriately applied to studies of vegetation stress and forest decline, as in the studies of Entcheva (2000), in which ASAS data was used to identify the early stages of decline to Norway spruce in the Czech Republic. There the focus is on degrees of change in reflected radiance for narrow bands at the pixel level, not a coarse spectral measure of green biomass.

In the absence of the success of ASAS, a simple and practical broadband approach is realized. The traditional vegetation indices, particularly NVDI and TM 5/4, are well suited to the task of measuring levels of green biomass, indicating levels of ice

damage, on the broadband spectral scale, with 30 x 30 m pixels, and nadir viewing. Landsat TM scenes are relatively inexpensive and provide forestland coverage on a regional scale, making them cost-effective. TM vegetation indices are simple algorithms and are easy to apply. Change detection adds a level of complexity and expense to broadband methods that may not be necessary. Further studies utilizing a larger study sample are needed to test the validity of the single post-event scene methods using NDVI and TM 5/4 with more precision.

APPENDIX

Figure A-1. 714nr by Damage ANOVA and Tukey-Kramer Test Results, 3 x 3 Pixel Sites (7.5 x 7.5 m), N = 210 (From SAS Institute, Inc., 1997. *JMP IN,* Version 3.2.1.) The points represent 714nr values. Values of 714nr are grouped according to their corresponding percent canopy damage measured on the ground (0-24.9% = Light, 25-49.9% = Moderate, 50-100% = Severe). The diamonds show the mean (horizontal center line) and one standard deviation (vertical dimension) for each damage class. The box-and-whisker plots for each group of points indicate the level up to which 10% (lower line), 25% (bottom of box), 50% (center of box), 75% (top of box), and 90% (upper line) of the data fall. The circles for the Tukey-Kramer test are centered on the mean 714nr value for each damage class. The size of a circle is determined by the variance from the group mean at the 95% confidence level. Separation between circles indicates a statistical difference between their means.

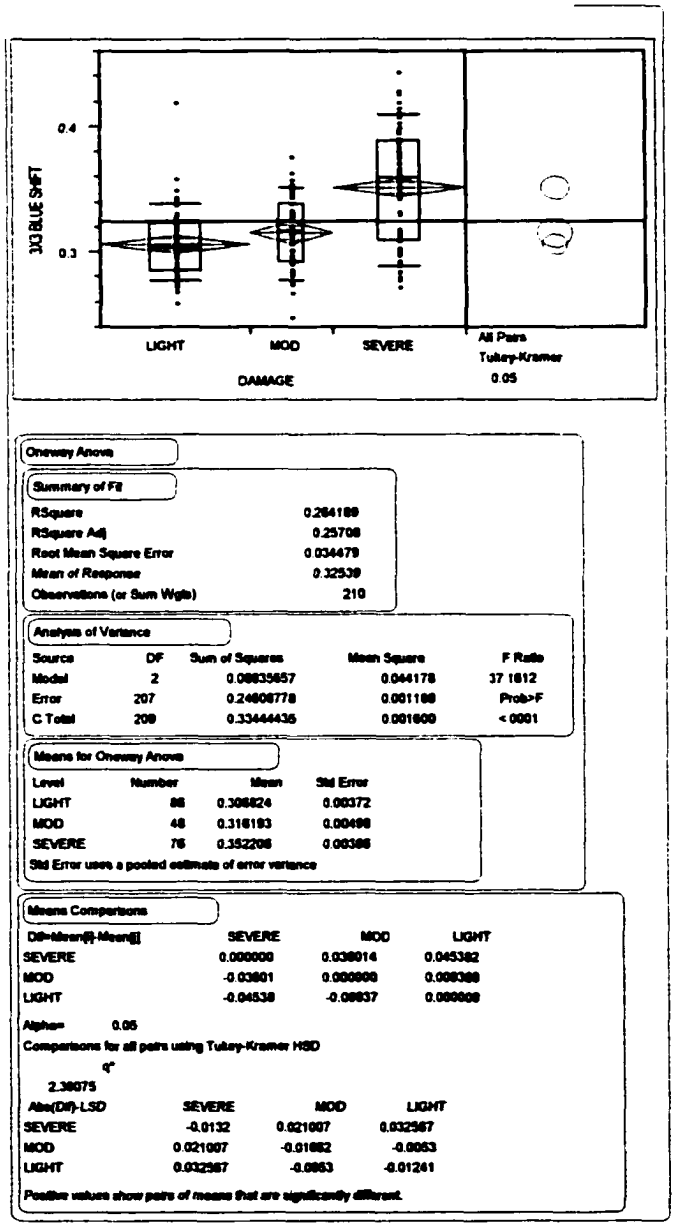

Figure A-2. ANOVA and Tukey Test Results for ASAS -45° View 714nr by Damage, 90 x 90 m Sites, N = 50 (From SAS Institute, Inc., 1997. *JMP IN*, Version 3.2.1.)

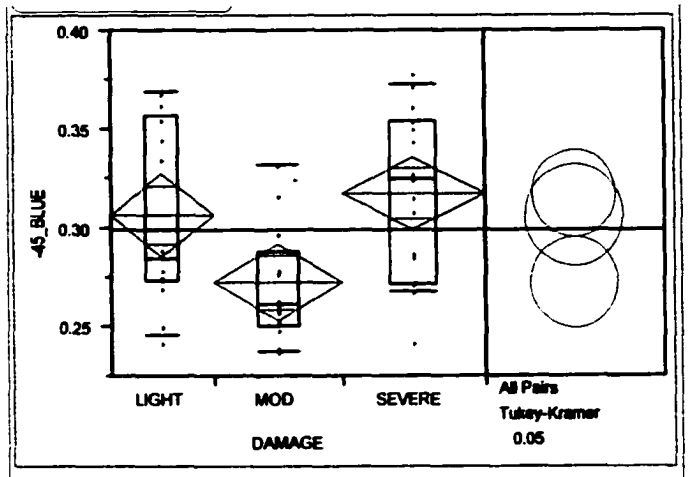

Oneway Anova

Summary of Fit

RSquare	0.202458
RSquare Adj	0.16852
Root Mean Square Error	0.040337
Mean of Response	0.299328
Observations (or Sum Wgts)	50

Analysis of Variance

Source	DF	Sum of Squares	Mean Square	F Ratio
Model	2	0.01941284	0.009706	5.9655
Error	47	0.07647304	0.001627	Prob>F
C Total	49	0.09588588	0.001957	0.0049

Means for Oneway Anova

Level	Number	Mean	Std Error
LIGHT	14	0.306925	0.01078
MOD	17	0.272544	0.00978
SEVERE	19	0.317695	0.00925

Std Error uses a pooled estimate of error variance

Means Comparisons

Dif=Mean[i]-Mean[j]	SEVERE	LIGHT	MOD
SEVERE	0.000000	0.010770	0.045151
LIGHT	-0.01077	0.000000	0.034381
MOD	-0.04515	-0.03438	0.000000

Alpha= 0.05

Comparisons for all pairs using Tukey-Kramer HSD

q*

2.42012

Abs(Dif)-LSD	SEVERE	LIGHT	MOD
SEVERE	-0.03167	-0.02361	0.012560
LIGHT	-0.02361	-0.0369	-0.00085
MOD	0.012560	-0.00085	-0.03348

Positive values show pairs of means that are significantly different.

Figure A-3. ANOVA and Tukey Test Results for ASAS -26° View 714nr by Damage, 90 x 90 m Sites, N = 45 (From SAS Institute, Inc., 1997. *JMP IN*, Version 3.2.1.)

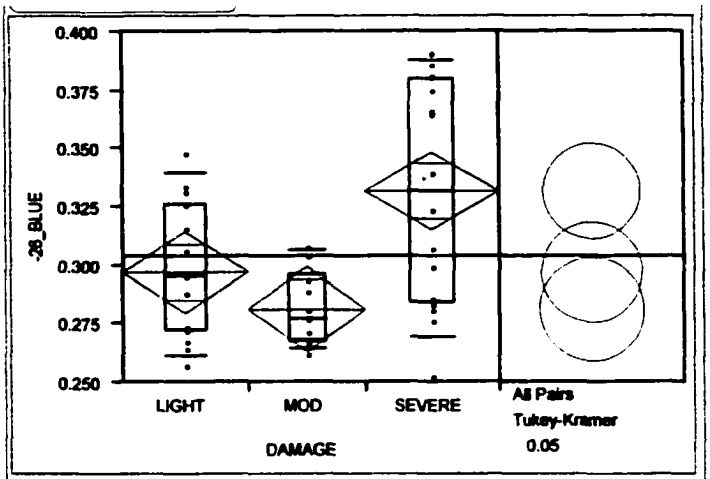

Oneway Anova

Summary of Fit

RSquare	0.289191
RSquare Adj	0.255343
Root Mean Square Error	0.034162
Mean of Response	0.304316
Observations (or Sum Wgts)	45

Analysis of Variance

Source	DF	Sum of Squares	Mean Square	F Ratio
Model	2	0.01994226	0.009971	8.5438
Error	42	0.04901661	0.001167	Prob>F
C Total	44	0.06895887	0.001567	0.0008

Means for Oneway Anova

Level	Number	Mean	Std Error
LIGHT	15	0.298850	0.00882
MOD	14	0.281386	0.00913
SEVERE	16	0.331395	0.00854

Std Error uses a pooled estimate of error variance

Means Comparisons

Dif=Mean[i]-Mean[j]	SEVERE	LIGHT	MOD
SEVERE	0.000000	0.034545	0.050029
LIGHT	-0.03454	0.000000	0.015484
MOD	-0.05003	-0.01548	0.000000

Alpha= 0.05

Comparisons for all pairs using Tukey-Kramer HSD

q*

2.42949

Abs(Dif)-LSD	SEVERE	LIGHT	MOD
SEVERE	-0.02934	0.004716	0.019655
LIGHT	0.004716	-0.03031	-0.01536
MOD	0.019655	-0.01536	-0.03137

Positive values show pairs of means that are significantly different.

Figure A-4. ANOVA and Tukey Test Results for ASAS Nadir View 714nr by Damage, 90 x 90 m Sites, N = 55 (From SAS Institute, Inc., 1997. *JMP IN*, Version 3.2.1.)

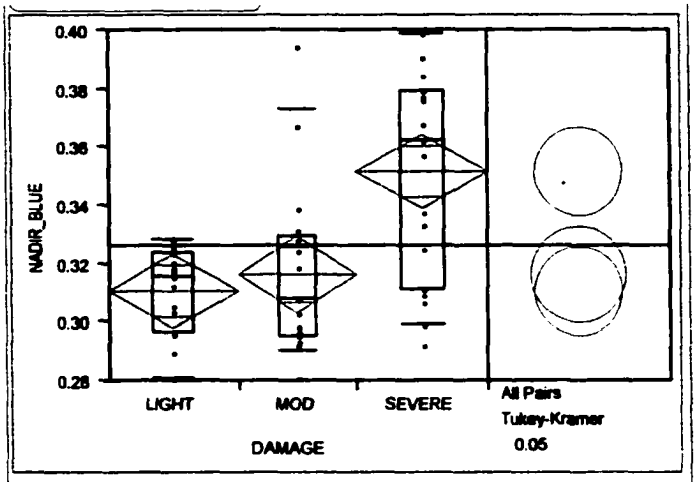

Oneway Anova

Summary of Fit

RSquare	0.314584
RSquare Adj	0.288232
Root Mean Square Error	0.028253
Mean of Response	0.326539
Observations (or Sum Wgts)	55

Analysis of Variance

Source	DF	Sum of Squares	Mean Square	F Ratio
Model	2	0.01905200	0.009526	11.9337
Error	52	0.04150885	0.000798	Prob>F
C Total	54	0.06056085	0.001121	<.0001

Means for Oneway Anova

Level	Number	Mean	Std Error
LIGHT	19	0.310344	0.00648
MOD	17	0.316242	0.00685
SEVERE	19	0.351947	0.00648

Std Error uses a pooled estimate of error variance

Means Comparisons

Dif=Mean(i)-Mean(j)	SEVERE	MOD	LIGHT
SEVERE	0.000000	0.035705	0.041604
MOD	-0.03571	0.000000	0.005899
LIGHT	-0.0416	-0.0059	0.000000

Alpha= 0.05

Comparisons for all pairs using Tukey-Kramer HSD

q*

2.41260

Abs(Dif)-LSD	SEVERE	MOD	LIGHT
SEVERE	-0.02212	0.012949	0.019488
MOD	0.012949	-0.02338	-0.01686
LIGHT	0.019488	-0.01686	-0.02212

Positive values show pairs of means that are significantly different.

Figure A-5. ANOVA and Tukey Test Results for ASAS +26° View 714nr by Damage, 90 x 90 m Sites, N = 53 (From SAS Institute, Inc., 1997. *JMP IN*, Version 3.2.1.)

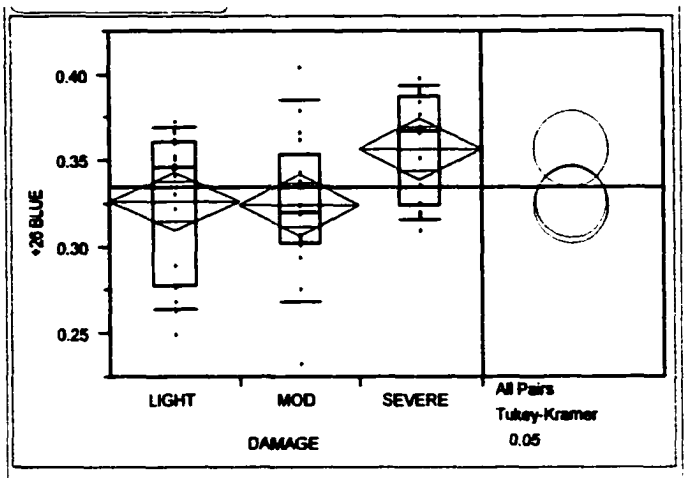

Oneway Anova

Summary of Fit

RSquare	0.136199
RSquare Adj	0.101646
Root Mean Square Error	0.038462
Mean of Response	0.335518
Observations (or Sum Wgts)	53

Analysis of Variance

Source	DF	Sum of Squares	Mean Square	F Ratio
Model	2	0.01166275	0.005831	3.9418
Error	50	0.07396781	0.001479	Prob>F
C Total	52	0.08563056	0.001647	0.0257

Means for Oneway Anova

Level	Number	Mean	Std Error
LIGHT	19	0.326309	0.00882
MOD	17	0.324259	0.00933
SEVERE	17	0.357070	0.00933

Std Error uses a pooled estimate of error variance

Means Comparisons

Dif=Mean(i)-Mean(j)	SEVERE	LIGHT	MOD
SEVERE	0.000000	0.030761	0.032811
LIGHT	-0.03076	0.000000	0.002050
MOD	-0.03281	-0.00205	0.000000

Alpha= 0.05

Comparisons for all pairs using Tukey-Kramer HSD

q*

2.41542

Abs(Dif)-LSD	SEVERE	LIGHT	MOD
SEVERE	-0.03187	-0.00025	0.000946
LIGHT	-0.00025	-0.03014	-0.02897
MOD	0.000946	-0.02897	-0.03187

Positive values show pairs of means that are significantly different.

Figure A-6. ANOVA and Tukey Test Results for ASAS +45° View 714nr by Damage, 90 x 90 m Sites, N = 34 (From SAS Institute, Inc., 1997. *JMP IN*, Version 3.2.1.)

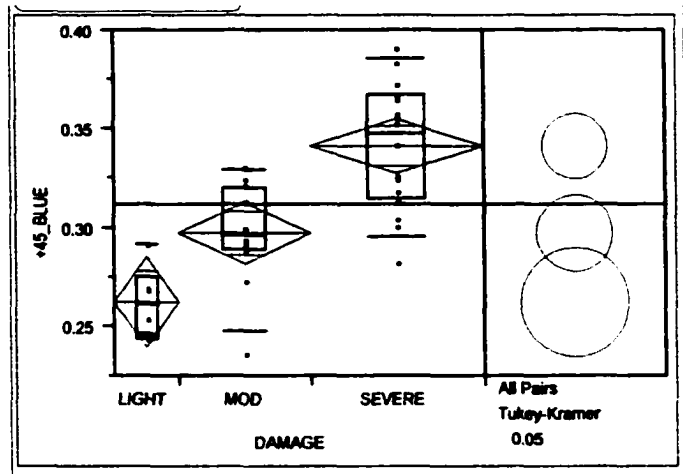

Oneway Anova

Summary of Fit

RSquare	0.563484
RSquare Adj	0.535322
Root Mean Square Error	0.028156
Mean of Response	0.312339
Observations (or Sum Wgts)	34

Analysis of Variance

Source	DF	Sum of Squares	Mean Square	F Ratio
Model	2	0.03172354	0.015862	20.0084
Error	31	0.02457539	0.000793	Prob>F
C Total	33	0.05629893	0.001706	<.0001

Means for Oneway Anova

Level	Number	Mean	Std Error
LIGHT	6	0.262407	0.01149
MOD	12	0.297629	0.00813
SEVERE	16	0.342096	0.00704

Std Error uses a pooled estimate of error variance

Means Comparisons

Dif=Mean[i]-Mean[j]	SEVERE	MOD	LIGHT
SEVERE	0.000000	0.044467	0.079689
MOD	-0.04447	0.000000	0.035222
LIGHT	-0.07969	-0.03522	0.000000

Alpha= 0.05

Comparisons for all pairs using Tukey-Kramer HSD

q*

2.46119

Abs(Dif)-LSD	SEVERE	MOD	LIGHT
SEVERE	-0.0245	0.018004	0.046516
MOD	0.018004	-0.02629	0.000573
LIGHT	0.046516	0.000573	-0.04001

Positive values show pairs of means that are significantly different.

Figure A-7. ANOVA and Tukey Test Results for 714nr by Damage, 90 x 90 m Sites, N = 53 (From SAS Institute, Inc., 1997. *JMP IN*, Version 3.2.1.)

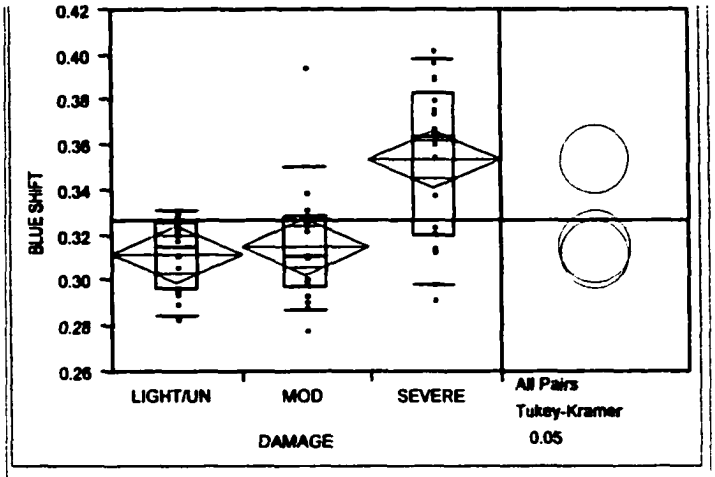

Oneway Anova

Summary of Fit

RSquare	0.345695
RSquare Adj	0.319523
Root Mean Square Error	0.027428
Mean of Response	0.326996
Observations (or Sum Wgts)	53

Analysis of Variance

Source	DF	Sum of Squares	Mean Square	F Ratio
Model	2	0.01987382	0.009937	13.2065
Error	50	0.03761566	0.000752	Prob>F
C Total	52	0.05748948	0.001106	<.0001

Means for Oneway Anova

Level	Number	Mean	Std Error
LIGHT/UN	18	0.311599	0.00646
MOD	17	0.314770	0.00665
SEVERE	18	0.353938	0.00646

Std Error uses a pooled estimate of error variance

Means Comparisons

Dif=Mean[i]-Mean[j]	SEVERE	MOD	LIGHT/UN
SEVERE	0.000000	0.039168	0.042339
MOD	-0.03917	0.000000	0.003171
LIGHT/UN	-0.04234	-0.00317	0.000000

Alpha= 0.05

Comparisons for all pairs using Tukey-Kramer HSD

q*
2.41542

Abs(Dif)-LSD	SEVERE	MOD	LIGHT/UN
SEVERE	-0.02208	0.016762	0.020255
MOD	0.016762	-0.02272	-0.01924
LIGHT/UN	0.020255	-0.01924	-0.02208

Positive values show pairs of means that are significantly different.

Figure A-8. ANOVA and Tukey Test Results for TM VI by Damage, 90 x 90 m Sites, N = 66 (From SAS Institute, Inc., 1997. *JMP IN*, Version 3.2.1.)

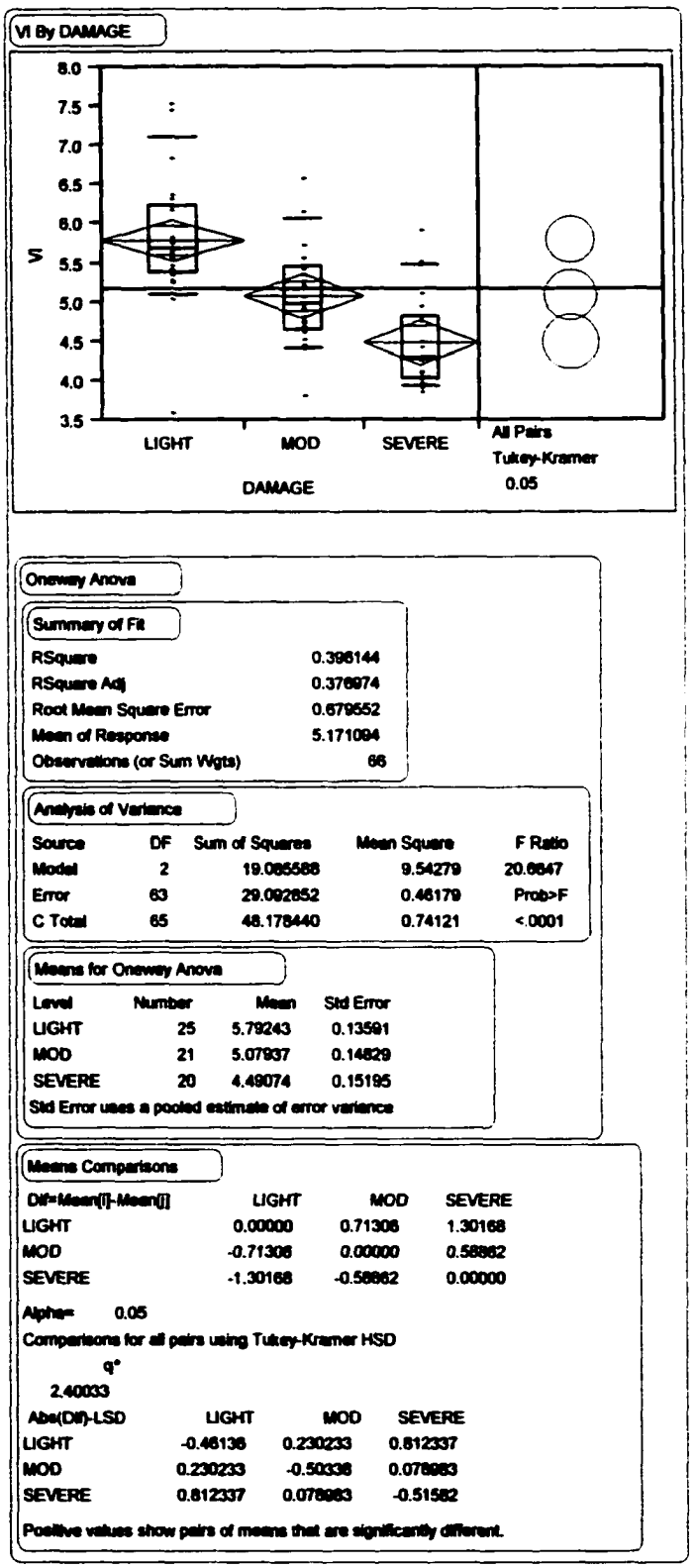

Figure A-9. ANOVA and Tukey Test Results for TM NDVI by Damage, 90 x 90 m Sites, N = 66 (From SAS Institute, Inc., 1997. *JMP IN,* Version 3.2.1.)

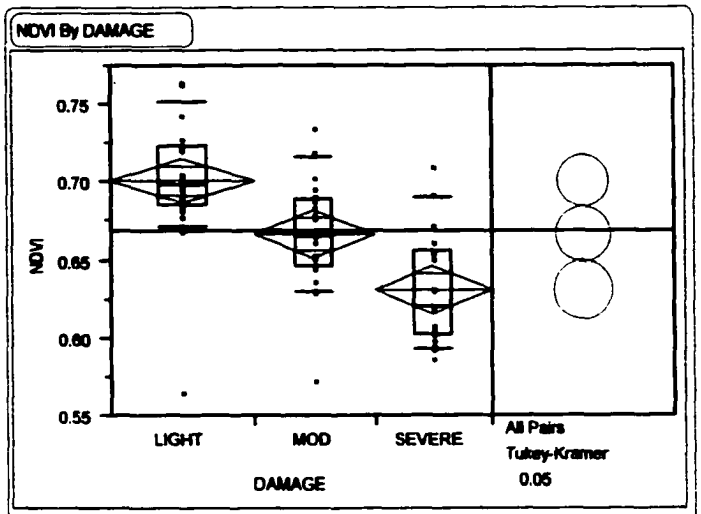

Oneway Anova

Summary of Fit

RSquare	0.395141
RSquare Adj	0.375839
Root Mean Square Error	0.036172
Mean of Response	0.668591
Observations (or Sum Wgts)	66

Analysis of Variance

Source	DF	Sum of Squares	Mean Square	F Ratio
Model	2	0.05384857	0.026924	20.5783
Error	63	0.08242819	0.001308	Prob>F
C Total	65	0.13627676	0.002097	<.0001

Means for Oneway Anova

Level	Number	Mean	Std Error
LIGHT	25	0.700508	0.00723
MOD	21	0.666413	0.00789
SEVERE	20	0.630984	0.00809

Std Error uses a pooled estimate of error variance

Means Comparisons

Dif=Mean[i]-Mean[j]	LIGHT	MOD	SEVERE
LIGHT	0.000000	0.034092	0.069521
MOD	-0.03409	0.000000	0.035429
SEVERE	-0.06952	-0.03543	0.000000

Alpha= 0.05

Comparisons for all pairs using Tukey-Kramer HSD

q*

2.40033

Abs(Dif)-LSD	LIGHT	MOD	SEVERE
LIGHT	-0.02456	0.008392	0.043474
MOD	0.008392	-0.02679	0.008302
SEVERE	0.043474	0.008302	-0.02746

Positive values show pairs of means that are significantly different.

Figure A-10. ANOVA and Tukey Test Results for TM 5/4 by Damage, 90 x 90 m Sites, N = 66 (From SAS Institute, Inc., 1997. *JMP IN,* Version 3.2.1.)

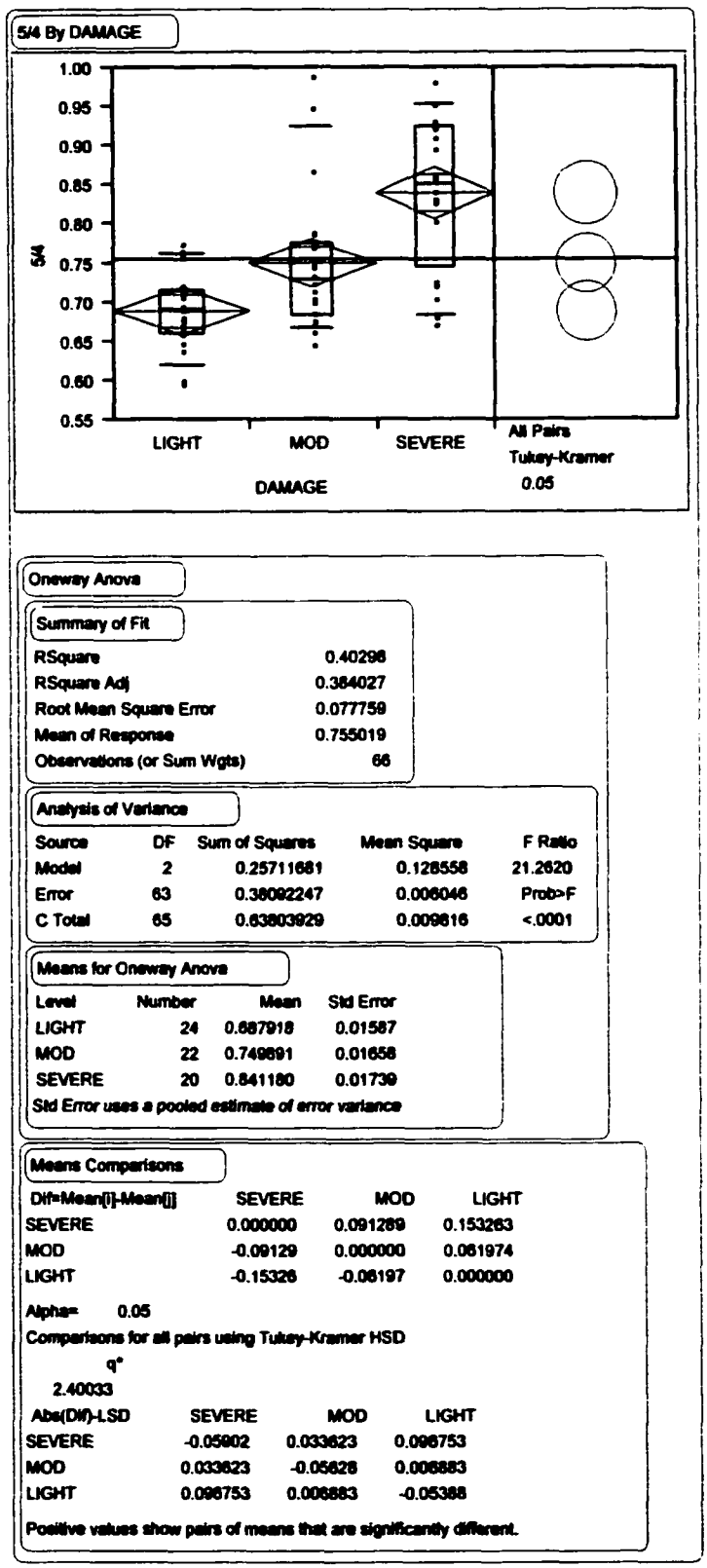

Figure A-11. ANOVA and Tukey Test Results for TM VI 1998-1996 by Damage, 90 x 90 m Sites, N = 66 (From SAS Institute, Inc., 1997. *JMP IN,* Version 3.2.1.)

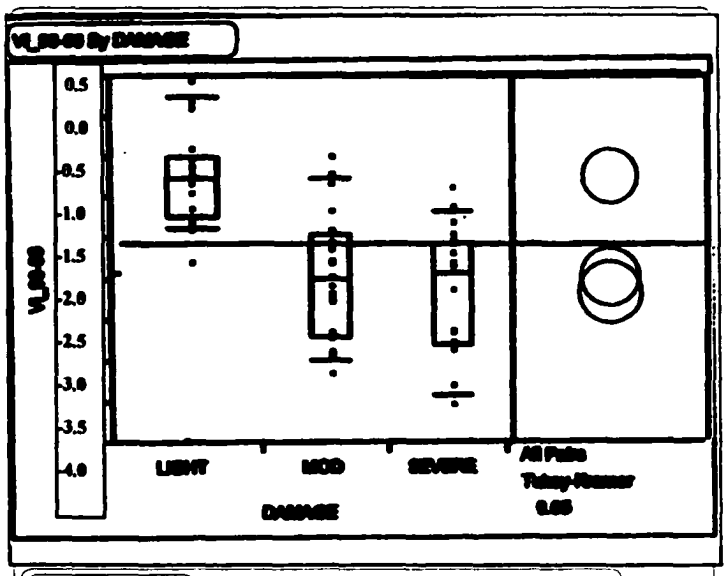

Oneway Anova

Summary of Fit

RSquare	0.469944
RSquare Adj	0.453117
Root Mean Square Error	0.707732
Mean of Response	1.567884
Observations (or Sum Wgts)	66

Analysis of Variance

Source	DF	Sum of Squares	Mean Square	F Ratio
Model	2	27.977104	13.9886	27.9277
Error	63	31.555761	0.5009	Prob>F
C Total	65	59.532865	0.9159	<.0001

Means for Oneway Anova

Level	Number	Mean	Std Error
LIGHT	25	0.74015	0.14155
MOD	21	1.97567	0.15444
SEVERE	20	2.17438	0.15825

Std Error uses a pooled estimate of error variance

Means Comparisons

Dif=Mean[i]-Mean[j]	SEVERE	MOD	LIGHT
SEVERE	0.00000	0.19871	1.43422
MOD	-0.19871	0.00000	1.23551
LIGHT	-1.43422	-1.23551	0.00000

Alpha= 0.05

Comparisons for all pairs using Tukey-Kramer HSD

q*

2.40033

Abs(Dif)-LSD	SEVERE	MOD	LIGHT
SEVERE	-0.53721	-0.33206	0.924585
MOD	-0.33206	-0.52426	0.732661
LIGHT	0.924585	0.732661	-0.48049

Positive values show pairs of means that are significantly different.

Figure A-12. ANOVA and Tukey Test Results for TM NDVI 1998-1996 by Damage, 90 x 90 m Sites, N = 66 (From SAS Institute, Inc., 1997. *JMP IN*, Version 3.2.1.)

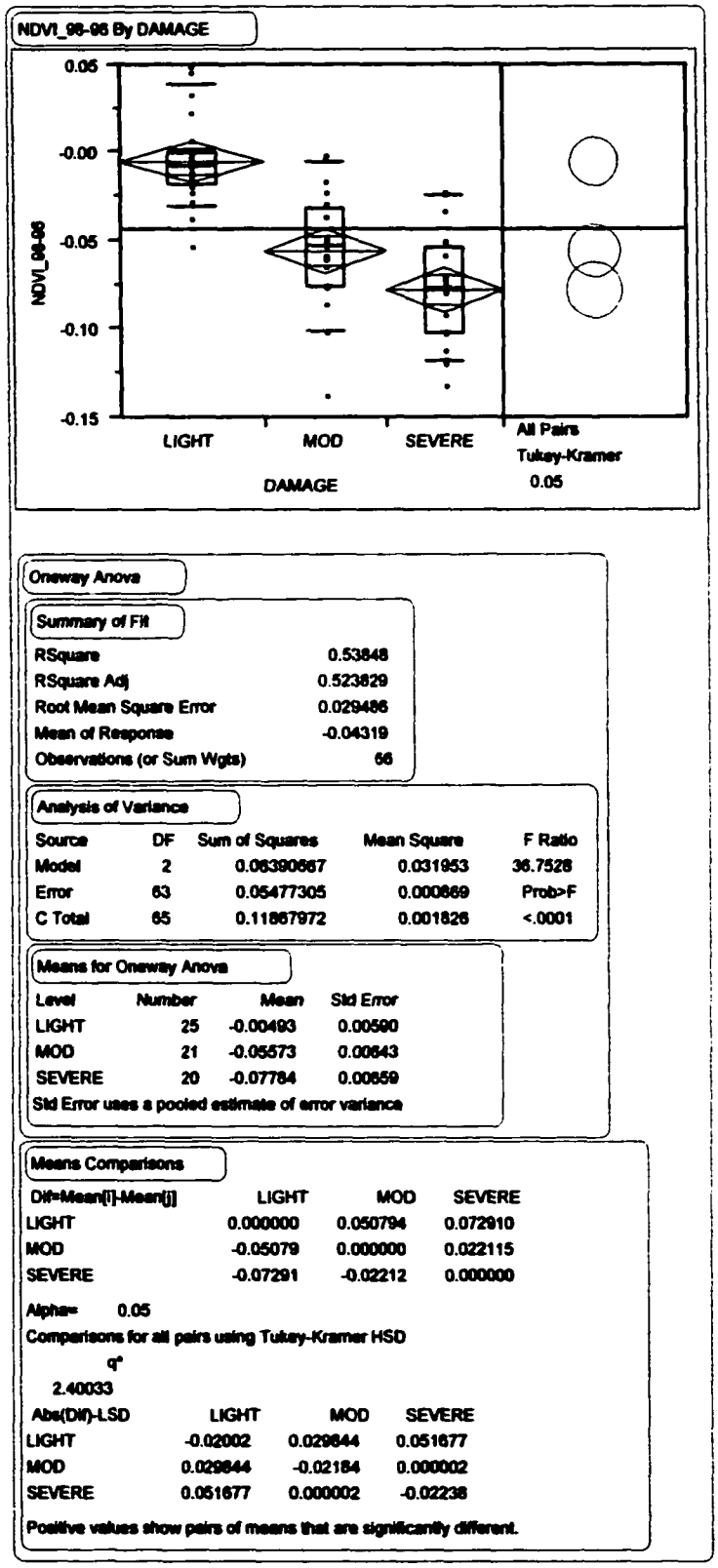

Figure A-13. ANOVA and Tukey Test Results for TM 5/4 1998-1996 by Damage, 90 x 90 m Sites, N = 66 (From SAS Institute, Inc., 1997. *JMP IN*, Version 3.2.1.)

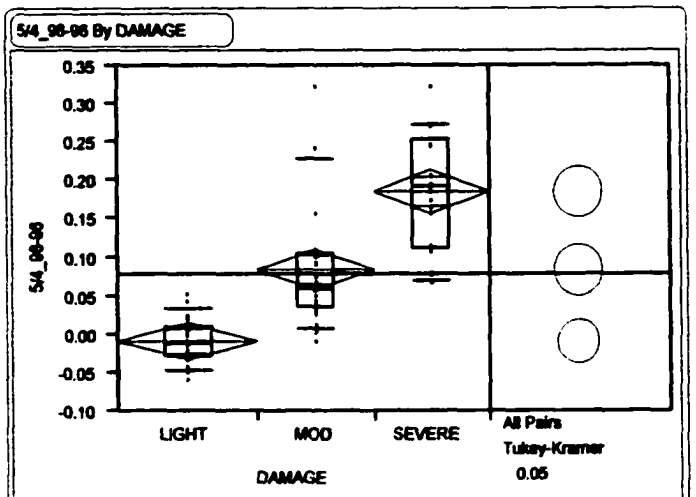

Oneway Anova

Summary of Fit

RSquare	0.617282
RSquare Adj	0.605111
Root Mean Square Error	0.064256
Mean of Response	0.07974
Observations (or Sum Wgts)	66

Analysis of Variance

Source	DF	Sum of Squares	Mean Square	F Ratio
Model	2	0.41950572	0.209753	50.8017
Error	63	0.26011800	0.004129	Prob>F
C Total	65	0.67962372	0.010456	<.0001

Means for Oneway Anova

Level	Number	Mean	Std Error
LIGHT	25	-0.00854	0.01285
MOD	21	0.083986	0.01402
SEVERE	20	0.185636	0.01437

Std Error uses a pooled estimate of error variance

Means Comparisons

Dif=Mean[i]-Mean[j]	SEVERE	MOD	LIGHT
SEVERE	0.000000	0.101649	0.194179
MOD	-0.10165	0.000000	0.092530
LIGHT	-0.19418	-0.09253	0.000000

Alpha= 0.05

Comparisons for all pairs using Tukey-Kramer HSD

q*
2.40033

Abs(Dif)-LSD	SEVERE	MOD	LIGHT
SEVERE	-0.04877	0.053460	0.147908
MOD	0.053460	-0.0476	0.046875
LIGHT	0.147908	0.046875	-0.04362

Positive values show pairs of means that are significantly different.

LIST OF REFERENCES

Abuelgasim, A.A., S. Gopal, J.R. Irons, and A.H. Strahler, 1996. Classification of ASAS multiangle and multispectral measurements using artificial neural networks, *Remote Sensing of Environment*, 57(2):79-87.

Biging, G., R. Congalton, and E. Murphy, 1991. A comparison of photointerpretation and ground measurements of forest structure, *Proc. of the 56th Annual Meeting of the American Society of Photogrammetry and Remote Sensing*, Baltimore, MD, 3:6-15.

Burnett, J. S., 1999. Detection, assessment, classification, and mapping of differing levels of ice storm damage to northern hardwood forests in the White Mountain National Forest in New Hampshire using hyperspectral airborne sensor Advanced Solid-State Array Spectroradiometer (ASAS), *Proc. of the International Symposium on Spectral Sensing Research*, Las Vegas, NV, pp. 121-136.

Burnett, J. S., 2001. Assessing differing levels of ice storm damage to northern hardwood forest canopies using Advanced Solid-State Array Spectroradiometer (ASAS), *Proc. Fifth International Airborne Remote Sensing Conference*, San Francisco, CA, in press.

Carter, G. A., R. J. Mitchell, A. H. Chappelka, and C. H. Brewer, 1992. Response of leaf spectral reflectance in loblolly pine to increased atmospheric ozone and precipitation acidity, *Journal of Experimental Botany*, 43(249):577-584.

Chang, S. H., and W. Collins, 1983. Confirmation of the airborne biogeophysical mineral exploration technique using laboratory methods, *Economic Geology*, 78:723-736.

Ciesla, W. M., 1998. Assessment of aerial survey classification of damage caused by the 1998 ice storm in the northeastern United States, *Plan of Work*, USDA Forest Service, Durham, NH.

Clevers, J. G., S. M. De Jong, and G. F. Epema, 1999. The use of MERIS standard band setting for deriving the red edge index, *Proc. of the International Symposium on Spectral Sensing Research*, Las Vegas, NV, pp. 145-153.

Collins, W., S. H. Chang, G. Raines, F. Chaney, and R. Ashley, 1983. Airborne geophysical mapping of hidden mineral deposits, *Economic Geology*, 78:737-749.

Committee on Earth and Environmental Sciences (CEES), 1991. Our changing planet: the FY 1992 U.S. Global Change Research Program, *Committee on Earth and Environmental Sciences of the Office of Science and Technology Policy Federal Coordinating Council on Science, Engineering, and Technology*, Washington, D.C., USA.

Congalton, R. G., and K. Green, 1999. *Assessing the Accuracy of Remotely Sensed Data: Principles and Practices,* Lewis Publishers, New York, NY, 137 p.

Congalton R. G., Oderwald, R. G., and R. A. Mead, 1983. Assessing Landsat classification accuracy using discrete multivariate analysis statistical techniques, *Photogrammetric Engineering & Remote Sensing,* 49(12):1671-1678.

Coppin, P. R., and M. E. Bauer, 1994. Processing of multitemporal Landsat TM imagery to optimize extraction of forest cover change features, *IEEE Trans. Geoscience and Remote Sensing,* 32(4):918-927.

DeFries, R.S., and J.R.G. Townsend, 1994. NDVI-derived landcover classification at global scales, *International Journal of Remote Sensing,* 15:3567-3586.

Dunham, J.W., and K.P. Price, 1996. Comparison of nadir and off-nadir multispectral response patterns for six tall grass prairie treatments in eastern Kansas, *Photogrammetric Engineering & Remote Sensing,* 62(8):961-967.

Entcheva, P., 2000. Remote sensing of forest damage in the Czech Republic using hyperspectral methods, *PhD Thesis,* University of New Hampshire, Durham, NH.

GSFC, 1998. Goddard Space Flight Center ASAS website, URL:http://asas.gsfc.nasa.gov/

Gopal, S., and C. Woodcock, 1994. Theory and methods for accuracy assessment of thematic maps using fuzzy sets, *Photogrammetric Engineering & Remote Sensing,* 60(2):181-188.

Hare, E. W., G. R. Edwards, and J. R. Miller, 1984. Geobotanical remote sensing of small localized swamps and bogs in northern Ontario, *Proc. of the International Symposium on Remote Sensing, 3rd Thematic Conference, Remote Sensing for Exploration Geology,* Ann Arbor: ERIM, pp. 671-682.

Horler, D.N.H., J. Barber, and A.R. Barringer, 1980. Effects of heavy metals on absorbance and reflectance spectra of plants, *International Journal of Remote Sensing,* 1:121-136.

Horler, D.N.H., M. Dockray, J. Barber, and A.R. Barringer, 1983. Red edge measurements for remotely sensed plant chlorophyll content, *Advanced Space Research,* 3(2):273-277.

Ingram, K., E. Knapp, and J. W. Robinson, 1981. Change detection technique development for improved urbanized area delineation, *Technical Memorandum* CSC/TM-81/6087, Computer Sciences Corporation, Silver Springs, Maryland.

Irons, J. R., K. J. Ranson, D. L. Williams, R. R. Irish, and F. G. Huegel, 1991. An off-nadir-pointing imaging spectroradiometer for terrestrial ecosystem studies, *IEEE Trans. Geosciences and Remote Sensing*, 29:66-74.

Jensen, J. R., 1996. *Introductory Digital Image Processing: A Remote Sensing Perspective*, Prentice Hall, Upper Saddle River, NJ, 316 p.

Kennedy, R.E., W.B. Cohen, and G. Takao, 1997. Empirical methods to compensate for a view-angle-dependent brightness gradient in AVIRIS imagery, *Remote Sensing of Environment*, 62: 277-291.

Kimes, D.S., B.N. Holben, and C.J. Tucker, 1984. Optimal directional view angles for remote-sensing missions, *International Journal of Remote Sensing*, 5(6): 887-908.

Knipling, E. B., 1969. Leaf reflectance and image formation on color infrared film, *Remote Sensing in Ecology*, P. L. Johnson, ed., Univ. of Georgia Press, Atlanta, GA, pp. 17-29.

Lambert, N.J., J. Ardo, B.N. Rock, and J.E. Vogelmann, 1995. Spectral characterization and regression-based classification of forest damage in Norway spruce stands in the Czech Republic using Landsat Thematic Mapper data, *International Journal of Remote Sensing*, 16(7):1261-1287.

Leroy, M., J.L. Deuze, F.M. Breon, O. Hautecoeur, M. Herman, J.C. Buriez, D. Tanre, S. Bouffies, P. Chazette, and J.L. Roujean, 1997. Retrieval of atmospheric properties and surface bidirectional reflectances over land from POLDER/ADEOS, *Journal of Geophysical Resources*, 102(14):17,023-17,037.

Linnane, J., 1998. Interim status report, Ice Storm 1998: Cooperating for forest recovery, *USDA Forest Service*, Durham, NH, July 1998, 13 p.

Ludlum, D. M., 1976. *The Country Journal: New England Weather Book*, Houghton Mifflin, Boston, MA.

Miller, J. R., E. W. Hare, R. A. Neville, R. P. Gauthier, W. D. McColl, and S. M. Till, 1985. Correlation of the metal concentrations with anomalies in narrow band multispectral imagery of the vegetation red reflectance edge, *Proc. of the International Symposium on Remote Sensing, 4th Thematic Conference, Remote Sensing of Exploration Geology*, Ann Arbor: ERIM, pp. 143-153.

Miller, J. R., M. G. Boyer, J. Wu, R. P. Gauthier, E. W. Hare, and M. Belanger, 1988a. Detection of spectral effects in individual tree crowns of metal-injected trees using high-resolution pushbroom imagery, *Proc. of the 16th Congress of the International Society of Photogrammetry and Remote Sensing*, Commission VII, 27 Part B, pp. 847-856.

Miller J. R., E. W. Hare, A. B. Hollinger, and D. R. Sturgeon, 1988b. Imaging spectrometry as a tool for botanical mapping, *Imaging Spectrometry II*, Greg Vane, ed., *Proc. of the Society for Photo-Optical Instrument Engineering (SPIE)*, 834:108-113.

Miller, J. R., E. W. Hare, and J. Wu, 1990. Quantitative characteristics of vegetation red reflectance, I, An inverted-Gaussian reflectance model, *International Journal of Remote Sensing*, 11:1755-1773.

Milton, J. R., W. Collins, S. H. Change, and R. G. Schmidt, 1983. Remote detection of metal anomalies on Pilot Mountain, Randolph County, NC, *Economic Geology*, 78:605-617.

Moss, D.M., and B.N. Rock. 1991. Analysis of red edge spectral characteristics and total chlorophyll values for red spruce (*Picea rubens*) branch segments from Mt. Moosilauke, NH, USA, *Proc. of the 11th Annual IGARSS '91 Symposium*, 3:1529-1532.

Nelson, R. F., 1983. Detecting forest canopy change due to insect activity using Landsat MSS, *Photogrammetric Engineering & Remote Sensing*, 49(9):1303-1314.

Oliver, C., and S. Quegan, 1998. *Understanding Synthetic Aperture Radar Images*, Boston, MA, Artech House.

Ranson, K. J., J.R. Irons, and D.L. Williams, 1994. Multispectral bidirectional reflectance of northern forest canopies with the Advanced Solid- State Array Spectroradiometer (ASAS), *Remote Sensing of Environment*, 47:276-289.

Rencz, A. N., G. F. Bonham-Carter, C. van der Greint, J. R. Miller, and E. W. Hare, 1986. Preliminary results from modeling vegetation spectra derived from MEIS data, *Proc. of the 10th Canadian Symposium on Remote Sensing, Canadian Remote Sensing Society, Canadian Aeronautic and Space Institute*, Ottawa, Ontario, pp. 909-917.

Rock, B.N., J.E. Vogelmann, D.L. Williams, A.F. Vogelmann, and T. Hoshizaki, 1986. Remote detection of forest damage. *Bioscience*, 36(7):439-445.

Rock, B. N., T. Hoshizaki, and J. R. Miller, 1988. Comparison of *in situ* and airborne spectral measurements of the blue shift associated with forest decline, *Remote Sensing of Environment*, 24:109-127.

Rock, B. N., D. L. Skole, and B. J. Choudhury, 1991. Monitoring vegetation change using satellite data, *Vegetation Dynamics and Global Change*, ed. A. M. Solomon and H. H. Shugart, Chapman and Hall, New York, NY.

Rohde, W. G., and C. E. Olson, Jr. 1971. Estimating foliar moisture content from infrared reflectance data, *Third Biennial Workshop: Color Aerial Photography in the Plant Sciences and Related Fields*, American Society of Photogrammetry, Falls Church, VA, pp.144-164.

Russell, C.A., J.R. Irons, and P.W. Dabney, 1993. Bidirectional reflectance of selected BOREAS sites from multiangle airborne data, *Journal of Geophysical Resources,* 102(D24):29,505-29,516.

Sandimeier, S., C. Muller, B. Hosgood, and G. Andreoli, 1998. Physical mechanisms in hyperspectral BRDF data of grass and watercress, *Remote Sensing of Environment,* 66:222-233.

SAS Institute, 1997. *JMP IN,* Version 3.2.1, Cary, NC.

Schowengerdt, R. A., 1983. *Techniques of image processing and classification in remote sensing*, Academic Press, New York, NY, 522 p.

Singh, A., 1984. *Tropical forest monitoring using digital Landsat data in northeastern India*, Ph.D. Thesis, Univ. Reading, Reading, England.

Singh, A., 1989. Digital change detection techniques using remote-sensed data, *International Journal of Remote Sensing*, 10(12):989-1003.

Smits, P. C., Dellepiane, S. G., and R. Schowengerdt, 1999. Quality assessment of image classification algorithms for land-cover mapping: A review and a proposal for a cost-based approach, *International Journal of Remote Sensing*, 20:1461-1486.

Smits, P. C., and A. Annoni, 2000. Toward specification-driven change detection, *IEEE Trans. Geoscience and Remote Sensing*, 38(3):1484-1488.

Stauffer, M. L., and R. L. McKinney, 1978. Landsat image differencing as an automated land cover change detection technique, *Technical memorandum* CSC/TM-78/6215, Computer Science Corporation, Silver Springs, MD.

Story, M., and R. Congalton, 1986. Accuracy assessment: A user's perspective, *Photographic Engineering & Remote Sensing*, 52(3):397-399.

Townshend, J. R., Justice, C. O., Gurney, C., and J. McManus, 1992. The impact of misregistration on change detection, *IEEE Trans. Geoscience and Remote Sensing*, 30:1054-1060.

Tucker, C. J., 1980. Remote sensing of leaf water content in the near infrared, *Remote Sensing of Environment,* 10:23-32.

Tukey, J. W., 1953. Problems of multiple comparison, Princeton University.

Vermote, E. F., D. Tanre, J. L. Denze, M. Herman, and J.-J. Morcrette, 1997. Second simulation of the satellite signal in the solar spectrum, 6S: An overview, *IEEE Trans. Geoscience and Remote Sensing*, 35(3):675-686.

Vogelmann, J.E., 1988. Detection of forest change in the Green Mountains of Vermont using Multispectral Scanner data, *International Journal of Remote Sensing*, 9(7):1187-1200.

Vogelmann, J. E., and B. N. Rock, 1988. Assessing forest damage in high-elevation coniferous forests in Vermont and New Hampshire using Thematic Mapper data, *Remote Sensing of Environment*, 24:227-246.

Vogelmann, J.E., and B.N. Rock, 1989. Use of Thematic Mapper data for the detection of forest damage caused by the pear thrips, *Remote Sensing of Environment*, 30:217-225.

Vogelmann, J.E., B.N. Rock, and D.M. Moss, 1993. Red edge spectral measurements from sugar maple leaves, *International Journal of Remote Sensing*, 14(8):1563-1575.

Zadeh, L.A., 1965. Fuzzy sets, *Information and Control*, 8:338-353.

Zar, J. H., 1996. *Biostatistical Analysis*, Prentice Hall, NY, 662 p.

Zarco-Tejeda, P. J., 2000. *Hyperspectral remote sensing of closed forest canopies: Estimation of chlorophyll fluorescence and pigment content*, PhD Thesis, York University, Toronto, Canada, 210 p.